A multiscale analysis of summer temperature variability in Southern South America during the 20th century

Inauguraldissertation
der Philosophisch-naturwissenschaftlichen Fakultät
der Universität Bern

vorgelegt von

Martín Jacques Coper

von Chile

Leiter der Arbeit:
Prof. Dr. S. Brönnimann

Geographisches Institut, Universität Bern

Von der Philosophisch-naturwissenschaftlichen Fakultät angenommen

Der Dekan:
Prof. Dr. G. Colangelo

Bern, den 10. Oktober 2014

A mis abuelos:
Flora y Walter,
Lydia y Arturo;

gracias a ustedes estoy acá.

Su fe en las ciencias

"Una esperanza creía en los tipos fisonómicos, tales como los ñatos, los de cara de pescado, los de gran toma de aire, los cetrinos y los cejudos, los de cara intelectual, los de estilo peluquero, etc. Dispuesto a clasificar definitivamente estos grupos, empezó por hacer grandes listas de conocidos y los dividió en los grupos citados más arriba. Tomó entonces el primer grupo, formado por ocho ñatos, y vio con sorpresa que en realidad estos muchachos se subdividían en tres grupos, a saber: los ñatos bigotudos, los ñatos tipo boxeador y los ñatos estilo ordenanza de ministerio, compuestos respectivamente por 3, 3 y 2 ñatos. Apenas los separó en sus nuevos grupos (en el Paulista de San Martín, donde los había reunido con gran trabajo y no poco mazagrán bien frappé) se dio cuenta de que el primer subgrupo no era parejo, porque dos de los ñatos bigotudos pertenecían al tipo carpincho, mientras el restante era con toda seguridad un ñato de corte japonés. Haciéndolo a un lado con ayuda de un buen sandwich de anchoa y huevo duro, organizó el subgrupo de los dos carpinchos, y se disponía a inscribirlo en su libreta de trabajos científicos cuando uno de los carpinchos miró para un lado y el otro carpincho miró hacia el lado opuesto, a consecuencia de lo cual la esperanza y los demás concurrentes pudieron percatarse de que mientras el primero de los carpinchos era evidentemente un ñato braquicéfalo, el otro ñato producía un cráneo mucho más apropiado para colgar un sombrero que para encasquetárselo. Así fue como se le disolvió el subgrupo, y del resto no hablemos porque los demás sujetos habían pasado del mazagrán a la caña quemada, y en lo único que se parecían a esa altura de las cosas era en su firme voluntad de seguir bebiendo a expensas de la esperanza."

Julio Cortázar

"Historias de Cronopios y de Famas" (1962)

"Aller Anfang ist schwer, gilt in jeder Wissenschaft."

Karl Marx

"Das Kapital" (1867)

Summary

South America is a key region for the study of climate processes and dynamics in the Southern Hemisphere due to its extension from the tropics into the midlatitudes and also due to its geographic particularities, which cause a fabulous climate diversity. However, the climate research of the southern latitudes of the continent, especially of Patagonia, during the instrumental period, is a relatively young scientific field. This is mainly a consequence of a rather scarce instrumental network with limited record lengths. In particular, the mechanisms of temperature variability have remained underexplored in comparison with other regions of the world. Although the anthropogenic regional warming signal is less marked than in most of the rest of the world, climate variability in Patagonia directly affects the cryosphere and biosphere. Thus, the understanding of natural temperature variability is especially important in this region. Many recent studies have focused on this region; however, they were mostly restricted to the few decades covered by the meteorological information. Nevertheless, a more comprehensive picture of the climate of this region has been emerging in the last years from diverse scientific efforts. In this context, the Twentieth Century Reanalysis (20CR), a novel observation-based global climate reconstruction spanning 1871 to present date, is an unprecedented source of climatic information that offers a big potential for climate studies. Despite the fact that conclusions derived from this dataset can be associated with large uncertainties in regions poorly covered by instruments –an issue affecting especially the Southern Hemisphere around the South Pacific Ocean–, it is possible to combine the 20CR with independent long-term instrumental information to validate the results drawn from the reanalysis.

    In the present work, we analyse the variability of summer temperature in Southern South America (SSA), in particular of Patagonia, with a multiscale temporal perspective in order to gain insight into different temporal variability ranges. We consider the intraseasonal timescale (*processes happening within each summer*), the interannual timescale (*summer-to-summer*), as well as the interdecadal timescale (*processes with periods longer than ~10 years*). The research is mainly based on signals extracted from the 20CR and instrumental records in Eastern Patagonia, where the data density is highest and the temporal coverage largest. The three chapters presented in this thesis

are self-contained but strongly interrelated. They contribute to an improved understanding of the large-scale and regional mechanisms associated with our study subject. Thus, our research is of relevance for the interpretation of climate events in the last century and also for projections of future climate change.

In the first study, the 1907-2001 interannual and the interdecadal temperature variability in the eastern part of SSA ia examined. Instrumental-based indices for the main modes of temperature variability within both timescales are defined. The main interdecadal index reveals a warm-to-cold (cold-to-warm) transition in the early 1930s (late 1970s). Although it has been in phase with the Pacific Decadal Oscillation (PDO) index since the 1960s, they diverged in the preceding decades. The main interannual index represents roughly the southern half of the continent and shows its peak at ~3.4 years. Running correlation coefficients between this index and summer indices of Niño3.4 and the Southern Annular Mode (SAM) reveal significant out-of-phase decadal fluctuations. The large-scale spatial correlation fields between the interannual index and several atmospheric variables show a wave-train circulation pattern in the South Pacific. This feature suggests a teleconnection mechanism that induces an interannual anticorrelation between SAT in SSA and precipitation in Oceania. This relationship, however, was disrupted in the late 1970s, presumably due to the subsequent PDO warm phase.

In the second study, an analogy to the subject investigated in the previous work (namely the occurrence of *warm summers* within the interannual timescale) is established, by investigating the occurrence of summer heat wave events in the intraseasonal timescale. The corresponding signal, extracted from 20CR for Southeastern Patagonia (SEPG, a more restricted area as in the previous study) covering 1872-2010, is validated for 1957-2010 with local instrumental records of daily resolution. The mean regional and large-scale dynamical development of the heat waves is described. The mean heat wave, which affects a broad area on both sides of the Andes, is mainly driven by horizontal temperature advection and enhanced radiative heating. Its anomaly signal lasts for approximately two weeks and reaches a peak perturbation of +4.3°C, eventually leading to temperature extremes in SEPG. Intraseasonal heat waves in SEPG are related to a wave-train circulation pattern in the South Pacific. This structure, which resembles the one found for the interannual timescale in our previous study, induces furthermore a similar teleconnection with Oceania. As for the interannual timescale, its existence provides a means to indirectly validate the temperature signal obtained for SEPG from 20CR. As an attempt to interrelate different frequencies of variability, this study shows that the spatial characteristics of the intraseasonal wave train pattern leading to heat waves in SEPG seem to be modulated in the interannual and interdecadal timescales.

The third study shows that the intraseasonal component of summer temperature in Eastern Patagonia is highly driven by the intraseasonal activity and, in particular, by that related to the Madden-Julian Oscillation (MJO), the dominant mode of intraseasonal variability of the tropical coupled ocean-atmosphere system. Using a long-term 20CR-based reconstruction of the MJO index defined by Wheeler and Hendon, this work reveals that active MJO phases modulate the mean instrumental temperature signal (1957-2008) with an amplitude of ca. 1.5°C. The warmest (coldest) conditions are found during days exhibiting an active MJO phase 8 (4). These results are also found for the subregion SEPG using 20CR (1906-2008). Besides, a link is established with the preceding work and it is shown that, in particular, intraseasonal heat waves detected in SEPG tend to culminate in an active MJO phase 8. Finally, based on composite fields and a case study, this work introduces a mechanism by which the tropical intraseasonal activity may constructively interact with extratropical dynamics and favour the occurrence of heat waves in SEPG.

Contents

Abbreviations

Climate products

20CR, 20CRv2	Twentieth Century Reanalysis v2
ERA-40	ECMWF reanalysis
GHCN	Global Historical Climate Network v2
NNR	NCEP/NCAR reanalysis I
UDel	University of Delaware gridded data v2.01 (SAT and precipitation)

Climate modes

EN	El Niño
ENSO	El Niño-Southern Oscillation
IPO	Interdecadal Pacific Oscillation
LN	La Niña
MJO	Madden-Julian Oscillation
PDO	Pacific Decadal Oscillation
PSA	Pacific-South American mode
SAM	Southern Annular Mode

Toponyms

CWA	Central Western Argentina
SA	South America
SESA	Southeastern South America
SSA	Southern South America
SH	Southern Hemisphere
SEQ	Southeast Queensland
SEPG	Southeastern Patagonia
SACZ	South Atlantic Convergence Zone

Variables

OLR	Outgoing longwave radiation
prate	Precipitation rate
RCF	Relative cyclone frequency
SAT	Surface air temperature
sf200	Streamfunction at 200 hPa
SLP	Sea level pressure
SST	Sea surface temperature
T	Surface air temperature
Tm, Tn, Tx	Mean, minimum, and maximum teperatures, respectively
u	Zonal component of the wind
v	Meridional component of the wind
wind200	Wind at 200 hPa
z500	Geopotential height at 500 hPa
ω500	Vertical velocity at 500 hPa

Physical units

°C	Degree Celsius
hPa	Hectopascal
K	Degree Kelvin
m	Meter
m a.s.l.	Meter above mean sea level
Pa	Pascal
s	Second
W	Watt

Institutions

CONICYT	Comisión Nacional de Investigación Científica y Tecnológica, Chile
ECMWF	European Centre for Medium-Range Weather Forecasts
NCAR	National Center for Atmospheric Research
SDC	Swiss Agency for Development and Cooperation

Other abbreviations

C	Cluster
d0	First day of a heat wave (day 0)
DJF	December-January-February
LLJ	Low-level jet
PC	Principal component
PCA	Principal component analysis
R	Region

Chapter 1

Introduction

*"De tous les sujets qui peuvent solliciter notre attention studieuse,
seraut-il possible d'en trouver un qui fût d'un intérêt plus direct, plus perpétuel, plus
important, que celui dont nous allons nous occuper? L'atmosphère fait vivre la terre."*

Camille Flammarion
"L'Atmosphère: Météorologie Populaire" (1888)

*"Why… have these arid wastes [of Patagonia] taken so firm a hold on my memory?
… I can scarcely analyse these feelings:
but it must be partly owing to the free scope given to the imagination."*

Charles Darwin
"Voyage of the Beagle" (1839) [quoted by Nouzeilles (1999)]

*"Para llorar, dirija la imaginación hacia usted mismo,
y si esto le resulta imposible por haber contraído el hábito de
creer en el mundo exterior, piense en un pato cubierto de hormigas o en
esos golfos del estrecho de Magallanes en los que no entra nadie, nunca."*

Julio Cortázar
"Historias de Cronopios y de Famas" (1962)

1.1 Motivation

Climatology, among the diversity of modern scientific specializations, is a relatively young discipline. This fact, however, contrasts with the fundamental role that climate has played in the story of mankind and is surely not a consequence of disinterest. In all corners of the world, actions that would be nowadays called *climatological observations* were and are still carried out within the development of the everyday life. Thus, it would not be exaggerated to affirm that, in practice, the *apparently young* climatology is the depositary of a century-long tradition.

In this sense, there is a parallel to South America, which, as a constitutive entity of the major American continent, is also a relatively young part of the world known to the European Civilization. The process of colonization of America began with the arrival of Columbus in 1492 in the Bahamas and expanded thereafter over the whole continent, giving place to one of the most intense and dramatic histories of cultural encounter, mixture, suppression, and replacement, a phenomenon that is still taking place (Galeano 1971). Because of its remote location, the southernmost part of South America remained an almost unexplored territory for the European eye. Indeed, the territory which is now known as Patagonia (Fig. 1.1) was almost a no man's land until the last decades of the 19th century, when the border between Argentina and Chile was established and the first settlements were founded, with a considerable European component. Notwithstanding, the remoteness of this region and its extreme environmental conditions, among other factors, have limited until now the population density in Patagonia.

Therefore, being climatology a quite recent research discipline and South America a continent with a young scientific tradition, it is not surprising that the climatology of the southern part of the continent, and in particular of Patagonia, is a quite novel area of study when compared with the research dedicated to other regions of the world. This fact still offers an interesting opportunity for expanding the climatological knowledge frontier, an aspect that constitutes our first motivation for this thesis.

The reasons for pursuing this work are not just of scientific but also of emotional nature. On the emotional side of the motivations, the focus on SSA is a natural consequence of the author's personal experience and interests. Although I was then not consciously devoted to the study of climate, my childhood and adolescence were impregnated by the features of the mid-latitude climate in the austral city of Valdivia, in the northwestern corner of Patagonia. Unending storms and many consecutive days of rain are features that forge not only the physical but also the human geography of that region. A series of travels undertaken during that phase of my life allowed me to discover the landscape diversity

Fig. 1.1: *Historical French map of Patagonia from the 19th century: "Patagonie, et Detroit de Magellan, Terres Australes. Atlas spheroidal & universel de geographie dresse par F.A. Garnier, geographe. Vve. Jules Renouard, Editeur, Rue de Tournon, no. 6, Paris. 1860. Sarazin, imp., r. Git-le-Coeur, 8, Paris.".*

of Patagonia. I was fascinated by it. That natural heterogeneity is mainly a consequence of its immense latitudinal extension and also of the presence of the Andes Cordillera, a towering obstacle to the humid westerly atmospheric flow from the Pacific Ocean and thus a major meridional divide between the climatic characteristics of the hyperhumid western part and the highly arid eastern part of that region. The particularities caused by the geographic setting of the continent were commented maybe already before Hahn (1897) asserted that "South America is the only continent in the Southern Hemisphere which extends beyond the subtropical zone, even into the region of the predominant westerly winds of the temperate zone. Moreover, South America differs from Africa and Australia in that the western edge of the mountains of the continent is the highest and, in contrast to that feature, the eastern side remains quite accessible for the sea winds. This fact causes some remarkable climatic differences" (personal translation).

With respect to science, this PhD thesis is the continuation of the first stages of my research activities. As a scientist in formation, I carried out my first work on climatology during my Master's Thesis at the Universidad de Chile, far from Patagonia. This work characterised the 1970s *climate shift* in South America and has been published very recently (Jacques-Coper and Garreaud 2014). That experience gave me a good opportunity to get a general but deep understanding of the large-scale climatology of South America. From a continental perspective, we described an outstanding abrupt change in the means of sea surface temperature (SST), surface air temperature (SAT), precipitation, and sea level pressure (SLP). In particular, we found a conspicuous shift-like summer warming in Southern South America during the late 1970s and, coinciding with previous studies, we concluded that both the interannual (El Niño-Southern Oscillation, ENSO) and the interdecadal (Pacific Decadal Oscillation, PDO) variability modes had an incidence in its manifestation. However, that analysis was mainly restricted to 1961-1990. The results obtained from that research, described below in more detail, encouraged us to overcome that temporal limitation and perform a further investigation still focused on Southern South America but considering a larger temporal context. Hence, we selected *the variability of temperature in Southern South America (SSA) in the 20th century* as our subject of study. The long-term perspective of the analysis of present work is of relevance for the climatology of South America, because most of the studies based on instrumental records have covered just a few decades. By taking a long-term perspective into account, our scientific contribution could acquire a higher profile. This potential is undoubtedly another motivation for the present thesis.

A further reason to choose the specific research subject of this thesis is the importance of understanding the behaviour of this variable within the present debate on climate variability and climate change. In the context of global warming, this part of the world has shown neutral and even negative temperature trends in the last decades

of the 20th century, a feature that is even more pronounced during summer (Falvey and Garreaud 2009; Trenberth et al. 2007). Moreover, the future climate projections of the Intergovernmental Panel on Climate Change (IPCC) show that this region is one of those exhibiting minimum warming over land, considering various scenarios and time periods (Meehl et al. 2007). Thus, as has been remarked in several contexts and especially regarding the research in climatology, *in order to be able to make projections for the future, it is necessary to understand the past.*

An additional impetus for attempting to seek answers to climatological questions in a relatively unexplored region such as the southernmost part of South America is related to the unprecedented opportunity offered by the availability of recent century-long global climate reconstructions. Despite its youth, climatology has developed in a vertiginous way. Lots of work devoted to data recovery, to the development of applied mathematical techniques, and to the enhancement of the computation capacity of modern machines have made possible that these datasets are currently available. Undoubtedly, they constitute a data source that can be explored in almost infinite ways.

The University of Bern has been a relevant international actor in the recovery of climatological data and the reconstruction of (paleo)climates worldwide. This fact, described also in more detail below, has been in its own a strong impulse to write this PhD thesis in Bern.

1.2 Southern South America: from Terra Incognita into the annals of climatology

1.2.1 Southern South America and Patagonia

SSA is defined in this work as the austral part of the continent, extending roughly from 30°S until the Drake Passage. Patagonia, covering from 40°S southward, is thus included in SSA. This geographical configuration is nicely shown in an historical French map of the 19th century (Fig. 1.1). The present thesis focuses on climatological phenomena occurring mainly in Eastern Patagonia, i.e., south of 40°S and to the east of the Andes Cordillera, a region were historical meteorological measurements are scarce (Garreaud et al. 2012; Paruelo et al. 1998) and the climate proxy coverage poor (Neukom et al. 2011). As is shown throughout the present work, these climatological phenomena are

consequence of the interaction between large-scale climate patterns and local features. Therefore, it can be expected to find climatic links —the so-called *teleconnections*— of these phenomena within South America, but also beyond its borders, even in a hemispheric scale. Hence, although the climatic signals to be explored are extracted mainly from Patagonia, it is more adequate to consider the whole SSA as the region of study of our work.

1.2.2 A brief historic climatological background of Patagonia

Although the geography of this region of the world was not explored in detail until the last decades of the 20th century, the characteristics associated with its remote location, especially its extreme climatic conditions, always attracted the attention of the foreigners who visited it. Patagonia awakened the fascination of renowned European scholars during exploration voyages that brought them to this edge of the world. This was the case of Louis Antoine de Bougainville in 1766, and Charles Darwin and Robert FitzRoy (a pioneer in meteorology) in 1832, among others.

Until recent years, the attempts to describe the climate of Patagonia were centred on a particular variable (Paruelo et al. 1998). The wind intensity has been historically the most salient meteorological feature of this region. Prohaska (1976) asserted that "in few parts of the world is the climate of the region and its life so determined by a single meteorological element, as is the climate of Patagonia by the constancy and strength of the wind". In fact, the wind cooling effect in Patagonia leads to an annual equivalent temperature range smaller than the actual temperature range and enhances the oceanic character of its climate (Coronato 1993).

Nevertheless, more recent studies have tried to draw a more comprehensive picture of the climate of Patagonia. Because an exhaustive bibliography has been included in each chapter of this thesis, here we will mention only a few of them. In a broader spatial context, the patterns of precipitation and temperature variability in Argentina and Chile were analysed for 1931-1960 by Pittock (1980a, 1980b). In the large-scale context, he found that a major part of the climatic variations of these variables was accounted by few circulation anomaly mechanisms, such as the Southern Oscillation, the pressure difference across the Antarctic between Tasmania and the Falkland Islands region, the latitude of the high-pressure belt off the coast of Chile, and the pressure difference across the tropical Atlantic Ocean. Among other works, the temperature variations in Southern South America, including Patagonia, were studied based on linear

trends for 1933-1992 by Rosenblüth et al. (1997). A general description of the climate of Patagonia, considering also wind, humidity, and radiation, was provided by Paruelo et al. (1998). Recently, Garreaud et al. (2012) analysed the large-scale control of the climate of Patagonia using a 30-year high-resolution numerical simulation. The authors described the dependence of the year-to-year climate of Patagonia on the low-level zonal wind. Berman et al. (2012, 2013), based on local measurements and reanalysis products, described in detail the seasonal-to-interannual temperature variability and the seasonal precipitation variability in Eastern Patagonia and its surrounding regions for 1979-2009.

Most of the climate studies (and in particular about temperature) concerning our definition of Southern South America and Patagonia are restricted to a few decades within the 20th century. Thus, a research as the one presented here, which involves a longer temporal perspective, constitutes a contribution to the understanding of the regional climate and could serve as a means to compare results drawn from different periods.

1.3 A crucial aspect: data availability in Southern South America

1.3.1 Long-term multi-proxy climate reconstructions

Pittock (1980), in his seminal work on the climatic variation in Argentina and Chile, cited the comment by Knoch (1930), who stated that "Because reliable and comparable observational data always must be the principal basis for a description of the climate (of a large region), a climatology of South America can hardly satisfy high expectations". In fact, the density of stations in Patagonia has historically been very low (Paruelo et al. 1998). Nevertheless, a great deal of water has flowed under the bridge since then, and strong efforts have been made in order to have meteorological and climatological information available for further digital processing and analysis. This achievement is the result of long procedures. Concerning data within the instrumental period, it includes the digitizing of weather measurements, recorded originally in different analogical ways, their adaptation into universal standard formats, and eventually the post-processing of them in terms of quality control, such as the application of homogenization techniques. With regard to longer timescales, another important area of scientific progress is related to the (paleo)climatic reconstructions developed for this region.

The University of Bern has devoted huge scientific labour in both aspects.

Concerning paleo-climate, a comprehensive review and discussion on the datasets that were available until a few years ago is found in Villalba et al. (2009). The work undertaken by the "Long-term climate reconstruction and dynamics of Southern South America" (LOTRED-SA) group in the framework of the IGBP-PAGES project delivered data products that are an enormous contribution to the climatology of SSA. In particular, the corresponding century-long precipitation and temperature gridded reconstructions (Neukom et al. 2011; Neukom et al. 2010) are a crucial product that might inspire many further studies. Concerning longer timescales, relevant studies have recently been published by investigators of the University of Bern, among others the reconstructions of air temperature (Elbert et al. 2013a; Elbert et al. 2013b) and precipitation (Elbert et al. 2012) based on lake sediments from the Chilean mid-latitudes. All these results, together with the combined work done by many scientists worldwide, have recently led to achieve an improved big picture of the inter-hemispheric climate variability of the past millennium (Neukom et al. 2014).

1.3.2 A climatic revolution within the instrumental period — The Twentieth Century Reanalysis: general overview and its application in the Southern Hemisphere

The University of Bern has also contributed to the development of a revolutionary climatological project: the *Twentieth Century Reanalysis* (20CR, Compo et al. (2011)). This global atmospheric circulation dataset has a 6-hourly temporal resolution and a 2°x2° horizontal resolution in space, and spans 1871-2012. It is based on the HadISST Sea Ice and SST dataset (Rayner et al. 2003) and on SLP observations from the International Surface Pressure Databank (ISPD). Before its development, many studies demonstrated that reliable reanalysis of early periods (last decades of the 19th century and first decades of the 20th century) can be generated using only surface observations and advanced data assimilation methods (Compo et al. 2011).

In the Southern Hemisphere, this reanalysis includes SLP observations in Australia and South America already by 1900, increasing the network coverage since then (Yin et al. 2008). We are aware that data coverage in the Southern Pacific is poor compared to other regions of the world and especially to Northern Hemisphere standards. However, the 20CR incorporates available observations and produces a physically-consistent reconstruction, which has been used as a good estimate of climate parameters in earlier periods. Because of the reasons exposed above, this product has a major potential for possible applications in the Southern Hemisphere. As already stated, this fact constitutes

a main motivation for the present work. The 20CR is indeed employed throughout all the studies that form this PhD thesis.

Although since our best knowledge the 20CR has not been thoroughly validated in the Southern Hemisphere, its skill in southern mid-latitudes has been positively assessed. Here we mention some results that demonstrate this statement. During 1958-1978, 300 hPa geopotential height observations from radiosondes present higher correlations in the Southern Hemisphere extratropics with 20CR than with ERA-40 (Compo et al. 2011). For early periods, Brönnimann et al. (2011) found good agreement between 20CR and temperature observations from radiosondes launched on a cruise from Europe around South Africa and across the Indian Ocean to the western Pacific in 1906/1907, and close agreement between the 20CR and geopotential height and temperature data from a cruise that travelled from Europe to Antarctica across the Atlantic and back in 1938/1939. Good agreement was also found between 20CR and temperature measurements taken during 1925-1927 in the Atlantic Ocean by the German expedition ship Meteor I (Jörg and Storz 2013). Brönnimann and Compo (2012) found good correlations between historical ozone data and 20CR over Australia and New Zealand in the 1930s. Zhang et al. (2012) evaluated the performance of eight global reanalyses in reproducing monthly-mean precipitation observations over southern Africa during the available periods for each dataset and concluded that 20CR is the best-suited reanalysis for investigating the climate variability over southern Africa, also highlighting its value to investigate interannual to decadal variability. This reanalysis has been also used for studies focusing in the Southern Hemisphere during the whole 20th century, by instance for constructing a summer index of the Southern Annular Mode (SAM) (Wang and Cai 2013), and also to force an oceanic model by computing heat fluxes (Liu and Wu 2012).

In the present work, we are aware that conclusions arising from early periods should be taken cautiously. However, throughout this thesis we attempt to describe results based not only on 20CR but also on observations and other independent datasets in order to reduce the uncertainty associated with single products. Furthermore, by analysing various variables at different levels, we have strived in our research at describing consistent relationships.

1.4 The scientific questions awakened by an outstanding climate event

1.4.1 The late-1970s summer warming in Southern South America

The fundamental scientific motivation for this PhD thesis was triggered by the results of own previous work, which has been recently published (Jacques-Coper and Garreaud 2014). In the context of the analysis of the 1970s *climate shift* in South America, we found that the sudden warming signal was highest (>1.5°C) in eastern SSA. Two December-to-February (DJF) temperature composites reveal a robust step-like warming in SSA and southeastern South America (SESA) in 1977/1978 and 1978/1979, respectively (Fig. 1.2). In SESA, the increase in temperature was linked hypothetically to enhanced subsidence and clearer skies, which were favoured by the concomitant abrupt increase observed in sea level pressure (SLP), maybe related to the southward shift of the southwestern part of the South Atlantic Anticyclone (Barros et al. 2008). In SSA, the warming pattern was found to be related to a southward shift of the prevailing westerly winds due to the onset of an anticyclonic circulation anomaly in the southern tip of the

a) summer SAT shifts: 1976-79
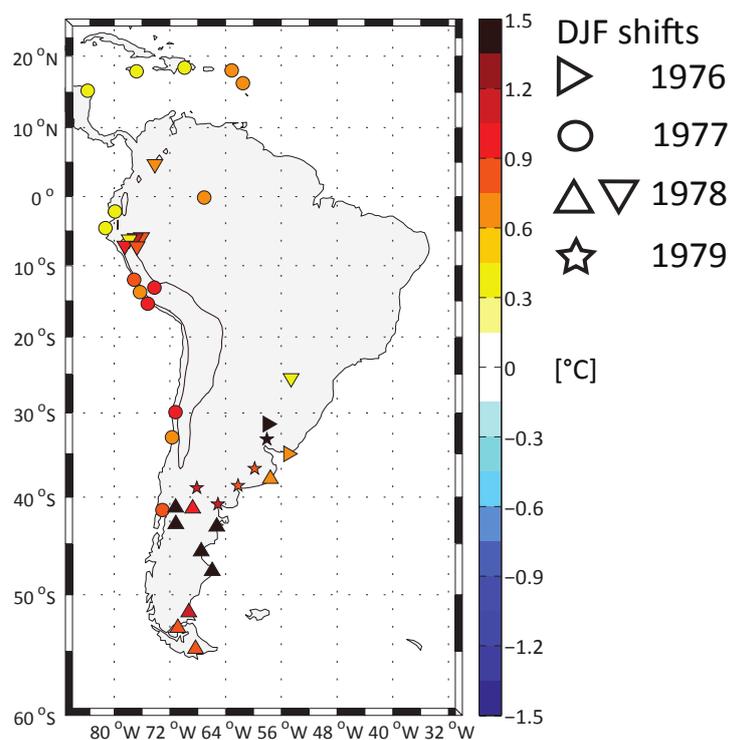
**Fig. 1.2 a)** *Surface air temperature (SAT) shifts identified between 1976 and 1979, shown as differences in the mean [°C] between periods of 10 years before and 10 years after their detection (see legend). Different symbols for the same year denote different clusters. Over the continent, the solid contour depicts the 2000 m isoline.*

continent. We showed that summer SAT in SSA is negatively correlated with zonal wind and positively correlated with low-level horizontal temperature advection. In SSA during summer, this term is always negative and mainly zonal. Its intensity weakened after the summer 1978/1979, leading to a net warming and probably also to less cloudiness and thus stronger solar radiation over that region.

1.4.2 Scientific curiosity and attractive research opportunities

The study mentioned in the previous subsection was limited to 1961-1990. Given the conspicuous and abrupt temperature rise found in SSA in the late 1970s, an inevitable scientific consequence was the curiosity to explore this event in a longer temporal context. Therefore, *the variability of summer temperature in SSA in the 20th century* was selected
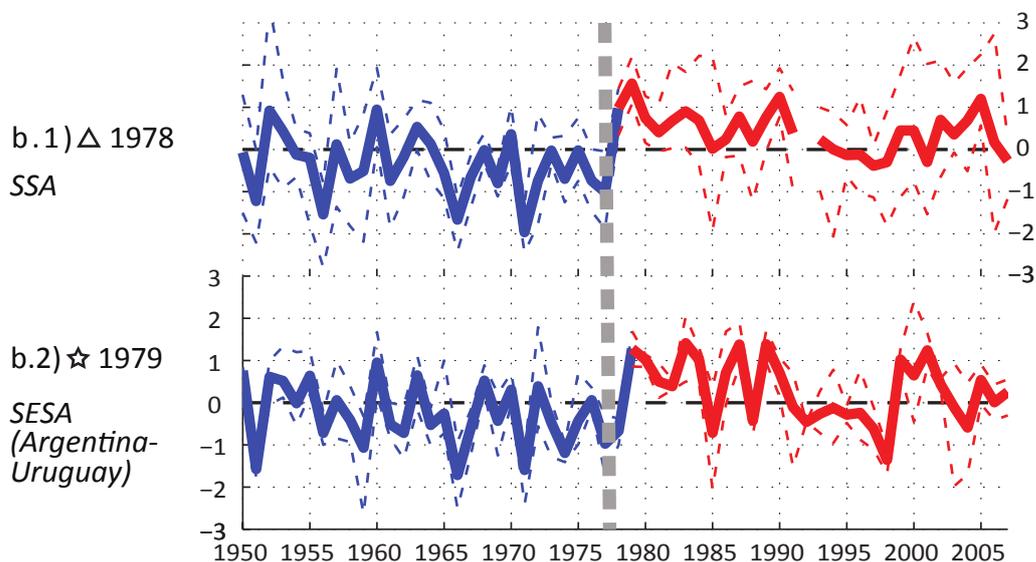
Fig. 1.2 b) *Composites of December-to-February (DJF) standardized anomalies of SAT with respect to 1961–1990 (zscores) showing a shift-like warming in (b.1) Southern South America (SSA) in 1978 and in (b.2) southeastern South America (SESA) in 1979; see legend in panel a. DJF values are depicted by solid curves; dashed lines show the minimum and maximum value of the composite for each year. The vertical dashed line indicates the 1976/1977 transition. Figure adapted from Jacques-Coper and Garreaud (2014).*

as a common subject for the studies presented in each chapter of this PhD thesis.

In particular, two main scientific questions were raised by our previous research:

– How does the remarkable 1970s *summer temperature shift in Southern South America* compare with other climatic transitions in a broader temporal context, namely within the whole 20th century?

– Which are the large-scale mechanisms driving the variability of the summer temperature in Southern South America within the 20th century *on various timescales,* beyond the global warming signal?

The availability of the 20CR enables a *multiscale temporal analysis of the temperature variability in SSA* during that period. As detailed in the next section, the consideration of various timescales is necessary for the understanding of phenomena related not only to the long-term seasonal climate, but also to the synoptic character of meteorological events, which, in the end, build up the climate. The comparison between phenomena occurring within different frequency bands constitutes a philosophical dimension of the present work.

Thus, since the beginning of this PhD thesis, an excellent opportunity was given to explore this subject in a very stimulating research atmosphere as the one offered by the Climatology group of the University of Bern.

1.5 Objectives of the PhD thesis

The objectives of this PhD thesis are related to the *multiscale analysis of the summer temperature variability in Southern South America in the 20th century*, i.e. considering both large spatial and temporal scales (namely the interannual and interdecadal timescales), and a more focalised area at the intraseasonal timescale. In the studies included in this thesis, we have removed the very long-term signal from the data, either by subtracting the linear trend of the seasonal mean values (to analyse the interannual variability) or the seasonal mean from each year (to analyse the intraseasonal variability). In this way, we focus on mechanisms other than those related to the long-term trend, possibly mainly related to the global warming signal.

The methodological approach has led us to formulate the following objectives for each of the three studies included in this PhD thesis:

1) Interannual-to-interdecadal variability: warm and cold summers in SSA

1.a) Definition and description of representative observation-based indices of the SAT variability in SSA for the interannual (i.e. *summer-to-summer*) and interdecadal timescales within the 20th century;

1.b) Analysis of the relationships between those SAT indices and large-scale climate variability modes;

1.c) Utilisation of the 20CR and further datasets covering the 20th century to explore the possible large-scale relationships of these indices, with special dedication to the interannual timescale, in order to explore atmospheric circulation features related to *cool* and *warm summers* in SSA.

2) Intraseasonal variability: occurrence of heat waves in southeastern Patagonia

2.a) Investigation of the intraseasonal variability of summer temperature in Southeastern Patagonia (SEPG), a region located within SSA, through the analysis of the occurrence of local heat waves in 20CR (an analog to *warm summers* for the interannual timescale);

2.b) Validation of the results obtained for the intraseasonal timescale by means of local temperature observations of daily resolution;

2.c) Dynamical description of the evolution of the large-scale patterns and possible teleconnections associated with the heat waves, and comparison to the patterns and relationships found for the interannual timescale.

3) Intraseasonal variability: tropical modulation of summer temperature in eastern Patagonia

3.a) Exploration of a possible link between summer intraseasonal anomalies of SAT in SEPG and the intraseasonal tropical activity associated with the Madden-Julian Oscillation (MJO);

3.b) Investigation of a potential relationship between the tropical modulation of intraseasonal summer temperature in SEPG and the occurrence of heat waves in SEPG.

1.6 Outline of the PhD thesis

The thesis is organised as follows: in Chapter 2, we analyse the 1907-2001 summer-to-summer SAT temperature variability in the eastern part of SSA, based on instrumental records and the 20CR (Jacques-Coper and Brönnimann 2014). We study the stability of the temporal correlations between the leading interannual and interdecadal SAT indices and those of large-scale climate variability modes during the 20th century. Moreover, we characterize the large-scale spatial correlation fields between the interannual index and several climatic variables and deduce from them a teleconnection between SAT in SSA and precipitation in Oceania. In Chapter 3, we explore the occurrence of summer heat wave events in the intraseasonal timescale in SEPG as depicted by 20CR during 1872-2010 (Jacques-Coper et al., in prep.). The SAT signal is validated with daily temperature observations for 1957-2010. We describe the regional and the large-scale dynamical development of these events, show the existence of an intraseasonal teleconnection between SEPG and Oceania (specifically: southeastern Australia and New Zealand), and include a brief discussion on the possible interannual and interdecadal modulation of the circulation anomalies that lead to heat waves in SEPG. In Chapter 4, we reveal that active phases of the MJO modulate the mean intraseasonal instrumental temperature signal in Eastern Patagonia and suggest how the related tropical intraseasonal activity may favour the occurrence of heat waves in SEPG. For that, we use both the 20CR and instrumental daily records, and a 20CR-based reconstruction of the MJO index defined by Wheeler and Hendon, available for 1905-2008. Finally, in Chapter 5, we summarize the conclusions derived from the results obtained in this thesis and propose research questions for further studies.

References

Barros VR, Doyle ME, Camilloni IA (2008) Precipitation trends in southeastern South America: relationship with ENSO phases and with low-level circulation. Theor Appl Climatol 93:19–33. doi: 10.1007/s00704-007-0329-x

Berman A, Silvestri G, Compagnucci R (2013) On the variability of seasonal temperature in southern South America. Clim Dyn 40:1863–1878. doi: 10.1007/s00382-012-1596-5

Berman AL, Silvestri G, Compagnucci R (2012) Eastern Patagonia Seasonal Precipitation: Influence of Southern Hemisphere Circulation and Links with Subtropical South American Precipitation. J Clim 25:6781–6795. doi: 10.1175/JCLI-D-11-00514.1

Brönnimann S, Compo GP (2012) Ozone highs and associated flow features in the first half of the twentieth century in different data sets. Meteorol Zeitschrift 21:49–59. doi: doi:10.1127/0941-2948/2012/0284

Brönnimann S, Compo GP, Spadin R, et al. (2011) Early ship-based upper-air data and comparison with the Twentieth Century Reanalysis. Clim Past 7:265–276. doi: 10.5194/cp-7-265-2011

Compo GP, Whitaker JS, Sardeshmukh PD, et al. (2011) The Twentieth Century Reanalysis Project. Q J R Meteorol Soc 137:1–28. doi: 10.1002/qj.776

Coronato F (1993) Wind chill factor applied to Patagonian climatology. Int J Biometeorol 37:1–6. doi: 10.1007/BF01212759

Elbert J, Grosjean M, Gunten L Von, et al. (2012) Quantitative high-resolution winter (JJA) precipitation reconstruction from varved sediments of Lago Plomo 47°S, Patagonian Andes, AD 1530–2002. The Holocene 1–10. doi: 10.1177/0959683611425547

Elbert J, Jacques-Coper M, Van Daele M, et al. (2013a) A 1500 yr warm-season temperature record from varved Lago Plomo, Northern Patagonia (47° S) and implications for the Pacific Decadal Oscillation (PDO). Clim Past Discuss 9:1771–1801. doi: 10.5194/cpd-9-1771-2013

Elbert J, Wartenburger R, Gunten L Von, et al. (2013b) Late Holocene air temperature variability reconstructed from the sediments of. Palaeogeogr Palaeoclimatol Palaeoecol 369:482–492. doi: 10.1016/j.palaeo.2012.11.013

Falvey M, Garreaud RD (2009) Regional cooling in a warming world: Recent temperature trends in the southeast Pacific and along the west coast of subtropical South America

(1979–2006). J Geophys Res Atmos 114:D04102. doi: 10.1029/2008JD010519

Galeano E (1971) Las venas abiertas de América Latina, 1st ed. 379.

Garreaud R, Lopez P, Minvielle M, Rojas M (2012) Large-Scale Control on the Patagonian Climate. J Clim 26:215–230. doi: 10.1175/JCLI-D-12-00001.1

Hahn J (1897) Klima der aussertropischen Südamerika. In: Ratzel F (ed) Handb. der Klimatologie, Bibliothek. J. Engelhorn, Stuttgart, p 576

Jacques-Coper M, Brönnimann S (2014) Summer temperature in the eastern part of southern South America: its variability in the twentieth century and a teleconnection with Oceania. Clim Dyn 1–20. doi: 10.1007/s00382-013-2038-8

Jacques-Coper M, Garreaud RD (2014) Characterization of the 1970s climate shift in South America. Int J Climatol 1–16. doi: 10.1002/joc.4120

Jörg C, Storz S (2013) Das Meteor Forschungsschiff I - Ein Vergleich mit Daten des 20th Century Reanalysis Project. University of Bern

Knoch K (1930) Klimakunde von Südamerika. In: Köppen W, Geiger R (eds) Handb. der Klimatologie. Borntraeger, Braunschweig, p 349

Liu C, Wu L (2012) An intensification trend of South Pacific Mode Water subduction rates over the 20th century. J Geophys Res Ocean 117:C07009. doi: 10.1029/2011JC007755

Meehl GA, Stocker TF, Collins WD, et al. (2007) Global climate projections. In: Solomon S, Qin M, Manning M, et al. (eds) Clim. Chang. 2007 Phys. Sci. Basis. Contrib. Work. Gr. I to Fourth Assess. Rep. Intergov. Panel Clim. Chang. Cambridge Univ. Press, Cambridge, UK, pp 747–846

Neukom R, Gergis J, Karoly DJ, et al. (2014) Inter-hemispheric temperature variability over the past millennium. Nat Clim Chang 4:362–367.

Neukom R, Luterbacher J, Villalba R, et al. (2011) Multiproxy summer and winter surface air temperature field reconstructions for southern South America covering the past centuries. Clim Dyn 37:35–51. doi: 10.1007/s00382-010-0793-3

Neukom R, Luterbacher J, Villalba R, et al. (2010) Multi-centennial summer and winter precipitation variability in southern South America. Geophys Res Lett 37:L14708. doi: 10.1029/2010GL043680

Nouzeilles G (1999) Patagonia as borderland: Nature, culture, and the idea of the state.

J Lat Am Cult Stud 8:35–48. doi: 10.1080/13569329909361947

Paruelo JM, Beltran A, Jobbagy E, et al. (1998) The climate of Patagonia: general patterns and controls on biotic. Ecol Austral 8:85–101.

Pittock AB (1980a) Patterns of Climatic Variation in Argentina and Chile—I Precipitation, 1931–60. Mon Weather Rev 108:1347–1361. doi: 10.1175/1520-0493(1980)108<1347:POCVIA>2.0.CO;2

Pittock AB (1980b) Patterns of Climatic Variation in Argentina and Chile—II. Temperature, 1931–60. Mon Weather Rev 108:1362–1369. doi: 10.1175/1520-0493(1980)108<1362:POCVIA>2.0.CO;2

Prohaska F (1976) The climate of Argentina, Paraguay, and Uruguay, Vol. 12, W. 57–69.

Rayner NA, Parker DE, Horton EB, et al. (2003) Global analyses of sea surface temperature, sea ice, and night marine air temperature since the late nineteenth century. J Geophys Res Atmos 108:4407. doi: 10.1029/2002JD002670

Rosenblüth B, Fuenzalida HA, Aceituno P (1997) Recent Temperature Variations in Southern South America. Int J Climatol 17:67–85. doi: 10.1002/(SICI)1097-0088(199701)17:1<67::AID-JOC120>3.0.CO;2-G

Trenberth KE, Jones PD, Ambenje P, et al. (2007) Observations: Surface and atmospheric climate change. In: Solomon S, Qin M, Manning M, et al. (eds) Clim. Chang. 2007 Phys. Sci. Basis. Cambridge Univ. Press, Cambridge, UK, pp 253–336

Villalba R, Grosjean M, Kiefer T (2009) Long-term multi-proxy climate reconstructions and dynamics in South America (LOTRED-SA): State of the art and perspectives. Palaeogeogr Palaeoclimatol Palaeoecol 281:175–179. doi: http://dx.doi.org/10.1016/j.palaeo.2009.08.007

Wang G, Cai W (2013) Climate-change impact on the 20th-century relationship between the Southern Annular Mode and global mean temperature. Sci. Rep. 3:

Yin X, Gleason BE, Compo GP, et al. (2008) The International Surface Pressure Databank (ISPD) land component version 2.2. 12.

Zhang Q, Körnich H, Holmgren K (2012) How well do reanalyses represent the southern African precipitation? Clim Dyn 40:951–962. doi: 10.1007/s00382-012-1423-z

Chapter 2

Summer Temperature in the Eastern Part of Southern South America: Its Variability in the 20th Century and a Teleconnection with Oceania

Martín Jacques-Coper and Stefan Brönnimann
Oeschger Centre for Climate Change Research and Institute of Geography, University of Bern, Bern, Switzerland

Abstract

The 1907-2001 summer-to-summer surface air temperature variability in the eastern part of Southern South America (SSA, partly including Patagonia) is analysed. Based on records from instruments located next to the Atlantic Ocean (36°S-55°S), we define indices for the interannual and interdecadal timescales. The main interdecadal mode reflects the late-1970s cold-to-warm climate shift in the region and a warm-to-cold transition during early 1930s. Although it has been in phase with the Pacific Decadal Oscillation index since the 1960s, they diverged in the preceding decades. The main interannual variability index exhibits high spectral power at ~3.4 years and is representative of temperature variability in a broad area in the southern half of the continent. Eleven-years running correlation coefficients between this index and December-to-February (DJF) Niño3.4 show significant decadal fluctuations, out-of-phase with the running correlation with a DJF index of the Southern Annular Mode. The main interannual variability index is associated with a barotropic wavetrain-like pattern extending over the South Pacific from

Oceania to SSA. During warm (cold) summers in SSA, significant anticyclonic (cyclonic) anomalies tend to predominate over Eastern Australia, to the north of the Ross Sea, and to the east of SSA, whereas anomalous cyclonic (anticyclonic) circulation is observed over New Zealand and west of SSA. This teleconnection links warm (cold) SSA anomalies with dry (wet) summers in Eastern Australia. The covariability seems to be influenced by the characteristics of tropical forcing; indeed, a disruption has been observed since late 1970s, presumably due to the Pacific Decadal Oscillation warm phase.

2.1 Introduction

South America (SA), the largest land mass south of the equator, is a key region for the study of climate processes and dynamics in the Southern Hemisphere (SH) (Luterbacher et al. 2011). The continent comprises diverse climatological regions, in part due to its meridional extent and prominent orography (Garreaud et al. 2008). However, a relatively dense network of surface and upper-air instrumental observations over SA is characteristic only of the second half of the 20th century (Garreaud et al. 2008). Thus, much research on climate processes in SA has been confined to the second half of the 20th century. Similarly, the scarce availability of long-term highly-resolved proxies limits reliable climate reconstruction from interannual to interdecadal timescales (Neukom et al., 2011).

As a result, the assessment of interannual and interdecadal climate variability in Southern South America (SSA), which is our first research motivation, has been restricted due to data availability. Despite this fact, some papers have dealt with multidecadal climate changes in SSA. Neukom et al. (2011) and Neukom et al. (2010) reconstructed by means of local and remote predictors both surface air temperature (SAT) and precipitation for summer over the last centuries for this region, reaching AD 900 and AD 1498, respectively. Considering this multi-centennial period, they found a moistening trend into the 20th century, whereas summer temperatures were found to be comparable to earlier warm periods.

The internal heterogeneity of SSA is stressed by papers focusing on recent climate mechanisms and trends of this region. Based on instrumental records, Rosenblüth et al. (1997) found local warming rates between 1.3 and 2°C per century (but twice as large in the last three decades analysed) over SSA for 1933-1992 and also a cooling trend from the 1950s to the 1970s around 41°S, which was mostly influenced by minimum temperature changes. Besides, in particular during summer, local 1960-1992 trends

showed large regional differences within SSA.

Particularly, as described by Garreaud et al. (2012), the southern part of SSA, Patagonia (40°S-55°S), is a diverse region: the southern Andes are a natural limit between its narrow western part, which presents a temperate and hyperhumid climate and the broad arid plains of eastern Patagonia, with windy and evaporative conditions at the surface, and a thermal amplitude between summer and winter of more than 10°C. Moreover, during the last 40 years, a drying trend west of the Andes and a subtle precipitation increase in the southern tip of the continent have been observed.

Eastern SSA exhibited a very pronounced and abrupt DJF SAT increase in late 1970s, embedded in a continent-wide climate shift (Jacques 2009; Jacques-Coper and Garreaud 2014). This large-scale event, whose origin is still not well understood, was firstly referred to as a North Pacific shift (Trenberth 1990) and its manifestations in the Northern Hemisphere have been well described.

In the context of global warming, Eastern SSA (and in general, the southern half of SA) is also a very particular region: after the abrupt DJF SAT increase in the late 1970s, it showed almost neutral and even negative SAT trends during the last decades of the 20th century, a feature that is even more pronounced during summer (Falvey and Garreaud 2009; Trenberth et al. 2007). Moreover, at a global scale, IPCC multi-model mean projections of SAT for the 21st century (Meehl et al. 2007) show a nonuniform spatial pattern, with SSA being one of the regions with minimum warming over land considering various scenarios and time periods.

All previous results motivate a specific research in Eastern Patagonia with a focus on summer and the exploration of possible relationships of this region with other areas of SA and the Southern Hemisphere. For this, we aim to extend the analysis to the whole of the 20th century and consider the interannual and interdecadal timescales separately. In particular, previous research on multidecadal regimes and regime changes leaves some questions unanswered. Is it possible to detect a previous rapid summertime climate shift in SSA in the 20th century, before the late 1970s? Are there any other evidences in instrumental records from SSA that could allow us to speak of a *shifty climate* (Kerr, 1992) there?

Our second research motivation deals with the stability of the effects of various climate modes at different timescales: mainly ENSO, the Southern Annular Mode (SAM, also known as the Antarctic Oscillation, AAO), and the Pacific Decadal Oscillation (PDO). Although their spatial patterns have been thoroughly examined and well established (Garreaud et al. 2008), the relatively short length of available local climate time series

hinders the in-depth exploration of possible instabilities of their effects and thus limits our understanding of natural and anthropogenic processes that may be crucial in the context of climate change. While ENSO does not have a strong impact on SAT there (Aceituno 1988), SAM seems to have a clear imprint in this part of the continent (Garreaud et al. 2012). Positive values of the SAM/AAO index have been related to warm and dry conditions over SSA due to a combination of horizontal thermal advection, subsidence (downward flux and positive SLP anomalies) and more incident solar radiation (Gillett et al. 2006; Sen Gupta and England 2006). In addition, the SAM index shows a positive trend from the late 1970s on, most evident during DJF (Marshall 2003; Thompson and Solomon 2002), which further impels a restricted analysis of this season. The stability in time of ENSO and SAM over SSA and the interaction between these two interannual modes at regional and global scales have been the subject of previous publications, although restricted to the second half of the 20th century and particular seasons (Fogt et al. 2011; Silvestri and Vera 2009; Silvestri and Vera 2003). Therefore, it is promising to explore the possible impact of both modes in SSA during austral summer in a long-term context.

The third motivation for this study are remote mechanisms related to the climate of Eastern SSA. Teleconnections identified as Rossby waves propagating eastward over the South Pacific towards SA have raised much attention, and have been documented in connection with various phenomena occurring at different timescales and seasons. Berbery and Nogués-Paegle (1993) analysed the intraseasonal interaction mechanics between tropical heating and circulation in the SH for summer and winter during 1980-1987 and found the strongest relationships, including the excitation of Rossby waves, in summer. Mo and Paegle (2001) found that tropical convection, dominated by the Madden-Julian Oscillation (MJO), modulates the intraseasonal Pacific-South American modes 1 and 2 (PSA1 and PSA2) for both summer and winter during 1949-2000, in both the interannual and intraseasonal bands. These modes are connected to rainfall anomalies over northeastern Brazil, the South Atlantic Convergence Zone (SACZ), and the subtropical plains. Díaz and Aceituno (2003) investigated large-scale circulation anomalies linked to submonthly convective cloudiness over Uruguay during austral spring and summer between 1979 and 1993 and found a wavelike quasi-barotropic structure showing alternating centres of negative and positive geopotential height and temperature anomalies in the southern portion of the continent and farther upstream in the southern Pacific. Berman et al. (2012) found a connection during austral summer between the SESA-SACZ dipole and precipitation variability over the southernmost part of SSA during 1979-2009 through a pattern which they associated with PSA2. Focusing on temperature modulation, analysing data from the period 1979-2003, Cerne and Vera (2011) showed that the circulation anomaly which leads to heat waves over subtropical

SA in the intraseasonal timescale, in association with an active SACZ, is embedded in a large-scale Rossby wave train that is linked to convection anomalies over the equatorial western and central Pacific Ocean. Nevertheless, no analysis of long-term records has been conducted in Eastern SSA in order to explore to what extent teleconnection patterns similar to PSA are related to the summer-to-summer local SAT variability, which is our concrete question.

In short, since to the authors' knowledge no long instrumental records have been used for these purposes, the research in this paper focuses on the main interdecadal and interannual summertime SAT variability patterns over SSA during the 20th century, the impacts of large-scale climate modes, and an associated teleconnection. The paper is organised as follows: Section 2.2 describes the datasets and methodology used to calculate summertime SAT indices for SSA at interannual and interdecadal timescales. The characteristics of these modes are described in Section 2.3, where we investigate interdecadal regime changes, compare our results with the PDO and Interdecadal Pacific Oscillation (IPO, Power et al. 1999), and include a brief discussion on the temporal stability of the incidence of ENSO and SAM over SSA in the interannual band. Section 2.4 presents local and remote relationships of the interannual SAT index with other climatic variables; in particular, a teleconnection between Oceania and SSA is described. Finally, Section 2.5 presents complementary discussions and summarizes our findings and the main conclusions.

2.2. Data and methodology

Instrumental SAT and sea level pressure (SLP) records were accessed from the Global Historical Climatology Network version 2 (GHCN; Table 2.1) (Peterson and Vose 1997). We also use precipitation observations from the Australian Bureau of Meteorology (Table 2.2) and SLP data from the New Zealand National Climate Database (Table 2.3). In addition, SAT and precipitation gridded datasets were obtained from the University of Delaware (UDel, version 2.01, 1901-2008) (Legates and Willmott 1990a; Legates and Willmott 1990b) and sea surface temperature (SST) data from ERSSTv3 (Smith and Reynolds 2004). We complement our research with different atmospheric variables from reanalysis products: ECMWF-ERA40 (1958-2002) (Uppala et al. 2005) and the Twentieth Century Reanalysis version 2 (20CRv2, 1871-2008) (Compo et al. 2011), and also with following indices: Niño3.4 index, JISAO PDO index, and the Zhang DJF AAO index (Zhang et al. 2010). This reconstruction used for its calibration period (1957-1989) proxies that were well correlated with the observation-based Marshall AAO index

(Marshall 2003). (See Acknowledgments section for details).

The datasets we use have been generated based on exhaustive research aimed at including various observational systems covering the longest time period possible. For that, sophisticated methods have been applied. In the case of 20CRv2, many studies have demonstrated that reliable reanalysis of earlier periods can be generated using only surface observations and advanced data assimilation methods (Compo et al., 2011). Although the quality of 20CRv2 in the Southern Hemisphere is still an open question, previous studies have positively assessed this product there. During 1958-1978, 300 hPa geopotential height observations from radiosondes present higher correlations in the Southern Hemisphere Extratropics with 20CRv2 than with ERA40 (Compo et al., 2011). For earlier periods, Brönnimann et al. (2011) found good agreement between this reanalysis and temperature observations on a cruise from Europe around South Africa and across the Indian Ocean to the western Pacific in 1906/1907, and close agreement between this reanalysis and geopotential height and temperature measurements from a cruise that traveled from Europe to Antarctica across the Atlantic and back in 1938/39. Brönnimann and Compo (2012) found good correlations between historical ozone data and 20CRv2 over Australia and New Zealand in the 1930s. Zhang et al. (2012) found that 20CRv2 is the best suited reanalysis for investigating the climate variability over

a.
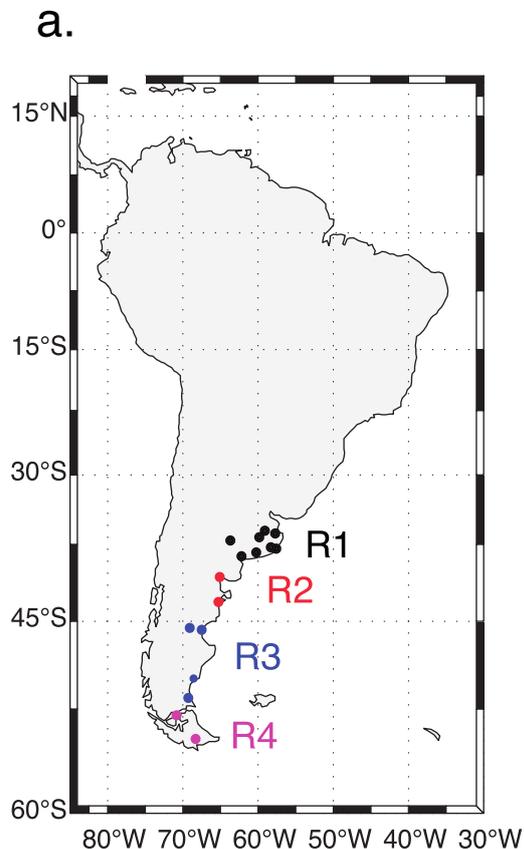
Fig. 2.1: *a) Stations used to form the 4 meridional composites of DJF surface air temperature in Eastern SSA (R1, R2, R3 and R4; see Table 2.1). b) Time series of the composites, detrended and standardized with respect to 1950-1979; magenta lines show the mean values between temperature shifts identified by the ad-hoc Rodionov test.*

southern Africa, also highlighting its value to investigate interannual to decadal variability. Furthermore, 20CRv2 has been used by studies focusing in the Southern Hemisphere during the whole 20th century (e.g. Wang and Cai 2013).

Nevertheless, note that station coverage is scarce in the SH compared to Northern Hemisphere standards, especially during early periods (late 19th and early 20th centuries) and in the southern Pacific region. Thus, conclusions arising from these early times should be taken cautiously. However, in this study we describe results based on partially independent datasets in order to reduce the uncertainty associated with single products. Furthermore, by analysing various variables at different levels, in the following we describe relationships that are consistent among them.

Our methodology consists of following steps: firstly, we formed 4 composites of austral summer (DJF) SAT time series which correspond to latitude belt averages. They group well-intercorrelated records from a total of 19 stations located next to the Atlantic coast of SSA between 36° and 55°S (regions 1-4 [R1-R4], see Fig. 2.1a and Table 2.1). Summer values were calculated at every station as the average value of DJF (and assigned to the corresponding JF year) from at least two values from these three months. Missing data for the years 1902 and 1991 from individual instrumental records were filled by means of a least-square regression on previously interpolated UDel gridded

b.
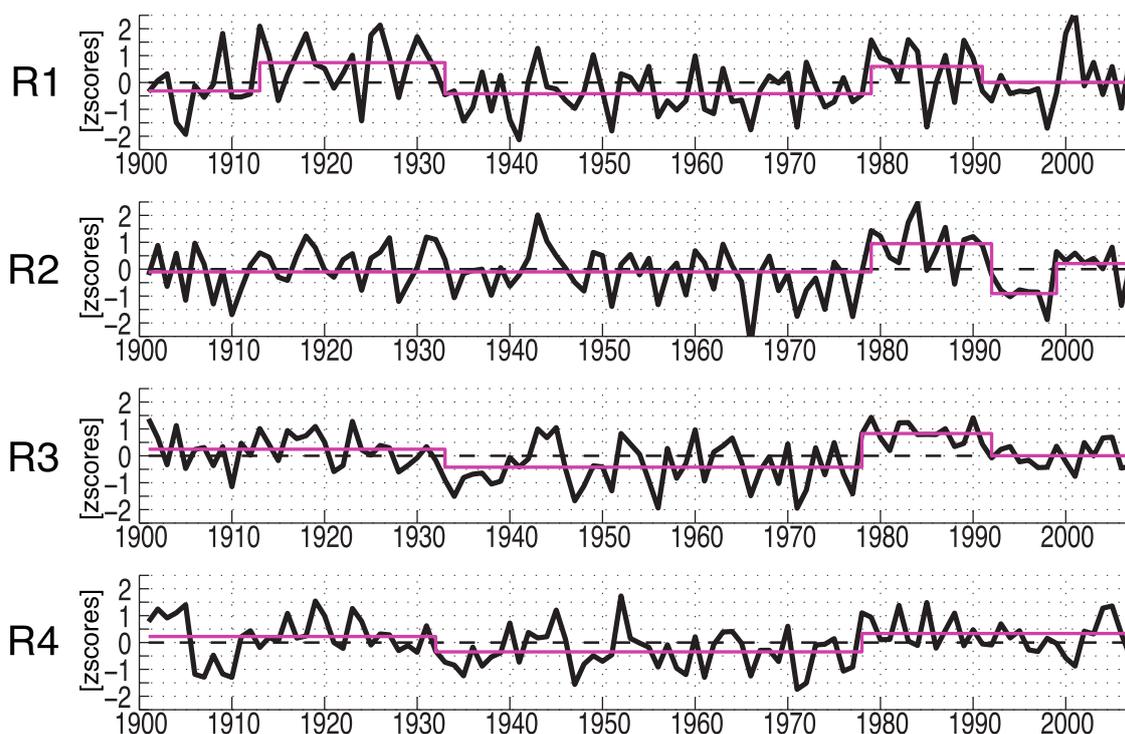
Table 2.1*: GHCN stations used to form the
4 surface air temperature composites in Eastern SSA*

| composite	GHCN station	latitude [°N]	longitude [°E]	elevation [m a.s.l.]	data length
R1	Las Flores Aero	-36.07	-59.10	38	1931-1960
	Dolores Aero	-36.35	-57.73	9	1931-2007
	Azul Aero	-36.75	-59.83	132	1931-1994
	Macachín	-37.10	-63.70	142	1931-1960
	Balcarce	-37.80	-58.30	130	1931-1960
	Mar del Plata	-37.93	-57.58	21	1931-2007
	Tres Arroyos	-38.33	-60.25	115	1931-2007
	Bahía Blanca Aero	-38.70	-62.20	72	1896-1960
R2	San Antonio	-40.78	-65.10	20	1931-2007
	Trelew Aero	-43.20	-65.27	43	1901-2007
R3	Sarmiento	-45.60	-69.10	268	1904-1963
	Comodoro Rivadavia	-45.78	-67.5	46	1931-2007
	Santa Cruz Aero	-50.02	-68.57	111	1901-1992
	Río Gallegos	-51.62	-69.28	19	1931-2007
R4	Punta Arenas	-53	-70.85	37	1888-2007
	Ushuaia Aero	-54.8	-68.32	14	1931-2007

Fig. 2.2: a) Surface air temperature time series of the composite of Region 3 (R3, see Table 2.1 and Fig. 2.1), detrended and standardized with respect to 1950-1979; b) residual interannual time series of Region 3, resulting from subtracting the corresponding R3 interdecadal component (panel d, thin black curve) from the series in a); c) standardized interannual T_PC1_ia of SSA, and d) standardized interdecadal T_PC1_id (thick black curve, scaled by 0.5), interdecadal time series of Region 3 (thin black curve), and 2x7-yr running mean of DJF PDO (thick blue curve) and of DJF IPO (thick cyan curve). Red (blue) markers denote years above (below) 1 (panel c, thin black curve) standard deviation of T_PC1_ia, depicted in panel c.

data. Individual series were normalized with respect to 1950-1979 and then averaged to form the 4 composites, covering the 1901-2007 period. Then, we substracted the long-term mean of each composite and applied a variance correction procedure (Jones et al. 1997) on the anomalies in order to reduce possible biases caused by the time-varying number of stations. We detrended the regional composites by subtracting the straight-line fit (least squares) from the data and thus removed the very low frequency variability. The resulting time series are shown in Fig. 2.1b. Finally, following Montecinos et al. (2003), we separated the interannual and the interdecadal variability bands by applying a 7-years running-mean twice on the detrended composite time series, which reduced the time series length to 1907-2001. Hence, we computed 4 interdecadal time series (the low-pass filtered component of the original values) and 4 interannual time series (the residuals of the detrended series minus their interdecadal components). Since in this work we deal with austral summer data (DJF), in the following the high-pass (low-pass) filtered component of the summer-to-summer time series will be denominated *interannual* (*interdecadal*) time series. We then performed a Principal Component Analysis (PCA) on the 4 time series of each time band. The corresponding leading principal components, named *T_PC1_ia* and *T_PC1_id*, respectively, are representative of all 4 original regions and will be used as SAT indices of Eastern SSA.

Figure 2.2 illustrates the application of the above-described methodology on the composite of Region 3. Although its original time series (Fig. 2.2a) is characterised by strong year-to-year variability, its interannual component (Fig. 2.2b) by definition does not exhibit interdecadal fluctuations and its autocorrelation is negligible. The correlation value between this series and *T_PC1_ia* index (Fig. 2.2c) reaches 0.9** for 1907-2001 (see Table 2.4 for all composites).

Throughout the paper, we calculate correlation fields between *T_PC1_ia* (*T_PC1_id*) and interannual (interdecadal) time series of various variables, which have also been computed by detrending their time series and applying a 7-years running mean twice to them to separate their interannual and the interdecadal variability components. In this paper, the use of one (two) asterisk(s) denotes statistical significance at 95% (99%) of the correlation between detrended series, considering the effective number of degrees of freedom of the data (Bretherton et al. 1999).

For the analysis of coming sections, we identify anomalously warm and cold summers, based *solely* on the interannual frequency range by defining a threshold of 1 standard deviation of the *T_PC1_ia* index (Fig. 2.2c). In total, this criterion results in 14 cold and 14 warm events, which roughly correspond to the 15% and 85% percentiles of our total sample of 95 years.

2.3. Summertime temperature variability over SSA

2.3.1 Description of SAT indices of Eastern SSA

The leading mode of interdecadal SAT variability over SSA, named *T_PC1_id* (Fig. 2.2d, thick black curve) explains around 80% of the original variance of the 4 interdecadal composites and suggests a frequency peak at around 64 years, which, however, cannot be statistically assessed due to limited data length. We correlate *T_PC1_id* with the interdecadal components of UDel SAT and ERSSTv3 for 1907-2001 (Fig. 2.3c). Over SA, the spatial correlation pattern shows positive coefficients over the southernmost part of the continent and negatively correlated values over the Gran Chaco region, eastern Brazil and the northernmost part of SA. A hemispheric-like dipole pattern is suggested in the SST correlation field, due to the prevailing positively (negatively) correlated regions in the Southern (Northern) Hemisphere. This meridionally asymmetric pattern shows particularly prominent positive correlation coefficients over the Eastern Tropical Pacific and the South Pacific, around 45°S; 150°W. Although the time series of *T_PC1_id* resembles the DJF PDO and IPO indices from 1960 on (both showing the 1970s phase change), this is not the case during the first half of the 20th century (Fig. 2.2d). The amount of interdecadal SAT variance over SSA explained by *T_PC1_id*, as measured by the coefficient of determination (r^2), exhibits a positive North-South gradient during the period 1907-2001 (Table 2.4). However, while during 1907-1979 the lowest r^2 coefficient is found for R2, the opposite happens during 1980-2001. This result possibly reveals the impact of the late-1970s climate shift.

At interannual level, *T_PC1_ia* explains ~60% of the total variance of the 4 interannual composites and exhibits a main significant spectral peak at ~3.4 years. As shown by Fig. 2.3a, the correlation pattern of this index with the interannual component of the UDel SAT data exhibits a broader area of positive coefficients in SSA in comparison with the interdecadal spatial pattern of Fig. 2.3c. The positively correlated region corresponds roughly to the southern half of the continent, including both sides of the Andes. A dipole-like anomaly is observed between this region and eastern Brazil, a region with negative correlation coefficients. This SAT structure seems to correspond to the easternmost part of a large-scale pattern of alternating negative and positive SST anomalies extending over the South Pacific.

During 1907-2001, *T_PC1_ia* reaches high correlation values especially with R2 and R3. This index represents 71% and 81% of the original interannual variance of these composites, respectively, whereas lower coefficients are found for R1 (48%) and R4 (35%). We notice that this result is similar during 1907-1979, but changes afterwards.

During 1980-2001, while this index mostly reflects the interannual variability of the northern part of Eastern SSA (R1: 54% and R2: 73%), it becomes less representative for R3 (39%) and is even anticorrelated with R4 (r:-0.30; r^2: 9%). Therefore, as for the interdecadal variability, we notice a regime difference around late-1970s. Agosta and Compagnucci (2008), describing circulation changes over SSA after the 1976/77 summer, found an expansion of the subtropical South Atlantic anticyclone over SA and lower midlatitude cyclone activity. Jacques (2009) and Jacques-Coper and Garreaud (2014) identified the establishment of an anticyclonic anomaly over the southern tip of SA and showed a southward shift of the westerlies during DJF after the 1970s climate shift, which resulted in weakened (enhanced) cold zonal advection over SSA between 40° and 45°S (around 53°S). The R4 composite is located where enhanced cool advection is found after late 1970s for DJF. There, temperature is anticorrelated with low-level zonal wind during this season (Garreaud et al. 2012). Hence, R4 is consequently strongly affected by the position and intensity of the westerlies. These atmospheric circulation changes seem to be at least partly responsible for the decoupling observed between R4 and the rest of the composites after late 1970s.

In order to get a deeper understanding of the spatial modes related to *T_PC1_ia* and *T_PC1_id*, we also performed a PCA analysis on all interannual and interdecadal UDel DJF SAT time series from SA, previously weighted by the cosine of their latitude. By doing so, resulting UDel interannual and interdecadal first (second) principal components, termed PC1s (PC2s) represent a fraction of 34.6% and 33.7% (19.6% and 12.6%) of the total continental SAT variance, respectively. The correlation coefficients between UDel interannual and interdecadal PC1s (PC2s) and the instrumental *T_PC1_ia* and *T_PC1_id* indices reach 0.62** and 0.22 (0.57** and -0.95) for the 1907-2001 period, respectively. At both timescales, the spatial correlation patterns of UDel PC2s with

Fig. 2.3: *a) Correlation fields of T_PC1_ia with various interannual variables for the period 1907-2001. For surface air temperature over SA and SST, warm/cold colours denote positive/negative values every 0.1 (see color scale), black contours denote absolute values greater than 0.3. Continuous red/dashed blue (continuous black/dashed black) contours correspond to positive/ negative anomalies of geopotential height at 500 hPa, Z500 (SLP). For these two variables, contours are drawn every 0.1 for absolute values greater than 0.3; zero contour omitted. Wind vectors at 850 and 200 hPa (red and black, respectively) are drawn at gridpoints showing a correlation coefficient greater than 0.3 for either their zonal or meridional components. In this case, statistical significance at 99% is reached at ~0.26 for all variables (considering autocorrelation, following Bretherton et al. (1999)). In this figure, areas of statistically significant Z500 anomalies at 99% (1907-2000) were also assessed following the random-phase method of Ebisuzaki (1997) and are denoted by asterisks. b) Correlation fields of T_PC1_ia with the interannual relative cyclone frequency (RCF, with respect to 1872-2008); zero contour omitted. RCF values are only shown where correlation coefficients are significant at 99% in at least 75% of the 56 20CRv2 ensemble members. c) Correlation fields of T_PC1_id with interannual surface air temperature and SST. Due to the strong autocorrelation of the time series, no statistical significance is reached at 99%. The color scale applies to all three plots.*
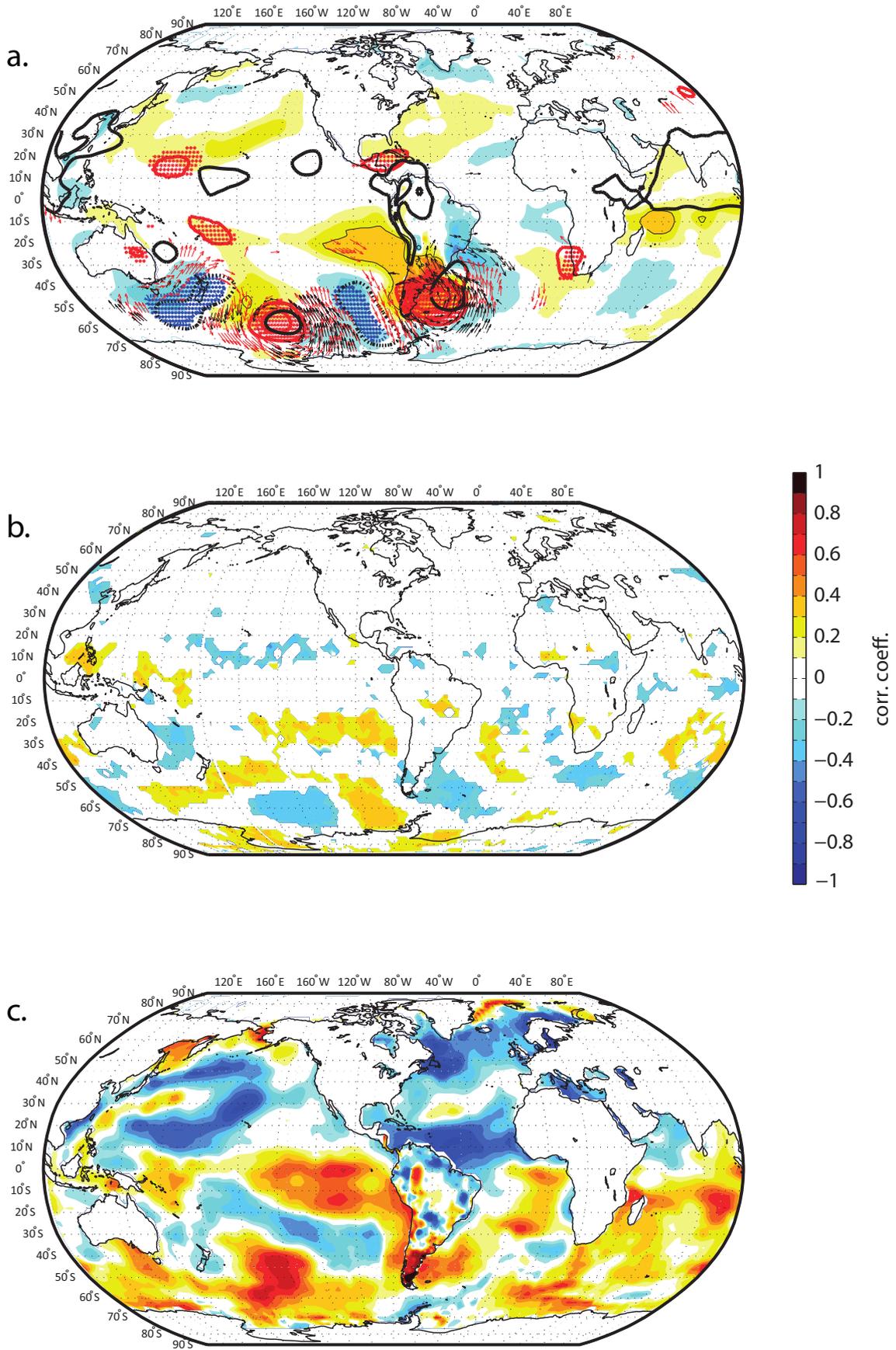
UDel SAT data over SA (not shown) greatly resemble those obtained from instrumental PC1s. Specifically, while UDel interannual PC1 represents mainly the SAT variability over central and northeastern Argentina and Uruguay, UDel interannual PC2 exhibits its highest scores over the southern tip of the continent, south of 40°S, at both sides of the Andes. Hence, *T_PC1_ia* combines and synthesizes the modes of variability of these two regions. These findings confirm that SSA, which extends from the subtropics into the extratropics, exhibits in fact leading patterns of DJF SAT variability within the continent.

2.3.2 On the stability of the correlations between interannual SAT, Niño3.4 and SAM/AAO

Although the impact of ENSO in SSA is subtle, as indicated by previous studies (Aceituno 1988; Garreaud et al. 2009), we advert that the correlation coefficient between DJF Niño3.4 and *T_PC1_ia* shows changes in time, in particular before and after the 1970s climate shift, reaching $r=0.10$ during 1907-1979 and $r=-0.23$ during 1980-2001. The 11-years running correlation values between these indices show significant decadal fluctuations at 90% after the method proposed by Gershunov et al. (2001) (Fig. 2.4a). Positively correlated periods in the 1930s, 1950s, 1970s and 1980s are separated by
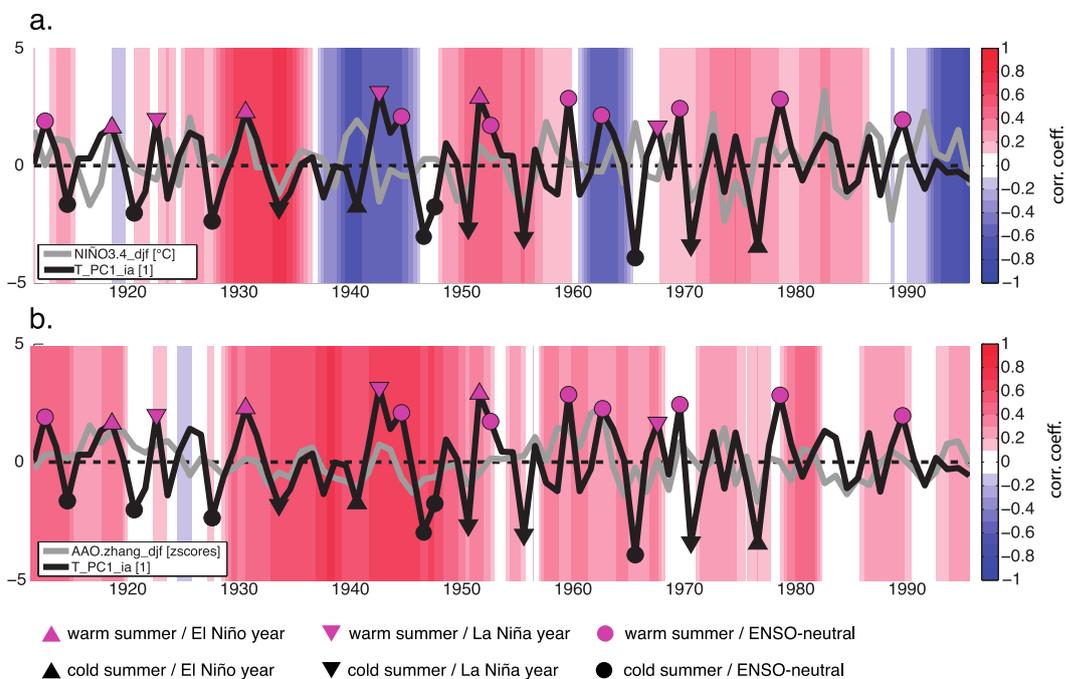

Fig. 2.4: *Time series of T_PC1_ia (black) and a) DJF Niño3.4 index (grey) and b) DJF Zhang AAO index (grey). Background colors indicate the 11-years running correlation between corresponding series, centred in the 5th year.*

anticorrelated periods in the 1940s, 1960s and 1990s. Hence, we conclude that there is no *stable* relationship between El Niño or La Niña events and SAT anomalies over SSA.

During 1907-2001, the correlation coefficient between the Zhang DJF AAO index and *T_PC1_ia* shows modest but significant coefficients (r=0.24**). However, when splitting this period, we find that the correlation values vary in time from r=0.29** in 1907-1979 to r=0.09 in 1980-2001. Hence, this suggests that the SAM-related variability is not modulating SAT in this region during 1980-2001. Furthermore, 11-years running correlation coefficients between these indices, although mostly positive during the 20th century (Fig. 2.4b), show a weak decadal fluctuation, with the highest positive coefficients reached in the 1930s and 1940s (r=0.59** for 1931-1950). Interestingly, relatively high running correlation values between *T_PC1_ia* and SAM are found for the anticorrelated periods calculated between *T_PC1_ia* and the DJF Niño3.4 index, namely early 1940s and 1960s. A possible explanation of the impact of these particular periods on the link between Oceania and South America is proposed in sections 4.4 and 5.

2.3.3 A shifty climate over SSA during the 20th century?

The shift observed in late 1970s in the 4 SAT composites of Fig. 2.1b marks the beginning of a new temperature regime. To objectively identify other possible abrupt changes in these time series, we apply an ad-hoc sequential Student's t-test (Rodionov 2005), considering a regime persistence of at least 10 years and a significance level of 90% (parameter values of L=10, p=0.1 and h=1, as specified therein). Besides the temperature shift in the late 1970s detected in all composites (Fig. 2.1b; R1: 1979, R2: 1979, R3: 1978 and R4: 1978), we identify a preceding warm-to-cold transition in all but one of them (R1: 1933, R3: 1933 and R4: 1932). Therefore, a warm-to-cold interdecadal transition took place in SSA around the beginning of the 1930s and not simultaneously with the positive-to-negative phase change of the PDO/IPO in the late 1940s (Fig. 2.2d). We also identify a more recent warm-to-cold transition in the early 1990s in three of the composites (R1: 1991, R2: 1992, R3: 1992). Thus, we can describe the interdecadal summertime temperature variability of SSA during the 20th century, beyond the temperature trend, as consisting of regimes separated by more or less sharp transitions, which are roughly depicted by *T_PC1_id*. The magnitude of the late-1970s transition is, however, the greatest of the century, and its abrupt nature is clearly observed.

2.4. Processes associated with interannual cold and warm summer anomalies

2.4.1 Relationships of the interannual SAT index with other variables over SSA

To further explore the physical implications of the *T_PC1_ia* signal, we correlate this index with 57 GHCN *summer-to-summer* non-filtered SLP records over the continent (Fig. 2.5a). Significant positive correlation coefficients are found in SSA to the East of the Andes, especially to the south of 20°S. This result shows that warm (cold) summers in Eastern SSA are linked to positive (negative) seasonal SLP anomalies there. Moreover, significant positive SLP anomalies are also found beyond that area, around 15°S, between 50°W and 70°W.

Furthermore, we also analyse the correlation field between *T_PC1_ia* and *summer-to-summer* interannual DJF precipitation from gridded UDel data (Fig. 2.5b). The most salient features are the anticorrelated regions of Southeastern SA (SESA, covering the La Plata Basin) and Patagonia. Nevertheless, also positive but weaker correlation values are found over the SACZ and Central-Western Argentina (CWA). Such a DJF dipole-like rainfall variability pattern between Central-Eastern SA and SESA was described for the intraseasonal scale by Liebmann et al. (2004) and is linked to the weakening (strengthening) of the South American low-level jet (LLJ) near 20°S, which leads to decreased (increased) precipitation over SESA and to the contrary over SACZ. It corresponds to the South American monsoon (Liebmann and Mechoso 2011), which is the leading mode of summer precipitation over the continent, not strongly connected with ENSO (Grimm and Zilli 2009).

SESA is well known as the depository of moist and warm air from the Atlantic Ocean and the Amazon Basin, partly advected by the LLJ. This intraseasonal phenomenon, which peaks in summer, originates in the tropical Easterlies from the Atlantic Ocean that are deflected southward by the Andes. Since the highest anticorrelation values of precipitation with *T_PC1_ia* are found there, we calculate a SESA precipitation index, named *sesa_P_PC1_ia*, by taking the standardized PC1 of all gridpoints that show a negative correlation value of -0.4 or stronger for the period 1907-2001 there (these gridpoints are denoted by black dots in Fig. 2.5b; a very similar index is obtained if those time series are averaged together). By definition, the correlation value between this index and *T_PC1_ia* reaches a high coefficient: -0.57** for 1907-2001. However, for the period 1907-1979 (after the 1970s climate shift), the corresponding coefficient is -0.66**. This result shows the robust physical coherence of the *T_PC1_ia* signal in the precipitation

field, highlights the imprint of higher frequency phenomena in the interannual timescale, and suggests a regime change since late-1970s.

2.4.2 Global correlation fields associated with the interannual SAT index

We analyse now the global correlation fields between the interannual *T_PC1_ia* signal and SLP, geopotential height at 500 hPa and wind fields (*u* and *v*) at 850 hPa and 200 hPa from 20CRv2 for the 1907-2001 period, depicted in Fig. 2.3a. The correlation fields shown in this figure resemble those obtained for the shorter period 1950-1979 (not shown), which adds confidence to our results. The most striking feature we observe is a wave train pattern of barotropic structure that extends from Australia to SA along the South Pacific. To the East of the Andes Cordillera, it shows a baroclinic structure. Thus, SAT anomalies over SSA associated with *T_PC1_ia* are linked to the alternation of large-scale circulation action centres. In particular, warm (cold) summers over SSA correspond to positive (negative) geopotential height and SLP anomalies, with mean positions over
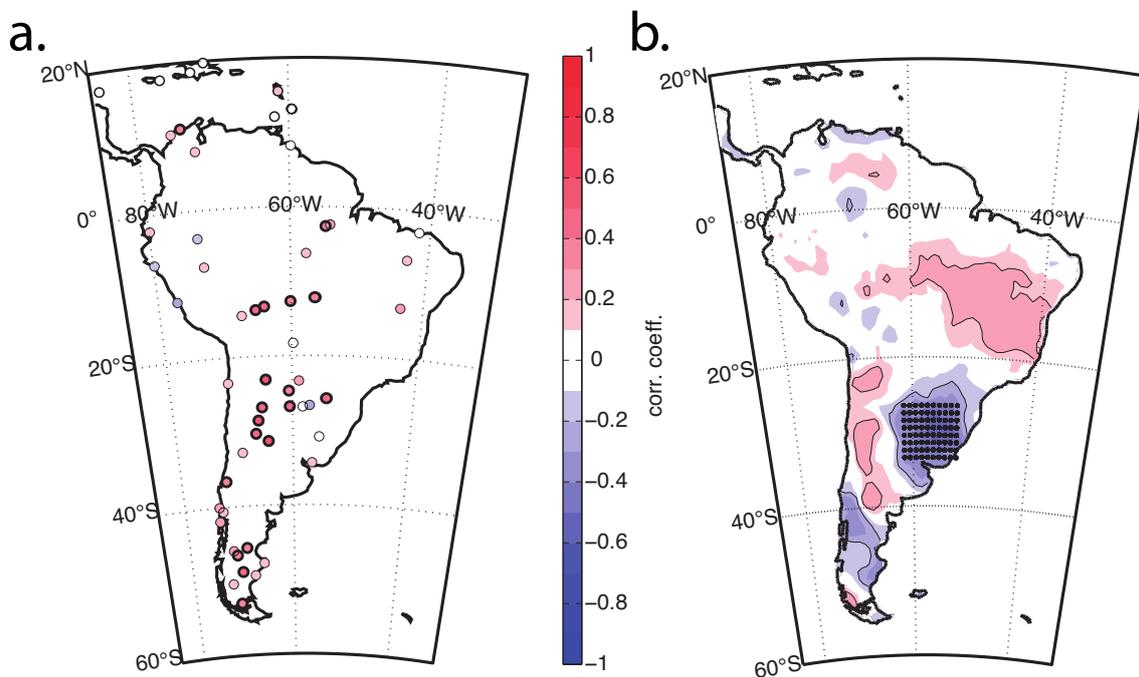

Fig. 2.5: *a) Correlation values between T_PC1_ia and non-filtered GHCN SLP records (see color scale); statistically significant coefficients (95%) are denoted by thick marker edges. b) Correlation field of T_PC1_ia with interannual UDel precipitation (see color scale; zero contour omitted). Black contours denote absolute values greater than 0.2, statistically significant at 95%. Selected gridpoints in SESA are depicted by black dots; their leading principal component defines the interannual sesa_P_PC1_ia index.*

eastern Australia [24°S; 144°E], to the north of the Ross Sea [56°S; 152°W], and to the east of SSA [46°S; 58°W], and negative (positive) anomalies to the west of New Zealand [42°S; 172°E] and over the South Pacific, west of SSA [46°S; 106°W]. Indeed, SAT and SST departures throughout this wave-train structure reveal the temperature advected by these circulation anomalies. The statistical significance of the spatial correlation patterns of *T_PC1_ia* was assessed at 99% taking into account the serial correlation of the time series (Bretherton et al. 1999). In addition, for geopotential height at 500 hPa during 1907-2000, we also applied the random-phase method proposed by Ebisuzaki (1997) and determined a statistically significant relationship at 99% between *T_PC1_ia* and the centres of action of the wave train pattern.

We compare these results with those obtained from ERA40 for SLP and geopotential height at 500 hPa. For that, we split the 20CRv2 fields into two periods, 1907-1963 and 1964-1996. Robust signals are found in 20CRv2 for both epochs and also in ERA40 during the overlapping second period, for which both datasets qualitatively agree (not shown). Although both datasets are still comparable when choosing a shorter second period (1970-1996), the imprint of the positive trends of SAM and PDO trends is stronger in this case and tends to weaken the wave train pattern in SLP and geopotential height at 500 hPa.

Furthermore, we also identify the wave train pattern in the correlation field between *T_PC1_ia* and the relative cyclone frequency (RCF), a dataset calculated with respect to the period 1872-2008 (Fig. 2.3b), which was generated using a cyclone identification algorithm on the 6-hourly SLP fields of the 56 members of the 20CRv2 ensemble (Welker and Martius 2012). In this case, correlation coefficients are only shown where they are significant at 99% in at least 75% of the 20CRv2 ensemble members. The spatial correlation pattern observed between *T_PC1_ia* and RCF is coherent with the signal observed in the 500 hPa geopotential height field. Our interpretation is that blocking (cyclonic anomalies) induced by the presence of ridges (troughs) throughout the troposphere to the North of the Ross Sea and East of SSA (over New Zealand and west of SSA), associated with the wave train pattern, is linked to the meandering shape of the polar front and the polar upper level jet in Fig. 2.3a, contrasting with their more zonal climatological shape, shown for the latter e.g. by Gallego et al. (2005). The correspondence between correlation fields obtained between *T_PC1_ia* and geopotential height at 500hPa and between *T_PC1_ia* and the relative cyclone frequency (RCF) reveals that, beyond the agreement between seasonal means, the synoptic activity depicted by the cyclone frequency is linked to the DJF SAT variability over Eastern SSA. This aspect seems to point to persistent circulation anomalies. Although derived from the same reanalysis product, this result further emphasizes the connection between synoptic and interannual anomaly patterns.

The linear components of the spatial correlation patterns of *T_PC1_ia* with some variables are analysed by means of the warm-minus-cold composite difference fields. For its calculation, we considered extreme events of this index, as described in Section 2.2 (depicted in Fig. 2.2c). In Fig. 2.6a-b, we can observe that the upper- and low-level wind anomalies in the Southern Hemisphere, between Australia and SA, resemble the wave train pattern as expected from geostrophic balance. The strong upper-level easterly (negative) anomaly over SSA around 40°S results from the anticyclonic anomaly over the southern tip of the continent and the Southwestern Atlantic. There, it implies the southward shift of the upper-level Polar Front Jet, due to a reduced meridional gradient of geopotential heigth at that latitude and to a stronger gradient to the South (Fig. 2.6c). We observe an enhancement of the prevailing low-level westerlies over the Drake Passage. A positive anomaly of low-level meridional wind is observed over eastern Brazil and subtropical SA. This pattern, together with the dipole of zonal wind anomalies identified over those regions, imply an opposite wind pattern as the one related to the low-level jet (LLJ), which is characterised by a southward flow east of the Andes, which deflects more to the Southeast at the exit region of the jet into La Plata Basin (Marengo et al. 2004). Thus, these circulation anomalies result in a weakened LLJ. The SLP and geopotential height fields (Fig. 2.6c) clearly exhibit the wave train pattern over the South Pacific and also reveal the existence of a similar structure over the North Pacific, which does not appear in the correlation fields of Fig. 2.3a. Nevertheless, while in the Northern Hemisphere the pattern seems to be weaker over the North American continent, in the Southern Hemisphere it develops until reaching South America. All these circulation anomalies are linked to a mean *interannual* difference of up to 1.5°C between warm and cold DJF composites over SSA and -0.6°C over eastern Brazil, at the location of the SACZ (Fig. 2.6d). This feature constitutes a characteristic meridional dipole pattern, observed also in the correlation fields of Fig. 2.3a and linked to the interannual rainfall variability during DJF, as already discussed.

The non-linear components of the fields (figures not shown) reveal that cold extreme events in SSA during summer are associated with stronger circulation anomalies related to the wave train pattern than their warm counterparts, and that these groups of extreme events are not exactly linearly associated with SST perturbations along the Equatorial Pacific.

a. zonal wind

[m/s]

b. meridional wind

[m/s]

c. SLP and gph at 500 hPa

[m]

d. SAT and SST

[°C]
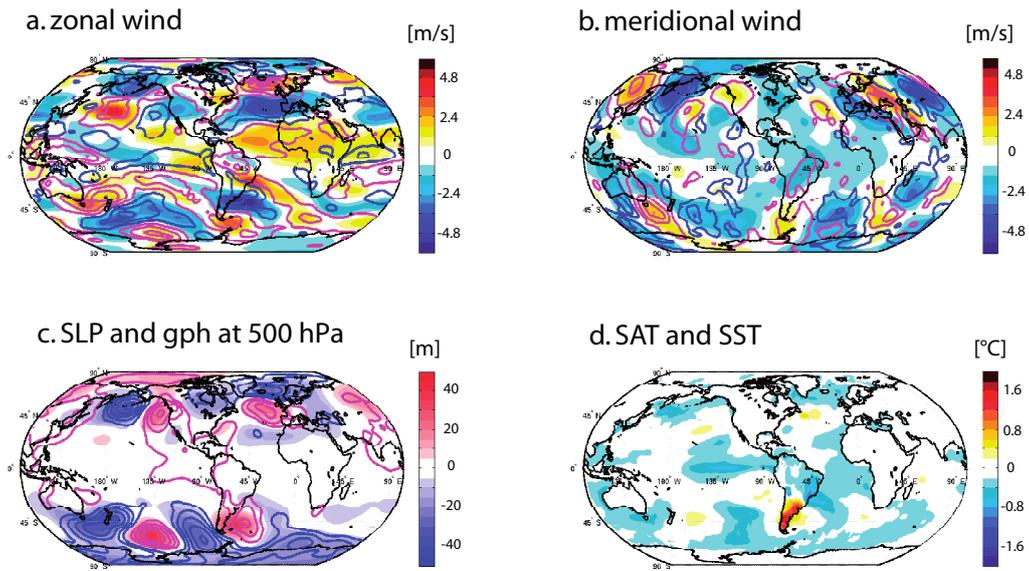
Fig. 2.6: *Warm-minus-cold composite difference fields of interannual variables, calculated from years exceeding 1 standard deviation of the T_PC1_ia time series (Fig. 2.2c): a) zonal wind at 200 hPa (filled) and 850 hPa (contours), b) meridional wind at 200 hPa (filled) and 850 hPa (contours), c) geopotential height at 500 hPa (filled) and SLP (contours), and d) surface air temperature over SA and SST. Color scales indicate the intervals of filled contours: a,b) 0.6 m/s, c) 5 gpm, d) 0.2°C. Units for not-filled contours are: a,b) 0.5 m/s, c) 0.5 hPa. Zero contours omitted.*
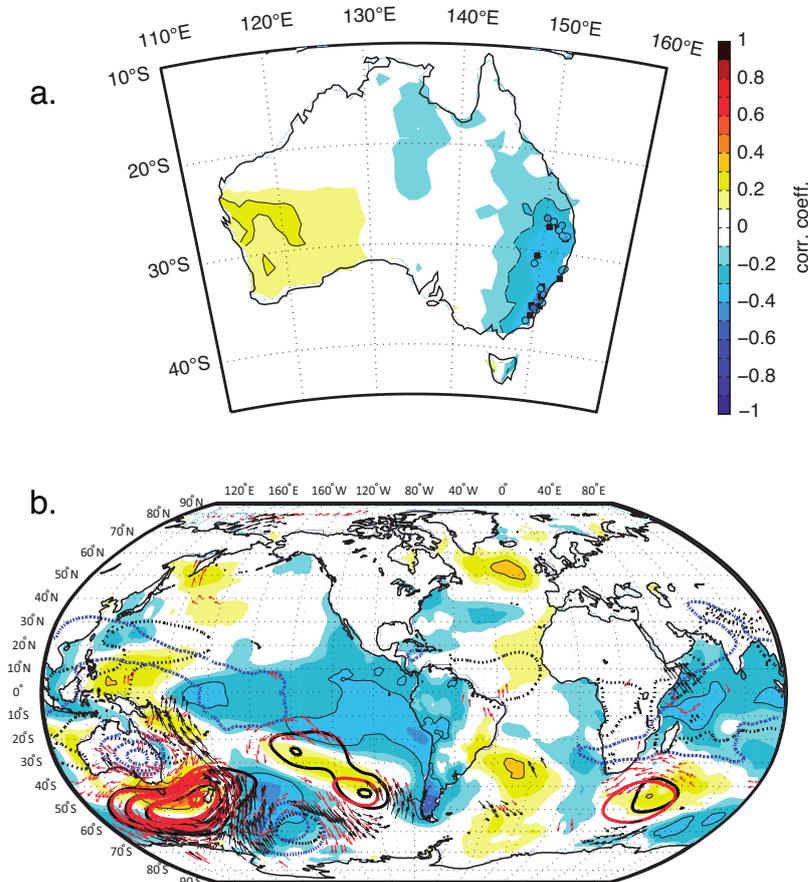
Fig. 2.7: *a) Correlation field of T_PC1_ia with interannual UDel precipitation over Australia (see color scale). Black contours denote absolute values greater than 0.2, statistically significant at 95%. Black squares indicate the gridpoints used to define the aus_P_PC1_ia index (see text). Circles show the correlation coefficients for individual interannual precipitation records (see Table 2.2). b) As Fig. 2.3a, but for aus_P_PC1_ia.*

Table 2.2: *Stations from Australia with rainfall records used to assess the correlation with T_PC1_ia and T_PC1_id. The considered period results as the intersection between 1907-2001 (1907-1979) and the available data length for each single rainfall record. One (two) asterisk(s) denote(s) statistical significance at 95% (99%) of the correlation between detrended series, considering the effective number of degrees of freedom of the data*

station name	latitude [°N]	longitude [°E]	elevation [m a.s.l.]	data length	*interannual correlation* coefficient, 1907-2001 (1907-1979)	*interdecadal correlation* coefficient, 1907-2001
Coonabarabran P.O.	-31.28	149.28	509	1907-2001	-0.37** (-0.40**)	-0.48
Bettowynd (Condry)	-35.70	149.78	160	1907-2001	-0.51** (-0.60**)	-0.39
Delegate (Cometville)	-37.05	148.98	765	1907-2001	-0.34** (-0.39**)	-0.48
Warra P.O.	-26.93	150.93	317	1907-1984	-0.34** (-0.35**)	-0.41
Miles P.O.	-26.66	150.18	305	1907-2001	-0.42** (-0.40**)	-0.48
Leura P.O.	-33.72	150.35	975	1916-1990	-0.43** (-0.45**)	-0.64
Cataract Dam	-34.27	150.80	340	1911-2001	-0.49** (-0.56**)	-0.45
Jervis Bay (Pt Perpendicular L/H)	-35.10	150.80	085	1907-1998	-0.32** (-0.42**)	-0.08
Moruya Head Pilot Stn	-35.92	150.15	017	1907-2001	-0.45** (-0.56**)	-0.27
Doctors Creek	-27.20	151.88	588	1913-2001	-0.29** (-0.29**)	-0.36
Pittsworth P.O.	-27.72	151.63	608	1907-2001	-0.36** (-0.40**)	-0.05
Warwick (Hermitage)	-28.20	152.10	475	1908-1995	-0.38** (-0.38**)	-0.13
Warwick (Canning Downs)	-28.23	152.07	456	1907-2001	-0.38** (-0.40**)	-0.54
Old Koreelah (McPherson)	-28.40	152.42	420	1919-2001	-0.43** (-0.45**)	-0.52
Port Macquaire Hill St	-31.45	152.92	007	1907-2001	-0.34** (-0.38**)	-0.42
Lorne (Hannam Vale Rd)	-31.67	152.62	050	1945-2001	-0.21 (-0.33*)	-0.60

2.4.3 The imprint of the teleconnection in Oceania

We suggest that the circulation anomalies induced by the wave train pattern could drive the atmospheric covariability over Oceania and SSA, e.g. by modifying convection and moisture transport, and thus affecting cloudiness and precipitation. Hence, we analyse the spatial correlation pattern between *T_PC1_ia* and DJF interannual precipitation over Australia from UDel. This variable exhibits a weak zonal dipole pattern, with negative (positive) coefficients over the Eastern (Western) region of the country (Fig. 2.7a). Therefore, we calculate the standardized PC1 of precipitation from the 10 most anticorrelated gridpoints of Southeastern Australia (anticorrelation higher than -0.4, denoted by black squares in the map), which define the *aus_P_PC1_ia* index (Fig. 2.8a). So, by definition, the significant correlation value between *T_PC1_ia* and *aus_P_PC1_ia* reaches r=-0.51** (-0.59**) for 1907-2001 (1907-1979), supporting the existence of a teleconnection that dynamically links both signals.

The correlation fields between *aus_P_PC1* and various variables (Fig. 2.7b) exhibit indeed a similar wave train pattern as the one observed for *T_PC1_ia* (Fig. 2.3a, note the reversed signs), showing in this case stronger (weaker) action centres over Oceania (South Pacific). A striking difference with Fig. 2.3a, however, resides in the ENSO (La Niña) signal observed in SST for this case. While it is known that ENSO variability is asymmetrically correlated with precipitation in eastern Australia (Cai et al. 2010), temperature over SSA does not show a strong relationship with ENSO (Garreaud et al. 2008), as already showed in previous sections. In order to explore the existence of the teleconnection beyond reconstructed data, we calculate the correlation coefficients between *T_PC1_ia* and precipitation records from various stations located in SE Australia

Table 2.3: *Stations from Australia (Darwin) and New Zealand with SLP records used to calculate the anz_index_raw (1885-2011)*

station name	latitude [°N]	longitude [°E]	elevation [m a.s.l.]	data length
Darwin	-12.40	130.87	30	1867-2011
Le Bons Bay Aws	-43.746	173.119	236	1984-2011
Lincoln	-43.648	172.463	11	1885-1955
Lyttelton Harbour	-43.608	172.724	5	1971-2001
Christchurch Gardens	-43.531	172.619	7	2003-2011
Christchurch Aero	-43.493	172.537	37	1954-2011
Lake Coleridge	-43.365	171.529	364	1971-1991
Reefton Ews	-42.117	171.86	198	2007-2011

(Table 2.2). We find lower but comparable correlation values (coloured circles in Fig. 2.7a) as with *aus_P_PC1_ia.*

Furthermore, the associated atmospheric circulation variability is analysed through the *anz_index_raw*, defined for 1885-2011 as a linear combination of standardized SLP records from Darwin in Northern Australia and a composite of seven stations in New Zealand (Table 2.3). So defined, this index measures the SLP variability over one action centre of the wave-train patterns depicted in Figs. 2.3a and 2.7b. In this case, we again calculate the interdecadal and interannual components of *anz_index_raw*, named *anz_index_id* and *anz_index_ia*, respectively. The correlation coefficient between *anz_index_ia* and *T_PC1_ia* (Fig. 2.8b) reaches *r*=0.39** (0.45**) for the 1907-2001 (1907-1979) period. Moreover, the correlation coefficients between *anz_index_ia* and *aus_P_PC1_ia* (Fig. 2.8c) are *r*=-0.65** (-0.74**) for the 1907-2001 (1907-1979) period. This result highlights the fact that rainfall variability in SE Australia is partly accounted by this SLP modulation. In fact, as expected from found relationships, the two most negative years of *anz_index_raw* are 1887 and 1890, when major floods were documented in Eastern Australia.
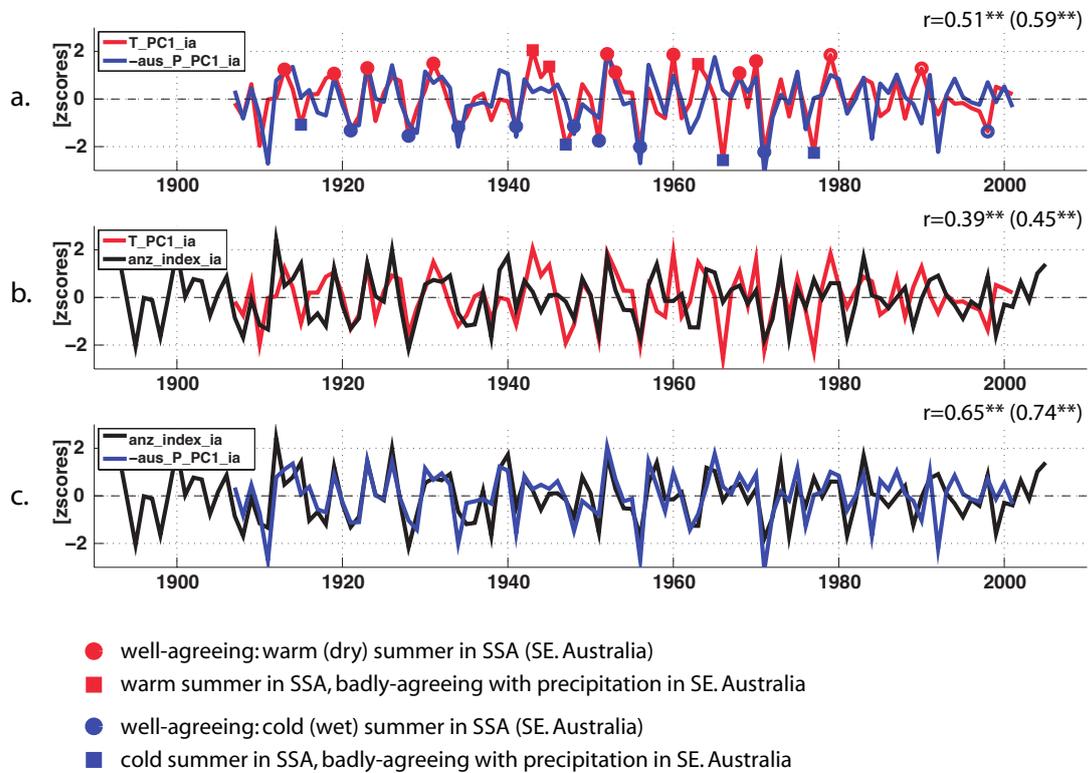

Fig. 2.8: *Normalized time series of T_PC1_ia (SSA, red), aus_P_PC1_ia (E. Australia, blue), and anz_index_ia (Australia-New Zealand, black). In a), extreme years of T_PC1_ia are indicated (see legend at the bottom). Correlation values (all statistically significant at 99%) for 1907-2001 (1907-1979) are shown.*

2.4.4 Stability of the Oceania-SSA teleconnection

We notice that some of the *T_PC1_ia* years agree better with *aus_P_PC1_ia* than others. In order to classify the extreme SAT events (as defined in Section 2.2, see Fig. 2.2c), a threshold of 1 standard deviation in the difference between the normalized series of *T_PC1_ia* and *-aus_P_PC1_ia* was defined (i.e., I*T_PC1_ia* + *aus_P_PC1_ia*I ≤ 1 for well-agreeing years). Table 2.5 lists warm and cold summers between 1912 and 1978 after this sorting. Furthermore, neutral (n), El Niño (EN), La Niña (LN), and volcanic eruption (v) years were identified based on Röthlisberger (2012), who used the ENSO definition of Yeh et al. (2009) on the Met Office Hadley Centre Interpolated sea ice and Sea Surface Temperature dataset (HadISST1 (Rayner et al. 2003)) for the 1891-2006 period, and a threshold of 0.6 W/m² in the estimated solar irradiation reduction for defining volcanic eruption events, after Crowley (2000). In Fig. 2.9, we compare the linear component of the spatial patterns of these extreme years, calculated as the positive minus negative composite difference fields of three groups of *T_PC1_ia* extreme years: a) all 28 extreme years (14 positive — 14 negative; similar to Fig. 2.6c,d; not shown), b) 17 well-agreeing years (9 positive — 8 negative, Fig. 2.9a,b) and c) 7 badly-agreeing years (3 positive — 4 negative, Fig. 2.9c,d). The badly-agreeing group clusters years which exhibit a drop in the covariability between *T_PC1_ia* and *aus_P_PC1_ia* and shows opposite SST and SAT anomalies over the Tropical Pacific and SSA, respectively (Fig. 2.9d).

Table 2.4: *Correlation coefficients r and coefficients of determination r² (in brackets) for the 4 composites in Eastern SSA, calculated between a) T_PC1_ia and corresponding interannual indices and b) T_PC1_id and corresponding interdecadal indices. First, second and third columns correspond to the 1) 1907-2001, 2) 1907-1979 and 3) 1980-2001 periods, respectively. One (two) asterisk(s) denote(s) statistical significance at 95% (99%) of the correlation between detrended series, considering the effective number of degrees of freedom of the data*

a) *T_PC1_ia* with interannual time series			
	1907-2001	**1907-1979**	**1980-2001**
R1	0.69** (0.48)	0.72** (0.52)	0.73** (0.54)
R2	0.84** (0.71)	0.86** (0.74)	0.85** (0.73)
R3	0.90** (0.81)	0.92** (0.85)	0.62** (0.39)
R4	0.59** (0.35)	0.71** (0.50)	-0.30 (0.09)
b) *T_PC1_id* with interdecadal time series			
	1907-2001	**1907-1979**	**1980-2001**
R1	0.85 (0.72)	0.80** (0.64)	0.75** (0.56)
R2	0.84 (0.71)	0.68** (0.46)	0.99** (0.98)
R3	0.94 (0.88)	0.85** (0.72)	0.86** (0.74)
R4	0.95 (0.90)	0.95** (0.90)	0.84** (0.71)

These results are summarized in an alternative manner by the 11-yr running correlation values between -*aus_P_PC1_ia*, *T_PC1_ia* and the DJF Niño3.4 index in Fig. 2.10 (comparable with the background of Fig. 2.4a). Note that during early 1940s and early 1960s the correlation coefficients between Niño3.4 and both -*aus_P_PC1_ia* and *T_PC1_ia* reverse sign. A similar phenomenon is observed for the 11-yr running correlation coefficients between -*aus_P_PC1_ia* and *T_PC1_ia*, although its decadal fluctuation just affects the amplitude and not the sign. Interestingly, these periods correspond to anomalous states of the climate system, namely after the strong and long-lasting 1940-42 El Niño event (Brönnimann et al. 2004) and the major eruption of Mt. Agung in 1963, respectively. In addition, we observe in the composite of badly-agreeing years (Fig. 2.9c,d) a La Niña-like anomaly over the Tropical Pacific together with a much more zonal geopotential height structure in the mid-latitudes, resembling the positive SAM phase. Furthermore, during these badly-agreeing years *less dry (less wet)* conditions are observed over southeast Australia, together with warm (cold) conditions over SSA. Although not evident in our results, Hendon et al. 2007 showed that during the positive SAM phase rainfall is enhanced over southeast Australia, partly due to an easterly upslope wind anomaly, which advects moisture from the Tasman Sea to the continent. Moreover, Fogt and Bromwich (2006) stated that high-latitude ENSO teleconnections amplify when the SAM index is positively correlated with the SOI during austral spring and summer, and L'Heureux and Thompson (2006) found a significant relationship between the warm phase of ENSO and the low index polarity of the SAM. Previous observations suggest a role of SST anomalies over the Tropical Pacific in modulating the found teleconnection.

2.5. Discussions and summary

In this work, the summertime temperature signal of Eastern SSA spanning the 20th century (1907-2001) has been analysed. The interdecadal leading mode, named *T_PC1_id*, explains ~80% of the total interdecadal variance of the station-based composites and suggests a highest frequency peak at 64 years. Its spatial pattern shows positive coefficients over the southernmost part of the continent and negative values over the Gran Chaco region, eastern Brazil and the northernmost part of SA. This mode modulates embedded higher frequency variability and is correlated with the PDO and IPO indices since the 1960s (showing the late 1970s climate shift), but not in the first half of the 20th century. This issue highlights the necessity of a proper definition of this particular variability mode. Besides the strong warming shift detected in *T_PC1_id* in the

late 1970s, in 3 of 4 of our interdecadal temperature composites, we observe a warm-to-cold shift-like transition in the early 1930s (and not in the late 1940s, as expected from a possible PDO-related or IPO-related variability) and a more recent abrupt warm-to-cold phase change in the early 1990s. Thus, we conclude that the interdecadal SAT variability in SSA during the 20th century consists of regimes separated by more or less sharp transitions.

The main focus of this paper, however, is the interannual summertime SAT variability over SSA. The corresponding index, named *T_PC1_ia*, represents ~60% of the interannual variance of our composites in this frequency range and exhibits its highest significant peak at ~3.4 years. Spatially, this mode represents the variability of roughly the southern half of SA and corresponds to one of the main SAT variability modes of the

Table 2.5: Well- and badly-agreeing extreme summers (see text for definition). Only warm (w) and cold (c) events between 1912 and 1978 have been considered and then classified as neutral (n), El Niño (EN), La Niña, and volcanic eruption (v) years. Positive (negative) DJF SAM phases correspond to departures greater than +1 (-1) std. dev. of the DJF Zhang AAO index (reference period: 1907-2001)

well-agreeing extreme years			
positive difference [std. dev.]		negative difference [std. dev.]	
1913	0.13 (w,v)	1951	-0.96 (c,LN,SAM-)
1919	0.19 (w,EN,SAM+)	1928	-0.51 (c,n)
1968	0.21 (w,LN)	1921	-0.20 (c,n)
1948	0.33 (c,n)	1923	-0.19 (w,LN)
1953	0.42 (w,n)	1952	-0.18 (w,EN)
1941	0.44 (c,EN,SAM-)		
1970	0.68 (w,v,SAM+)		
1956	0.68 (c,LN)		
1934	0.81 (c,LN)		
1931	0.81 (w,EN)		
1960	0.89 (w,n,SAM+)		
1971	0.90 (c,LN)		
badly-agreeing extreme years			
positive difference [std. dev.]		negative difference [std. dev.]	
1945	1.07 (w,n)	1966	-2.95 (c,v)
1943	1.77 (w,LN)	1977	-2.30 (c,EN,SAM-)
1963	2.24 (w,n,SAM+)	1947	-1.78 (c,n)
		1915	-1.14 (c,v)

whole continent.

A barotropic wave train pattern, extending from Oceania along the South Pacific to SSA, is the main large-scale feature associated with *T_PC1_ia* (Fig. 2.3a). The wavetrain-like pattern we identified at 500 hPa resembles that described by Cerne and Vera (2011) when studying the influence of intraseasonal variability in the development of heat waves over subtropical South America in summer in connection with an active SACZ, i.e. increased convection leading to more precipitation in this area. For that, these authors used SAT data from just one station located in Rosario, Argentina (32°55'S, 60°47'W, 25 m a.s.l.), and the NCEP-NCAR reanalysis for the 1979-2003 period. However, we advert a different phasing of the wave-train pattern linked to *T_PC1_ia*; that is, the location of the action centres of the corresponding large-scale anomalies differ between that study and the results presented here. Furthermore, Díaz and Aceituno (2003), in their study about enhanced (wet) and reduced (dry) episodes of convective cloudiness over Uruguay during the period 1979-1993, showed a wavelike structure in 11-day composites of 200 hPa geopotential height anomalies. Our results resemble their sub-monthly signal for dry conditions over Uruguay. In this way, we extend the results of previous papers into longer timescales by studying SAT variability over SSA during almost the whole 20th century.

The climatic implications of *T_PC1_ia* were also investigated through the relationships between this index and SLP and precipitation time series from SA. In
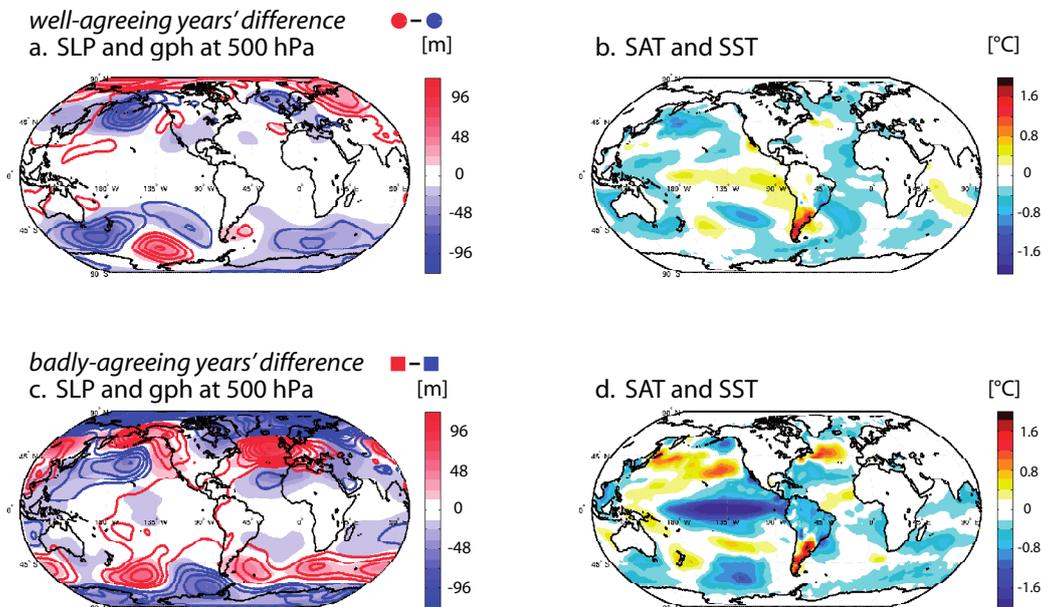

Fig. 2.9: *Composite difference fields (positive–negative) of interannual DJF variables, considering following groups of extreme events listed in Table 2.5 and depicted in Fig. 2.8a: a,b) well-agreeing years, and c,d) badly-agreeing years between T_PC1_ia and aus_P_PC1_ia. Anomaly fields correspond to: a,c).*

particular, the spatial correlation pattern with rainfall reveals the dipole between SESA and the SACZ, associated with the South American monsoon (Liebmann and Mechoso 2011). Doyle and Barros (2002) showed, for January, a positive feedback between weak (intense) SACZ activity and positive (negative) SST anomalies over the western subtropical South Atlantic Ocean (WSSA: 20°-30°S; 30°-50°W). In agreement with this, we observe in 2.3a and 2.5b, respectively, that the dry (wet) anomaly over SESA and wet (dry) anomalies over SACZ and CWA are concomitant with a cold (warm) anomaly over WSSA. We also note that such SST anomaly has at least partly an advective origin due to the anticyclonic circulation observed to its Southwest, which is indeed part of the described wave train pattern. The SACZ-SESA rainfall dipole, which modulates heavy precipitation events, has been identified also in connection with DJF sub-monthly variations of cloudiness (from 2 to 30 days) and referred to as the South American Seesaw Pattern (Liebmann et al. 1999; Nogués-Paegle and Mo 1997). Liebmann et al. (1999), showed a wave train in the 200 hPa streamfunction over the South Pacific, starting near New Zealand towards SA. They characterised it as a zonal wavenumber-5 pattern that occurs frequently within the austral westerlies, especially during summer (Kidson 1991), and referred to the Rossby wave guide along the South Pacific jet into the subtropics of the South Atlantic identified by Ambrizzi and Hoskins (1997) during austral summer as a preferred route of energy dispersion. Although derived from a submonthly signal associated with another variable in a different region as ours, and analysing the streamfunction at 200 hPa instead of geopotential height at 500 hPa, the wave train pattern of Liebmann et al. (1999) is comparable to the circulation pattern associated with our results, especially when their fields are lagged by -4 to -2 days with respect to the OLR signal. However, the strongest anomalies are, as expected, located where each signal originates. This supports the conclusion that our results are linked to findings by previous studies (in particular, the SACZ-SESA dipole shown in our Fig. 2.5), and that our approach (SAT seasonal analysis) masks the synoptic evolution of this teleconnection. At synoptic scale, Liebmann et al. (2004) showed that the intensity of the LLJ is forced by a wave train pattern that originates at midlatitudes over the Pacific Ocean, and then deflects equatorward after crossing the Andes Cordillera. These authors proposed that the MJO could modify the planetary basic-state flow, which would lead to a preferred phasing of synoptic waves towards SA.

The correlation pattern between *T_PC1_ia* and the relative cyclone frequency (a synoptic-to-intraseasonal phenomenon, Fig. 2.3b) shows that a warm (cold) anomaly over SSA is observed together with a lower (higher) frequency of cyclones over this region and the southwest Atlantic Ocean. Besides, the geopotential height and SLP correlation fields of Fig. 2.3a resemble features that are opposite to the pattern related to summertime incursions of cold air, which affect the whole region (Garreaud 2000; Garreaud and Wallace 1998). In particular, we observe the mid-level ridge to the east of

the Andes and over the southwest Atlantic, and the positive SLP anomaly over that latter region. Thus, we clearly identify how the signals of synoptic-scale phenomena, related to both precipitation and temperature variability, propagate into longer timescales and imprint the local pattern of DJF *interannual* climate variability.

In this context, regional SAT implications of *T_PC1_ia* could be associated with findings of previous studies focused on daily variability. Barrucand et al. (2008) found a 4-year signal in the occurrence of warm days and cold nights during summer for 1964-2003 and a decrease of the latter variable during 1964-1979. These results agree with the variability peak at ~3.4 years of *T_PC1_ia* and with the warming observed during the 1970s in *T_PC1_id*, respecitvely, but a possible connection should be explored in detail.

In a broader spatial perspective, we found a negative covariability between precipitation over eastern Australia and SAT over SSA (represented by *aus_P_PC1_ia* and *T_PC1_ia*, respectively). Although ENSO variability is known to impact the former, such a relationship is not evident for the latter, where the 11-years running correlation coefficients between DJF Niño3.4 and *T_PC1_ia* exhibit significant decadal fluctuations.
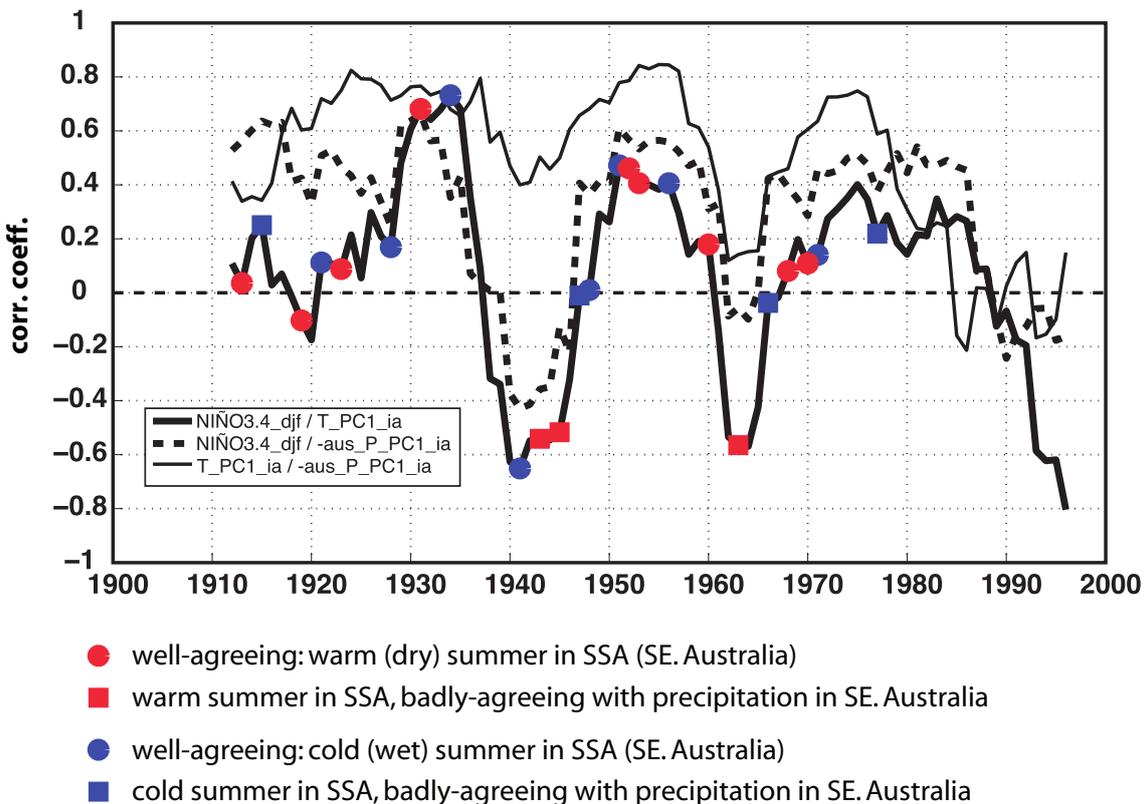
Fig. 2.10: *Time series of 11-yr running correlation coefficients (1912-1996) centered in the 5th year between DJF Niño3.4 and: a) T_PC1_ia (thick solid curve) and b) –aus_P_PC1_ia (dashed curve). The 11-yr running correlation coefficients calculated between T_PC1_ia and –aus_P_PC1_ia are also shown (thin solid curve). Red/blue markers denote warm/cold events listed in Table 2.5 (see legend at the bottom).*

Thus, disruptions of the Oceania-SSA teleconnection seem to be related to SST anomalies in the Tropical Pacific. Cai et al. (2001) described the non-stationarity of the relationship between ENSO and DJF precipitation in northeastern Australia. It was found that this relationship reversed sign in periods where the detrended global mean surface temperature was rising or anomalously high, as in 1931-1945. This period partially coincides with the first reversal of the running correlation values between T_PC1_ia and DJF Niño3.4 and the strengthening of the relationship between T_PC1_ia and DJF SAM/AAO (Figs. 2.4 and 2.10), which also occurs in the 1960s. In both periods, the low-pass-filtered SOI index shows anomalously low values (e.g. Power et al. (2006)). Moreover, Cai et al. (2010) studied the asymmetry of the relationship between ENSO and DJF precipitation in the eastern part of Australia (Southeast Queensland, SEQ) during 1950-1979 and found that, while La Niña events result in increased rainfall in that region, no robust signal is found for El Niño events. This study states, however, that before the mid-1930s and since the 1980s, this asymmetry no longer operates. This fact has caused a dramatic local rainfall reduction since then. They associate this breakdown partly to an eastward shift of the Walker circulation (and, consequently, an increase of the amplitude of La Niña Modoki thereafter) and of the convection centre near SEQ (particularly the South Pacific Convergence Zone), which they relate to a positive phase of the IPO (PDO). In summary, the new mean position of the main convection centre over the Tropical Pacific, related to the El Niño-like climate background after late 1970s (Mantua et al. 1997), seems to have modified the position of the action centres of the wave train pattern and its related dynamics. Hence, while after the 1970s shift this mechanism still appears to drive the interannual SAT variability over SSA, it would have stopped modulating the precipitation variability over eastern Australia, thus breaking the Oceania-SSA teleconnection documented here.

To this respect, Agosta and Compagnucci (2011) found that the precipitation variability of CWA (spanning [29-36°S; 65-70°W] in their case), positively correlated with T_PC1_ia (Fig. 2.5b), was associated with a barotropic quasi-stationary wave emanating from the tropical Indian Ocean and the South Pacific from the beginning of the 20th century until mid-1970s. After the 1976/77 climate shift, however, they identified the El Niño-like conditions over the Tropical Pacific and the possibly related strengthening of the Subtropical Atlantic Anticyclone as factors modulating the CWA precipitation variability. We found that the interdecadal precipitation variability of CWA (UDel data) greatly resembles T_PC1_id (not shown), although showing an earlier manifestation of the 1970s shift, which could be related to large-scale precipitation changes documented in the Pampean plains of Central Argentina (Piovano et al. 2002) and in the South American Monsoon System (Carvalho et al. 2011). These similarities reflect the broad climatic implications of the interannual and interdecadal variability modes documented in this paper.

The results presented here contribute to a better understanding of South American climate and its dynamical connections with remote regions. In comparison with previous studies, a broader spatiotemporal perspective has been introduced by using long instrumental records from this relatively poorly instrument-covered region and by means of the novel 20CRv2 reanalysis.

Acknowledgments

References

Aceituno P (1988) On the Functioning of the Southern Oscillation in the South American Sector. Part I: Surface Climate. Mon Weather Rev 116:505–524. doi: 10.1175/1520-0493(1988)116<0505:OTFOTS>2.0.CO;2

Agosta EA, Compagnucci RH (2008) The 1976/77 Austral Summer Climate Transition Effects on the Atmospheric Circulation and Climate in Southern South America. J Clim 21:4365–4383. doi: 10.1175/2008JCLI2137.1

Agosta EA, Compagnucci RH (2011) Central-West Argentina Summer Precipitation Variability and Atmospheric Teleconnections. J Clim 25:1657–1677. doi: 10.1175/JCLI-D-11-00206.1

Ambrizzi T, Hoskins BJ (1997) Stationary rossby-wave propagation in a baroclinic atmosphere. Q J R Meteorol Soc 123:919–928. doi: 10.1002/qj.49712354007

Barrucand M, Rusticucci M, Vargas W (2008) Temperature extremes in the south of South America in relation to Atlantic Ocean surface temperature and Southern Hemisphere circulation. J Geophys Res Atmos 113:D20111. doi: 10.1029/2007JD009026

Berbery EH, Nogués-Paegle J (1993) Intraseasonal Interactions between the Tropics and Extratropics in the Southern Hemisphere. J Atmos Sci 50:1950–1965. doi: 10.1175/1520-0469(1993)050<1950:IIBTTA>2.0.CO;2

Berman AL, Silvestri G, Compagnucci R (2012) Eastern Patagonia Seasonal Precipitation: Influence of Southern Hemisphere Circulation and Links with Subtropical South American Precipitation. J Clim 25:6781–6795. doi: 10.1175/JCLI-D-11-00514.1

Bretherton CS, Widmann M, Dymnikov VP, et al. (1999) The Effective Number of Spatial Degrees of Freedom of a Time-Varying Field. J Clim 12:1990–2009. doi: 10.1175/1520-0442(1999)012<1990:TENOSD>2.0.CO;2

Brönnimann S, Compo GP (2012) Ozone highs and associated flow features in the first half of the twentieth century in different data sets. Meteorol Zeitschrift 21:49–59. doi: doi:10.1127/0941-2948/2012/0284

Brönnimann S, Compo GP, Spadin R, et al. (2011) Early ship-based upper-air data and comparison with the Twentieth Century Reanalysis. Clim Past 7:265–276. doi: 10.5194/cp-7-265-2011

Brönnimann S, Luterbacher J, Staehelin J, et al. (2004) Extreme climate of the global troposphere and stratosphere in 1940-42 related to El Nino. Nature 431:971–974.

Cai W, van Rensch P, Cowan T, Sullivan A (2010) Asymmetry in ENSO Teleconnection with Regional Rainfall, Its Multidecadal Variability, and Impact. J Clim 23:4944–4955. doi: 10.1175/2010JCLI3501.1

Cai W, Whetton PH, Pittock AB (2001) Fluctuations of the relationship between ENSO and northeast Australian rainfall. Clim Dyn 17:421–432. doi: 10.1007/PL00013738

Carvalho LM V, Jones C, Silva AE, et al. (2011) The South American Monsoon System and the 1970s climate transition. Int J Climatol 31:1248–1256. doi: 10.1002/joc.2147

Cerne SB, Vera CS (2011) Influence of the intraseasonal variability on heat waves in subtropical South America. Clim Dyn 36:2265–2277. doi: 10.1007/s00382-010-0812-4

Compo GP, Whitaker JS, Sardeshmukh PD, et al. (2011) The Twentieth Century Reanalysis Project. Q J R Meteorol Soc 137:1–28. doi: 10.1002/qj.776

Crowley TJ (2000) Causes of Climate Change Over the Past 1000 Years. Sci 289 :270–277. doi: 10.1126/science.289.5477.270

Díaz A, Aceituno P (2003) Atmospheric Circulation Anomalies during Episodes of Enhanced and Reduced Convective Cloudiness over Uruguay. J Clim 16:3171–3185. doi: 10.1175/1520-0442(2003)016<3171:ACADEO>2.0.CO;2

Doyle ME, Barros VR (2002) Midsummer Low-Level Circulation and Precipitation in Subtropical South America and Related Sea Surface Temperature Anomalies in the South Atlantic. J Clim 15:3394–3410. doi: 10.1175/1520-0442(2002)015<3394:MLLCAP>2.0.CO;2

Ebisuzaki W (1997) A Method to Estimate the Statistical Significance of a Correlation When the Data Are Serially Correlated. J Clim 10:2147–2153. doi: 10.1175/1520-0442(1997)010<2147:AMTETS>2.0.CO;2

Falvey M, Garreaud RD (2009) Regional cooling in a warming world: Recent temperature trends in the southeast Pacific and along the west coast of subtropical South America (1979–2006). J Geophys Res Atmos 114:D04102. doi: 10.1029/2008JD010519

Fogt R, Bromwich D, Hines K (2011) Understanding the SAM influence on the South Pacific ENSO teleconnection. Clim Dyn 36:1555–1576. doi: 10.1007/s00382-010-0905-0

Fogt RL, Bromwich DH (2006) Decadal Variability of the ENSO Teleconnection to the High-Latitude South Pacific Governed by Coupling with the Southern Annular Mode*. J Clim 19:979–997. doi: 10.1175/JCLI3671.1

Gallego D, Ribera P, Garcia-Herrera R, et al. (2005) A new look for the Southern Hemisphere jet stream. Clim Dyn 24:607–621. doi: 10.1007/s00382-005-0006-7

Garreaud R (2000) Cold Air Incursions over Subtropical South America: Mean Structure and Dynamics. Mon Weather Rev 128:2544–2559. doi: 10.1175/1520-0493(2000)128<2544:CAIOSS>2.0.CO;2

Garreaud R, Lopez P, Minvielle M, Rojas M (2012) Large-Scale Control on the Patagonian Climate. J Clim 26:215–230. doi: 10.1175/JCLI-D-12-00001.1

Garreaud R, Wallace JM (1998) Summertime Incursions of Midlatitude Air into Subtropical and Tropical South America. Mon Weather Rev 126:2713–2733. doi: 10.1175/1520-0493(1998)126<2713:SIOMAI>2.0.CO;2

Garreaud RD, Vuille M, Compagnucci R, Marengo J (2008) Present-day South American climate. Palaeogeogr Palaeoclimatol Palaeoecol. doi: 10.1016/j.palaeo.2007.10.032

Garreaud RD, Vuille M, Compagnucci R, Marengo J (2009) Present-day South American climate. Palaeogeogr Palaeoclimatol Palaeoecol 281:180–195. doi: http://dx.doi.org/10.1016/j.palaeo.2007.10.032

Gershunov A, Schneider N, Barnett T (2001) Low-Frequency Modulation of the ENSO–Indian Monsoon Rainfall Relationship: Signal or Noise? J Clim 14:2486–2492. doi: 10.1175/1520-0442(2001)014<2486:LFMOTE>2.0.CO;2

Gillett NP, Kell TD, Jones PD (2006) Regional climate impacts of the Southern Annular Mode. Geophys Res Lett 33:1–4. doi: 10.1029/2006GL027721

Grimm AM, Zilli MT (2009) Interannual Variability and Seasonal Evolution of Summer Monsoon Rainfall in South America. J Clim 22:2257–2275. doi: 10.1175/2008JCLI2345.1

Sen Gupta A, England MH (2006) Coupled Ocean–Atmosphere–Ice Response to Variations in the Southern Annular Mode. J Clim 19:4457–4486. doi: 10.1175/JCLI3843.1

Hendon HH, Thompson DWJ, Wheeler MC (2007) Australian Rainfall and Surface Temperature Variations Associated with the Southern Hemisphere Annular Mode. J Clim 20:2452–2467. doi: 10.1175/JCLI4134.1

Jacques M (2009) Caracterización del salto climático de mediados de los 1970s en Sudamérica. MSc Thesis. Universidad de Chile

Jacques-Coper M, Garreaud RD (2014) Characterization of the 1970s climate shift in South America. Int J Climatol 1–16. doi: 10.1002/joc.4120

Jones PD, Osborn TJ, Briffa KR (1997) Estimating Sampling Errors in Large-Scale Temperature Averages. J Clim 10:2548–2568. doi: 10.1175/1520-0442(1997)010<2548:ESEILS>2.0.CO;2

Kerr RA (1992) Unmasking a Shifty Climate System. Science (80-) 255:1508–1510. doi: 10.1126/science.255.5051.1508

Kidson JW (1991) Intraseasonal Variations in the Southern Hemisphere Circulation. J Clim 4:939–953. doi: 10.1175/1520-0442(1991)004<0939:IVITSH>2.0.CO;2

L'Heureux ML, Thompson DWJ (2006) Observed Relationships between the El Niño–Southern Oscillation and the Extratropical Zonal-Mean Circulation. J Clim 19:276–287. doi: 10.1175/JCLI3617.1

Legates DR, Willmott CJ (1990a) Mean seasonal and spatial variability in global surface air temperature. Theor Appl Climatol 41:11–21. doi: 10.1007/BF00866198

Legates DR, Willmott CJ (1990b) Mean seasonal and spatial variability in gauge-corrected, global precipitation. Int J Climatol 10:111–127. doi: 10.1002/joc.3370100202

Liebmann B, Kiladis GN, Marengo J, et al. (1999) Submonthly Convective Variability over South America and the South Atlantic Convergence Zone. J Clim 12:1877–1891. doi: 10.1175/1520-0442(1999)012<1877:SCVOSA>2.0.CO;2

Liebmann B, Kiladis GN, Vera CS, et al. (2004) Subseasonal Variations of Rainfall in South America in the Vicinity of the Low-Level Jet East of the Andes and Comparison to Those in the South Atlantic Convergence Zone. J Clim 17:3829–3842. doi: 10.1175/1520-0442(2004)017<3829:SVORIS>2.0.CO;2

Liebmann B, Mechoso CR (2011) The South American Monsoon System. In: Chang C-P, Ding Y, Lau N-C, et al. (eds) Glob. Monsoon Syst. Res. Forecast, 2nd Editio. World Scientific Publication Company, pp 137–157

Luterbacher J, Neukom R, González-Rouco F, et al. (2011) Reconstructed and simulated Medieval Climate Anomaly in southern South America. PAGES news 19:20–21.

Mantua NJ, Hare SR, Zhang Y, et al. (1997) A Pacific Interdecadal Climate Oscillation with Impacts on Salmon Production. Bull Am Meteorol Soc 78:1069–1079. doi: 10.1175/1520-0477(1997)078<1069:APICOW>2.0.CO;2

Marengo JA, Soares WR, Saulo C, Nicolini M (2004) Climatology of the Low-Level Jet East of the Andes as Derived from the NCEP–NCAR Reanalyses: Characteristics and Temporal Variability. J Clim 17:2261–2280. doi:

10.1175/1520-0442(2004)017<2261:COTLJE>2.0.CO;2

Marshall GJ (2003) Trends in the Southern Annular Mode from Observations and Reanalyses. J Clim 16:4134–4143. doi: 10.1175/1520-0442(2003)016<4134:TITSAM>2.0.CO;2

Meehl GA (2007) Global climate projections. In: Solomon S (ed) Clim. Chang. 2007 Phys. Sci. Basis. Cambridge Univ. Press, Cambridge, UK, pp 747–846

Mo KC, Paegle JN (2001) The Pacific–South American modes and their downstream effects. Int J Climatol 21:1211–1229. doi: 10.1002/joc.685

Montecinos A, Purca S, Pizarro O (2003) Interannual-to-interdecadal sea surface temperature variability along the western coast of South America. Geophys Res Lett 30:1570. doi: 10.1029/2003GL017345

Neukom R, Luterbacher J, Villalba R, et al. (2011) Multiproxy summer and winter surface air temperature field reconstructions for southern South America covering the past centuries. Clim Dyn 37:35–51. doi: 10.1007/s00382-010-0793-3

Neukom R, Luterbacher J, Villalba R, et al. (2010) Multi - centennial summer and winter precipitation variability in southern South America. 37:1–6. doi: 10.1029/2010GL043680

Nogués-Paegle J, Mo KC (1997) Alternating Wet and Dry Conditions over South America during Summer. Mon Weather Rev 125:279–291. doi: 10.1175/1520-0493(1997)125<0279:AWADCO>2.0.CO;2

Peterson TC, Vose RS (1997) An Overview of the Global Historical Climatology Network Temperature Database. Bull Am Meteorol Soc 78:2837–2849. doi: 10.1175/1520-0477(1997)078<2837:AOOTGH>2.0.CO;2

Piovano EL, Ariztegui D, Moreira SD (2002) Recent environmental changes in Laguna Mar Chiquita (central Argentina): a sedimentary model for a highly variable saline lake. Sedimentology 49:1371–1384. doi: 10.1046/j.1365-3091.2002.00503.x

Power S, Casey T, Folland C, et al. (1999) Inter-decadal modulation of the impact of ENSO on Australia. Clim Dyn 15:319–324. doi: 10.1007/s003820050284

Power S, Haylock M, Colman R, Wang X (2006) The Predictability of Interdecadal Changes in ENSO Activity and ENSO Teleconnections. J Clim 19:4755–4771. doi: 10.1175/JCLI3868.1

Rayner NA, Parker DE, Horton EB, et al. (2003) Global analyses of sea surface temperature, sea ice, and night marine air temperature since the late nineteenth century. J Geophys Res Atmos 108:4407. doi: 10.1029/2002JD002670

Rodionov SN (2005) A sequential method for detecting regime shifts in the mean and variance. In: Velikova V, Chipev N (eds) Large-Scale Disturbances (Regime Shifts) Recover. Aquat. Ecosyst. Challenges Manag. Towar. Sustain. Varna, Bulgaria, pp 68–72

Rosenblüth B, Fuenzalida HA, Aceituno P (1997) Recent Temperature Variations in Southern South America. Int J Climatol 17:67–85. doi: 10.1002/(SICI)1097-0088(199701)17:1<67::AID-JOC120>3.0.CO;2-G

Röthlisberger M (2012) Vergleich des El Niño Signals in unterschiedlichen Datensätzen und anhand verschiedener El Niño Definitionen. BSc Thesis. Universitat Bern

Silvestri G, Vera C (2009) Nonstationary Impacts of the Southern Annular Mode on Southern Hemisphere Climate. J Clim 22:6142–6148. doi: 10.1175/2009JCLI3036.1

Silvestri GE, Vera CS (2003) Antarctic Oscillation signal on precipitation anomalies over southeastern South America. Geophys Res Lett 30:2115. doi: 10.1029/2003GL018277

Smith TM, Reynolds RW (2004) Improved Extended Reconstruction of SST (1854–1997). J Clim 17:2466–2477. doi: 10.1175/1520-0442(2004)017<2466:IEROS>2.0.CO;2

Thompson DWJ, Solomon S (2002) Interpretation of Recent Southern Hemisphere Climate Change. Sci 296 :895–899. doi: 10.1126/science.1069270

Trenberth KE (2007) Observations: Surface and atmospheric climate change. In: Solomon S (ed) Clim. Chang. 2007 Phys. Sci. Basis. Cambridge Univ. Press, Cambridge, UK, pp 253–336

Trenberth KE (1990) Recent Observed Interdecadal Climate Changes in the Northern Hemisphere. Bull Am Meteorol Soc 71:988–993. doi: 10.1175/1520-0477(1990)071<0988:ROICCI>2.0.CO;2

Uppala SM, Kållberg PW, Simmons AJ, et al. (2005) The ERA-40 re-analysis. Q J R Meteorol Soc 131:2961–3012. doi: 10.1256/qj.04.176

Wang G, Cai W (2013) Climate-change impact on the 20th-century relationship between the Southern Annular Mode and global mean temperature. Sci. Rep. 3:

Welker C, Martius O (2012) Variability of cyclones over the North Atlantic and Europe since 1871. Geophys Res Abstr 14:2507–2507.

Yeh S-W, Kug J-S, Dewitte B, et al. (2009) El Nino in a changing climate. Nature 461:511–

514.

Zhang Q, Körnich H, Holmgren K (2012) How well do reanalyses represent the southern African precipitation? Clim Dyn 40:951–962. doi: 10.1007/s00382-012-1423-z

Zhang Z-Y, Gong D-Y, He X-Z, et al. (2010) Statistical Reconstruction of the Antarctic Oscillation Index Based on Multiple Proxies. Atmos Ocean Sci Lett 3:283–287.

Chapter 3

Heat waves in Southeastern Patagonia during austral summer: an analysis of the intraseasonal timescale

Martín Jacques-Coper[1], Stefan Brönnimann[1], Olivia Martius[1], Carolina Vera[2], and Bibiana Cerne[2]

[1]*Oeschger Centre for Climate Change Research and Institute of Geography, University of Bern, Bern, Switzerland*

[2]*Centro de Investigaciones del Mar y la Atmósfera, CIMA/CONICET-UBA, DCAO/ FCEN, UMI-IFAECI/CNRS, Buenos Aires, Argentina*

Abstract

We explore the occurrence of intraseasonal summertime heat wave events in Southeastern Patagonia (SEPG, 46°-52°S;65°-70°W) since the late 19th century by means of the Twentieth Century Reanalysis version 2 (20CRv2). In total, 201 cases were identified for 1872-2010 according to criteria of intensity and persistence. They were centred around the heat day of each cluster of days fulfilling those conditions (named day 0, *d0*). Composites of intraseasonal surface air temperature anomaly (T') in Southern South America (SSA) indicate that heat waves detected over SEPG affect a broad area on both sides of the Andes, a result that is also confirmed by instrumental records. A high pressure system over SSA precedes the T' rise in SEPG. The local warming is caused by temperature advection and enhanced radiative heating. The mean warm perturbation over SEPG lasts

approximately two weeks and exhibits a mean T' peak of 4.3°C on *d0*. Preceding these events, a cyclonic anomaly progresses eastward over the Tasman Sea in Oceania, from southeastern Australia (day -6, causing a dry anomaly there) over New Zealand (day -3, inducing a wet anomaly on its Southern Island). These atmospheric perturbations are embedded in a wavetrain-like pattern with negative (positive) action centres over New Zealand and to the west of South America (north of the Ross Sea and SSA). The anomalous circulation induced by this pattern is the origin of a teleconnection between SSA and Oceania, documented in previous work for the interannual level. Two thirds of the heat wave events are linked to enhanced ascent in the South Atlantic Convergence Zone (SACZ) and around one third of them leads to absolute maximum temperatures exceeding the 99 percentile of the instrumental record at Comodoro Rivadavia in 1957-2010. Furthermore, for SEPG, we explore the link between the intraseasonal anomalies associated with heat waves and those related to summer seasonal mean anomalies of temperature. We suggest that circulation anomalies favouring heat waves tend to be stronger (weaker) during years with extreme positive (negative) summer temperatures. Finally, a possible interdecadal modulation of the wave train pattern is discussed.

3.1 Introduction

3.1.1 General aspects on the climate of Patagonia

Southern South America (SSA) is defined in this work as the part of the continent to the south of 30°S. Patagonia, within SSA, is the region that spans from 40°S until the southern tip of the continent. Although the current climate of Patagonia has been reviewed in a regional and comprehensive context, including its links with the large-scale circulation (e.g. Garreaud et al. 2012; Paruelo et al. 1998; Prohaska 1976), and also with focus on particular aspects of single variables such as temperature (e.g. Berman et al. 2013; Garreaud 2000) and precipitation (e.g. Berman et al. 2012; Carrasco et al. 2002), it still remains a relatively unexplored topic in the climate sciences. The relative lack of studies about this region is due in part to the low density of instrumental coverage, especially in the interior regions (Paruelo et al. 1998). Moreover, detailed analysis on a broad variety of meteorological and climatological phenomena in Patagonia are needed in order to understand their impacts on natural aspects, such as the biosphere (Hertel et al. 2008; Lara et al. 2005) and cryosphere (Carrasco et al. 2002; Rasmussen et al. 2007; Rignot et al. 2003), but also on socioecological subjects, such as desertification (Del Valle et al. 1998).

On the western side of Patagonia the interaction between the westerly flow from

the Pacific Ocean and the southern Andes leads to a temperate and hyperhumid climate. The eastern side of Patagonia exhibits a continental climate with high aridity caused by the rain shadow effect of the Andes, along with a high annual thermal amplitude and extremely windy conditions associated with the westerlies (Garreaud et al. 2012). In this paper, our region of study is Southeastern Patagonia (SEPG), defined as the region confined within 46°-52°S; 65°-70°W (Fig. 3.1a), which roughly corresponds to the Argentinean province of Santa Cruz. Its northeast coast exhibits a mild semiarid climate. In that area, the 1961-1990 climatology for Comodoro Rivadavia (in the Chubut Province, 45°47'S; 67°30'W) features mean daily maximum (minimum) temperatures ranging between 24°C and 26°C (12°C and 14°C) during austral summer (December to February, DJF) and scarce annual precipitation (ca. 228 mm per year). Further to the south, mean temperatures decrease and the climate gets cooler and wetter. Río Gallegos (51°37'S; 69°17'W) features a local steppe climate, with maximum (minimum) temperatures fluctuating between 19°C and 21°C (7°C and 8°C). The inland of the Santa Cruz Province is formed by plateaus and river valleys at low to mid-altitudes, where stronger thermal amplitude and even more aridity than in the coastal areas are observed.

3.1.2 The variability of temperature in Southern South America

The modulation of surface air temperature (SAT) in SSA (and, in particular, in SEPG) involves various time scales and possible interactions between them. The interdecadal and interannual modulation of SAT in the eastern part of SSA during DJF was extensively studied by Jacques-Coper and Brönnimann (2014). In this region, an interdecadal warm-to-cold transition was detected during the early 1930s, followed by a relatively cold phase interrupted abruptly by a strong, step-like warming in the late 1970s, whose manifestations were especially striking in SEPG (Jacques 2009; Jacques-Coper and Brönnimann 2014; Jacques-Coper and Garreaud 2014). This result indicates that decadal variability plays a major role in the low-frequency evolution of local SAT.

Jacques-Coper and Brönnimann (2014) showed also that the interannual variability during summer (that is, the variability associated from one DJF season to another) leads to strong regional SAT departures from the climatology in SSA. This mode, whose strongest spectral peak appears at ~3.4 years, is related to a wave train pattern in geopotential height at 500 hPa over the South Pacific, which resembles the Pacific-South American (PSA) mode 2. In addition, the circulation induced by the centres of action of this circulation pattern causes an interannual teleconnection between temperature in SSA and precipitation in Southeastern Australia, in such a way that warm/cold summers

in SSA tend to be dry/wet in Southeastern Australia. The intraseasonal development of this particular wavetrain-like pattern and its climate impacts within that frequency band deserve attention and constitute a motivation for the present work.

3.1.3 Intraseasonal heat waves in Southern South America

In this paper we investigate the intraseasonal modulation of SAT in SEPG by studying the occurrence of local heat waves. Cerne and Vera (2011) analysed summertime intraseasonal heat waves recorded by a single station in Central-Eastern Argentina (Rosario Aero, 32°55'S;60°47›W) during 1979-2003 using the NNR. For that region, they ascribed 32% of SAT variance to intraseasonal variability. That study also found that 73% of the heat waves detected in Rosario were related to enhanced convection in the South Atlantic Convergence Zone (SACZ, Fig. 3.1a), located to the northeast of Rosario. The associated meridional circulation cell leads to subsidence conditions in Rosario, which reinforce the local anticyclonic anomaly and thus enhance the local SAT increase. Therefore, it is also of our concern to investigate whether there is a connection between heat wave events detected in SEPG and the SACZ activity. Furthermore, we aim at analysing to which extent the occurrences of heat waves in diverse regions of SSA are related.

3.1.4 Circulation patterns over the South Pacific

Interestingly, Cerne and Vera (2011) identified a large-scale Rossby wave train pattern in association to the heat waves in subtropical SA, which they linked to convection anomalies at the equatorial western and central Pacific Ocean. The development of atmospheric Rossby wave trains has been widely described in the literature (e.g. Hoskins et al. 1977) and it can be, indeed, partly induced by tropical forcing (Berbery and Nogués-Paegle 1993; Jin and Hoskins 1995). This pattern, although comparable to the one described for the interannual timescale in SSA by Jacques-Coper and Brönnimann (2014), shows a different phasing of its action centres. Moreover, Rossby wave trains between Oceania and South America have been identified in connection to the extensively-sudied subject of the intraseasonal variability of precipitation in subtropical and extratropical South America (e.g. Gonzalez and Vera 2013). Hence, as mentioned above, a main motivation for our study is to investigate whether warm intraseasonal anomalies in SEPG are also

related to a large-scale wavetrain-like circulation pattern over the South Pacific.

Also focusing on subtropical SA, the opposite phenomenon, namely the synoptic incursion of cold air was studied by Garreaud (2000) using 1979-1995 data from the NCEP-NCAR reanalysis (NNR). Northward-moving cold surges were found to be a leading mode of synoptic-scale variability of low-level circulation east of the Andes, causing temperature variations and even freezing conditions during winter and summer. Also based on NNR, Müller and Berri (2007) explored the atmospheric circulation leading to generalized frosts in central-southern SA during winter for 1961-1990 and found a double (single) pattern of Rossby waves over the South Pacific leading to persistent (less persistent) events. Recently, Sprenger et al. (2013) analysed from a potential vorticity perspective the precursor waves of cold surge episodes over southeastern Brazil.

As shown above, perturbations of circulation over the South Pacific leading to climate impacts in SA have been studied with various motivations and methodologies. In this context, the PSA modes 1 and 2 have been identified focusing on different seasons and time scales (e.g. Berbery et al. 1992; Mo and Paegle 2001; Müller and Ambrizzi 2007; Zamboni et al. 2012). These PSA modes, which represent arched wavetrain-like circulation patterns over the South Pacific towards SSA, appear as the leading EOFs of low-frequency variability and are in spatial-phase quadrature, which points to a propagating wave.

Robertson and Mechoso (2003) also documented an oscillation of 42.5 days dominated by the PSA 1 pattern, more pronounced in austral winter and spring, which shows a rapid attenuation and an eastward drift. In summary, they proposed an oscillation of circulation anomalies in the South Pacific that is predominantly stationary in space, but with regimes that account for the slow part of that oscillation. Thus, some predictability of the related circulation anomalies was suggested.

Relatively less work has focused on the way these circulation patterns spread throughout a broad frequency range. Cazes-Boezio et al. (2003), motivated by the analysis of seasonal precipitation in Uruguay, studied the ENSO teleconnections over SA and its seasonal dependence during OND, JF, and MAMJJ for the period 1968-1997 using the NNR. ENSO was found to be connected with SA through a pronounced Walker cell in all those seasons. For austral spring, they found an extratropical teleconnection between ENSO and Southeastern SA due to a wave train pattern over the South Pacific, which disappears during summer. A similar wave-like pattern, but not related to ENSO, appears in autumn again over the South Pacific. A cluster analysis performed on intraseasonal 700-hPa geopotential height fields revealed 3 similar wave-train like circulation regimes in all studied seasons. Finally, interannual 200-hPa circulation patterns were found to

be related to the frequency of occurrence of those intraseasonal regimes for spring and autumn but not for summer. While in spring latent heating anomalies related to ENSO seem to trigger Rossby waves and thus modify the circulation regime frequency, in autumn and winter the interannual teleconnection appears to be related to random changes of the frequency of occurrence of intraseasonal regimes. Therefore, their results show that the connection between different timescales during summer may not be due to the frequency of occurrence of distinct circulation patterns. Hence, one possible hypothesis would be that few but strong and/or persistent intraseasonal anomalies would imprint their signal in the seasonal means, thus contributing significantly to the construction of the interannual variability. Thus, we also aim to study the link between both timescales.

3.1.5 Aims of present work and structure

Consequently, in this paper we address the development of heat waves in the intraseasonal timescale over SEPG during 1872-2010. Our approach is based upon the Twentieth Century Reanalysis version 2 (20CRv2, Compo et al. 2011). That is, we explore the regional and large-scale aspects associated with our research subject reproduced by this reconstruction. In addition, century-long daily climatic records will be used in order to compare and partially validate the results obtained.

The data and methods used are detailed in Section 3.2. In Section 3.3, we describe the identification of heat waves in SEPG and discuss their regional manifestation. Besides, we interpret the large-scale circulation anomalies associated with these events, with a focus on Oceania in order to understand, in the intraseasonal band, the covariability between SAT in SSA and precipitation in SE Australia and New Zealand. In Section 3.4, we describe the fields associated with the intensity of the heat waves in SEPG and the link with the variability of the SACZ. Section 3.5 presents the analysis on the potential connection between the intraseasonal and interannual patterns that lead to SAT perturbations in SSA. A possible decadal variation of the waveguide of these intraseasonal circulation anomalies is briefly discussed in Section 3.6. Finally, Section 3.7 summarizes our findings and conclusions.

3.2 Data and methods

We use non-detrended daily fields of SAT (2m), mean pressure at sea level (SLP), geopotential height at 500 hPa (z500), precipitation rate (prate), and vertical velocity at 500 hPa (ω500) from the ensemble mean of 20CRv2. Vertical velocity at 500 hPa was selected as a proxy for large-scale ascent and descent due the lack of OLR fields in this dataset. We focus on DJF (December 1st to February 28, without considering leap years) during 1872-2010 (DJF seasons are assigned to the corresponding JF year). This period comprises a total of 12510 days. The intraseasonal anomalies are defined following the method of Cerne and Vera (2011) as the result of subtracting from the daily values the climatological daily mean (annual cycle) and the seasonal departures of every year from the climatology (i.e., the DJF mean of each year minus the long-term seasonal mean). In other words, we consider that the absolute temperature for a certain day is made of the sum of the expected long-term value defined by the yearly cycle plus the mean seasonal anomaly of the corresponding year plus the intraseasonal anomaly, which accounts for the higher-frequency perturbation. That is, the intraseasonal anomaly of a given variable for a certain day d and year y is calculated as:

$$
\begin{aligned}
\textit{intraseasonal anomaly}_{d,y} \\
= \textit{daily value}_{d,y} - \textit{climatological daily mean}_{d} \quad\quad (3.1)\\
- (\textit{DJF seasonal mean}_{y} - \textit{long--term DJF seasonal mean})
\end{aligned}
$$

The reference period for defining long-term statistics (mean, standard deviation, seasonal cycle, etc.) and anomalies is 1961-1990. For simplicity, in the rest of the paper, an apostroph will denote intraseasonal variables.

We first calculate daily SAT anomalies on the intraseasonal timescale (T') as the spatial mean of the 5 gridpoints within SEPG (Fig. 3.1a). Then, we detect heat waves according to both following criteria (Cerne and Vera 2011), which must be met at the same time: a) T'>0 for at least 5 consecutive days, and b) T' larger than its own standard deviation for at least 3 days.

For the comparison between different timescales, seasonal (interannual) DJF SAT anomalies were calculated for SEPG with respect to the 1961-1990 mean by subtracting from the detrended DJF seasonal mean series the interdecadal components, obtained previously by applying to it a 7-years running mean twice (which consequently reduced their length at the beginning and the end by 6 years each).

The observational temperature dataset used in this study spannig 1957-2010 was

supplied by the Argentinean National Weather Service. Their intraseasonal anomalies were obtained in a similar way as those from the reanalysis data. Precipitation records from Oceania were provided by the Australian Bureau of Meteorology and the New Zealand National Climate Database (see Acknowledgments section for details).

3.3 Intraseasonal heat waves in SEPG: regional and large-scale anomalies

A total of 460 days satisfy both conditions defined for detecting heat waves. Since many of these days occur in clusters, we select the first day of every group to characterize each single event and name that day $d0$. So defined, we obtain 201 heat waves within the studied period, which we consider to be independent. The mean duration of a heatwave (defined here as the number of consecutive days that satisfy the conditions presented in Section 3.2) is ~2.3 days. Single events within a season are separated by a median (mean) of 20.5 (24.9) days, with a minimum of 4 days and a maximum of 64 days. During 1872-2010 (1900-2010) the mean value of events per season is 1.45 (1.59), with a trend of 0.66 (0.30) events per 100 years, statistically significant (non-significant) at 95%.

3.3.1 Time evolution of heat waves and sequences of related composites

a) Heat waves in Southestern Patagonia (SEPG)

We start by analysing the 21-day composite sequence of T' centred on $d0$ (Fig. 3.1b) for all heat wave events identified at the SEPG region (Fig. 3.1a). T' does not deviate substantially from 0 until day -3, when the values increase sharply and reach a mean anomaly of 4.3°C on $d0$. After day 1, T' decreases less rapidly in comparison to the first half of the sequence (+1.6 K/day between days -1 and -3 compared to -1.1 K/day between days 1 and 3, and lower cooling rates thereafter). In fact, the +2°C anomaly is exceeded between days -2 and 3. Thereafter, positive anomalies over +0.5°C last almost day 8. The asymmetry of the T' signal partly reflects the fact that, by definition, $d0$ is the first day satisfying the conditions for a heat wave. Because some events include several of those days, they define a heat wave that begins on $d0$. A similar asymmetric evolution is observed for z500' over SEPG (Fig. 3.1c, red curve). This series shows its maximum amplitude of ~100 gpm on day -1; that is, it leads that of T' by one day. As expected
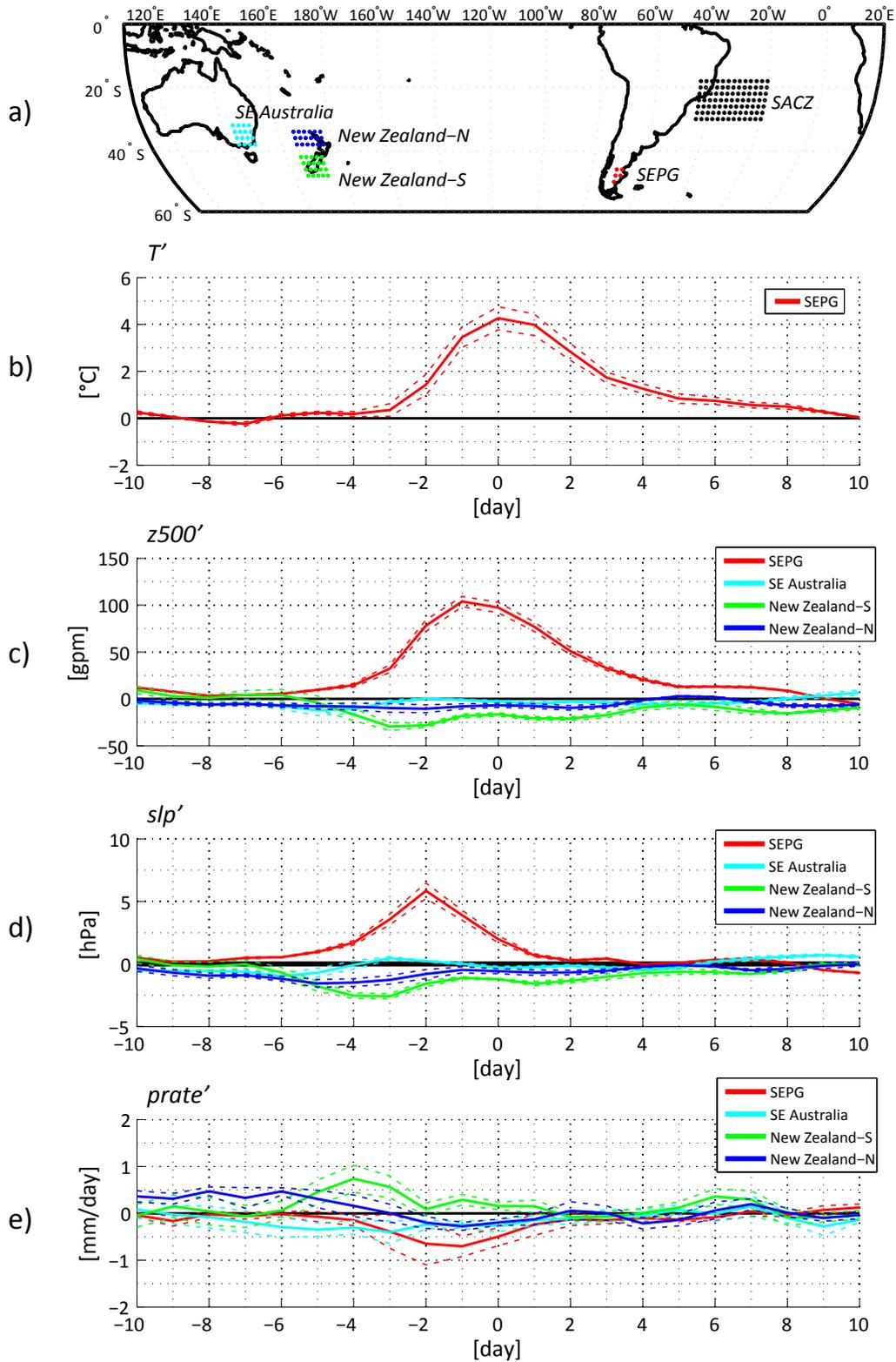
Fig. 3.1: *a) Definition of regions analysed in this study: SEPG (red, 46°-52°S;65°-70°W), SACZ (black, 18°-30°S; 20°-44°W), SE Australia (cyan, 30°-39°S;144°-150°E), North Island of New Zealand (blue, 32°-38°S;166-178°E), South Island of New Zealand (green 42°-50°S;166°-176°E). b-e) 21-day mean time series of T', z500', slp' and prate', respectively, centred on day 0 (d0), as defined for the 201 heat waves in SEPG. Continuous (dashed) curves correspond to the composite spatial mean (standard deviation) of the corresponding regions.*

within the development stage of a baroclinic wave, the positive slp' perturbation, whose sequence depicts an anticyclone over SEPG, leads that of z500' (T') by one day (two days) (Figs. 4.1c-d, red curves). Mirroring the slp' sequence and consistently with the accompanying subsidence conditions, we observe a negative prate' anomaly in SEPG between days -4 and 1 (Fig. 3.1e, red curve).

The spatial fields W these anomalies are displayed in Figure 3.2, restricted to the 7-day sequence between days -3 and 3. In the upper row, we observe the intrusion of the anticyclonic anomaly from the southwest into SSA, to the east of the Andes. As noted before, the slp' maximum is located directly to the east of SEPG on *d0*. This anomaly is associated with the development of a temperature dipole in the T' composite (Fig. 3.2, middle row) with warm (cold) anomalies to the south (north) of ~35°S. The mean T' perturbation exceeding 2°C over SEPG typically lasts from day -2 until day 3. During this sequence of days, dry anomalies persist in the southern tip of the continent (stronger in southwestern Patagonia), ahead of the anticyclonic anomaly (over the southwest Atlantic), and in southeastern SA (SESA; Fig. 3.2, lower row).

Summarizing all, the slp', T' and prate' fields show the expected relationships associated with the development of a mid-latitude disturbance. For instance, on day -1, the wet pattern shown by the prate' field is an imprint of the mid-latitude cyclonic anomaly centred at ca. 40°S; 25°W with SE-NW orientation towards the continent at 20°S. Behind that cyclonic anomaly, the anticyclonic anomaly peaking to the east of SSA seems to drive the dry anomaly ahead of it and the T' increase over the continent. Hence, heat waves in SEPG, large-scale ascent in the SACZ, and large-scale descent in Patagonia (inferred rom the prate' field) are related to the eastward evolution of alternating cyclonic and anticyclonic anomalies. These aspects are further explored in Section 3.4.

The possible drivers of the local heating in SEPG, expressed in the thermodynamic energy equation, are the temperature horizontal advection plus adiabatic and diabatic processes. Cerne and Vera (2011) showed, indeed, that the physical processes contributing to the occurrence of heat waves in subtropical South America are essentially the advection of temperature and diabatic effects. Although a detailed analysis of these terms lies beyond the aims of this work, we first study the radiative effect (one of the diabatic terms) and then the near-surface horizontal temperature advection.

The intraseasonal anomaly of the downward shortwave radiation flux at the surface (Fig. 3.2a) exhibits positive values between ca. 37°S and 50°S around *d0.* The signal is related to the easterly anomalies of wind at 10 m, which inhibit the moisture advection and the development of cloudiness and precipitation in the western part of the Andes. The positive anomaly of downward radiation flux moves eastward and peaks
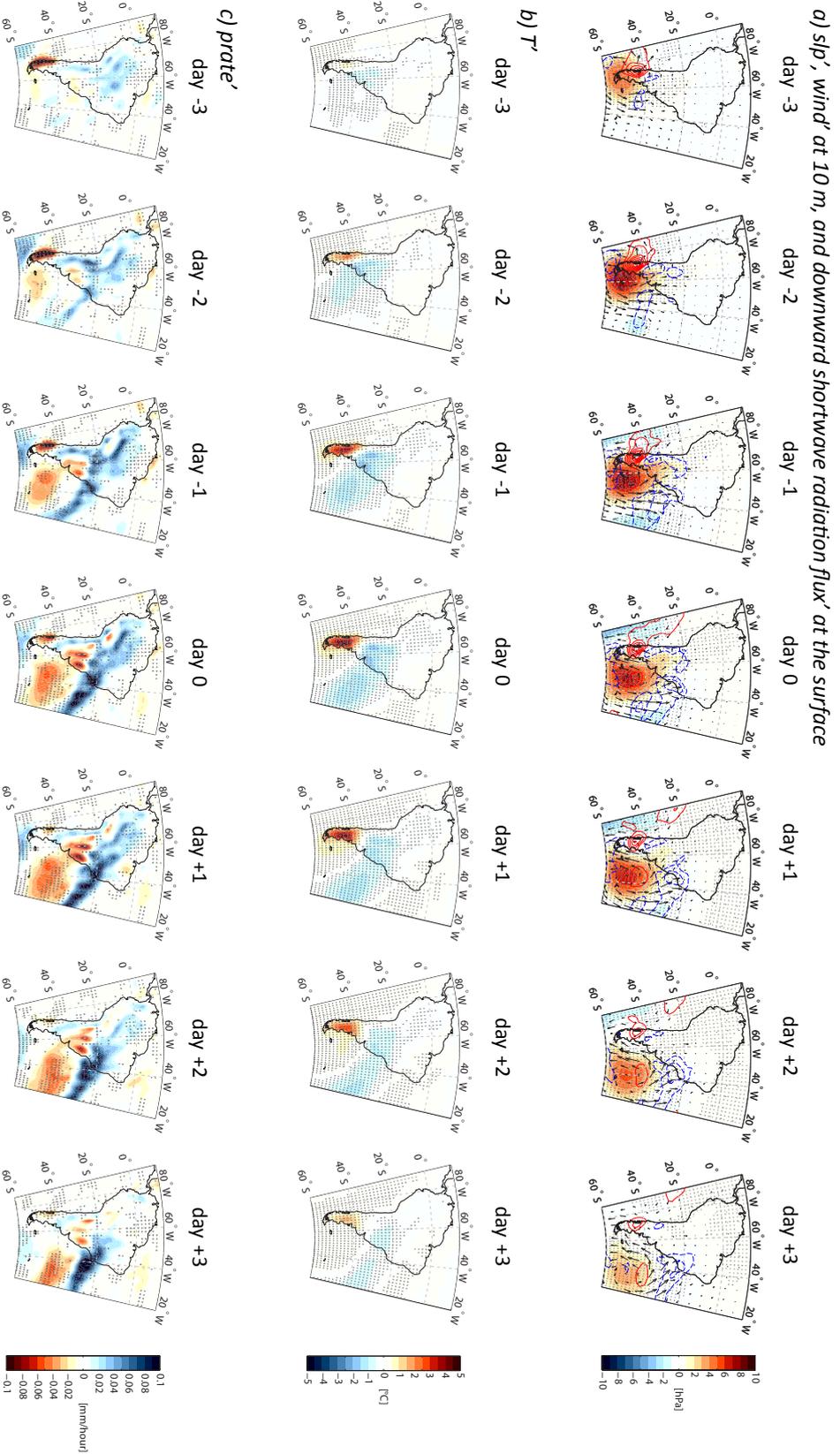
Fig. 3.2: *Composite fields of intraseasonal anomalies over South America of the 201 heat wave events, centred on day 0 (d0), from day -3 until day 3. Upper, middle and lower panels show the sequences of a) slp' (shaded contours every 1 hPa), wind' at 10m (vectors), and downward shortwave radiation flux' at the surface (empty contours every 10 W/m2), b) T' (shaded contours every 0.5°C), and c) prate' (shaded contours every 0.01 mm/hour). Reddish (bluish) colours denote positive (negative) anomalies; zero contour omitted. Black dotes denote values which are statistically significant at 95%; for prate' a Monte Carlo calculation was made with 500 composites of 201 members.*

on day -1 over SEPG. On that day, the positive anomaly reaches its highest value, exceeding 60 W/m^2 around 43°S; 73°W and decreasing towards the Atlantic coast to ~30 W/m^2. These results suggest a positive contribution of the solar radiation to the T' development in the northern part of SEPG. A negative anomaly is observed to the south of 50°S, covering also Tierra del Fuego and peaking over the Drake Passage with values around -25 W/m^2. The negative anomalies of downward shortwave radiation fluxes are associated with cloudiness and precipitation (Fig. 3.2c). However, given the negative anomaly of this variable in this region, another factor must drive the warming in the southern part of Patagonia.

In terms of circulation, we essentially identify three main patterns related to the anticyclonic anomaly that propagates over SSA: on day -3, when the anticyclone is located over the southern tip of the continent, it promotes weak easterly anomalies over the SEPG region; between days -2 and day 0, the anticyclone intensifies while it moves eastward causing northeasterly wind anomalies over SEPG; and, between days +1 and +3, as the anticyclone has moved eastward over the south Atlantic, wind anomalies are very weak over the continent.

From day -3 on, the intraseasonal anomaly of the near-surface horizontal temperature advection (not shown) exhibits positive values over Eastern SSA, south of ~43°S. The magnitude of the spatial pattern of this variable is highest on *d0* and increases towards the south with its maximum to the south of ~50°S. This anomaly of the horizontal temperature advection is mainly driven by its zonal (easterly) component to the north of ~50°S and by its meridional (northerly) component to the south of ~50°S.

In summary, in connection with the development of intraseasonal heat waves in SEPG, we observe an enhanced downward shortwave radiation flux in the northern part of SSA (between ~37°S and ~50°S) and warm horizontal temperature advection over most of SSA (south of ~43°S).

b) Regional dynamics associated with heat wave occurrences in SEPG

As demonstrated above, heat waves occurring in SEPG are embedded in an anomalous regional anticyclonic circulation which induces a notorious warm signal in Patagonia. Therefore, in this section we explore the regional circulation dynamics associated with the heat wave events detected in SEPG.

However, as a first step, we will assess the robustness of the 20CRv2 heat wave signal from SEPG by comparing it with instrumental T' anomalies for 1957-2010 from Comodoro Rivadavia Aero (45°47'S; 67°30'W, 46 m a.s.l.) and Río Gallegos Aero (51°37'S; 69°17'W, 19 m a.s.l.; their locations are shown in Fig. 3.3), which were obtained in the same way as the intraseasonal time series from the reanalysis. The statistics of the comparison between 20CRv2 and the station data is shown in Table 3.1. In the supplementary material, Fig. 3.S1 shows the mean T' composite for heat waves from SEPG of Fig. 3.1a together with the composite calculated for the closest gridpoint to each of both stations. The instrumental time series shown there correspond to the intraseasonal anomalies of minimum temperature (Tn'), maximum temperature (Tx') and mean temperature (Tm', calculated as the arithmetic average of Tn' and Tx'). The composites of Comodoro Rivadavia, which lies at the Atlantic coast directly to the north of SEPG, show a warm bias of ~1.5°C on *d0* for 20CRv2 with respect to Tm'. Although Tx' is closer to the signal extracted from 20CRv2 than Tm' during the whole 21-day sequence, the general evolution of the instrumental anomalies is well reproduced by the reanalysis, in particular according to the timing of the T' maximum on *d0*. The measurements taken at Río Gallegos, located also at the Atlantic coast but directly to the south of SEPG, are in better agreement in magnitude with the reanalysis. At this station, Tx' surpasses the 20CRv2 mean. However, the instrumental T' peak is recorded here on day -1 and not on *d0* as in 20CRv2, a result that suggests a northward propagation of the T' signal related to heat waves in SEPG within Patagonia.

In Comodoro Rivadavia, 17 out of the 49 (~35%) heat wave events registered in 20CRv2 within 1957-2010 are related to instrumental absolute maximum temperatures above their 99% percentile. This result highlights the fact that such extreme warm events are not necessarily persistent nor mainly due to intraseasonal perturbations and therefore not always associated with our definition of heat waves.

The regional circulation dynamics associated with the heat waves at SEPG are analysed using 20CRv2, through defining neighbouring regions of SEPG and comparing their T' evolution. As shown in Fig. 3.3a, these 4 regions correspond (from North to South) to the closest gridpoint to Rosario Aereo (32°55'S;60°47'W, whose intraseasonal heat wave signal was analysed by Cerne and Vera (2011)), and to regions formed by the gridpoints located within zonal bands to the east of 70°W: R1 (36°-39.5°S), R2 (40°-44°S), and R4 (53°-55°S), following the definition used in Jacques-Coper and Brönnimann (2014). Figure 3.2b previously showed that the T' signals at R1-R4 regions are affected by the passage of the same baroclinic disturbance. The temporal evolution of the regional T' composites are shown in Fig. 3.3b-e. In R4, to the south of SEPG, the warm anomaly begins almost synchronously with that of SEPG, due to the meridional temperature advection caused by the anticyclonic circulation depicted in Fig. 3.2a.

The warming in R4 shows lower magnitude than in SEPG and reaches a maximum of nearly 3°C on *d0*. The lags observed in R2, R1 and Rosario indicate that the T' anomaly propagates from South to North. In R2, directly to the north of SEPG, the magnitude of the warm anomaly is comparable with that of the heat wave in SEPG. Although the onset of the event in R2 occurs later than in SEPG, after *d0* both signals evolve similarly, and thus the local warm perturbation lasts less than in SEPG. In R1, we observe a cold perturbation on day -2 (associated with the cold advection promoted in that region by the southeasterly wind anomaly induced by the anticyclone) that evolves later into a local warming anomaly, reaching a moderate maximum of nearly 2°C on day 2. Further north, next to Rosario, we just recognize a cold perturbation which is almost in phase with the heat wave signal from SEPG. This subtropical cooling corresponds to the temperature dipole pattern induced by the trough-ridge system.

In summary, a typical heat wave in SEPG is accompanied by a regional warming effect throughout Patagonia, which is first observed at the southern tip of the continent and moves northward. Moreover, at subtropical latitudes, these events are related to moderate cooling. That is, heat waves in Rosario, described previously by Cerne and Vera (2011), do not occur in connection to those in SEPG. Although those events are also linked to a wave train pattern over the South Pacific Ocean, they bear different large-scale characteristics, such as different phasing.

3.3.2 The wave train pattern over the South Pacific

In this subsection, we analyse the midlevel circulation anomalies associated with intraseasonal heat waves in SEPG on the hemispheric scale. They are described by the intraseasonal anomalies of geopotential height at 500 hPa, i.e. z500'. The 15-day

Table 3.1: *Evaluation statistics of the temperature records of Comodoro Rivadavia and Río Gallegos (see Fig. 3.3a) with respect to the time series extracted from their closest gridpoints in 20CRv2. The bias [°C] and the correlation coefficient are calculated with respect to the ensemble mean of 20CRv2 and are shown for the instrumental absolute values (abs.) and their intraseasonal (IS) anomalies. The period of reference is 1957-2010*

|	Tn		Tx		Tm	
Station	abs.	IS	abs.	IS	abs.	IS
Comodoro Rivadavia	-3.73 / 0.64	-0.01 / 0.62	8.57 / 0.64	-0.01 / 0.63	2.42 / 0.71	-0.01 / 0.69
Río Gallegos	-2.41 / 0.59	0.00 / 0.56	9.70 / 0.63	0.00 / 0.61	3.67 / 0.69	0.01 / 0.67
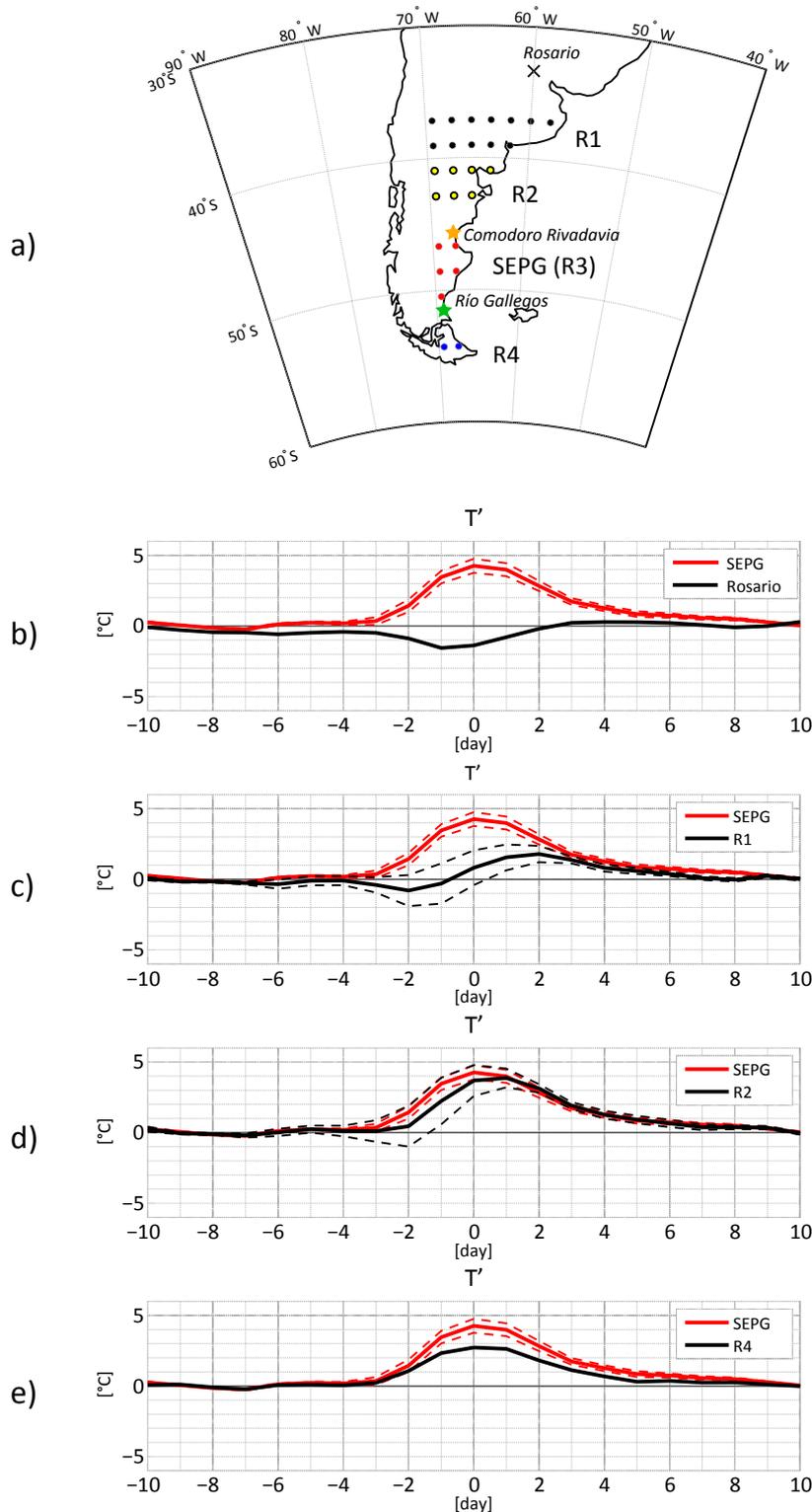
Fig. 3.3: *a) Definition of SEPG (red, 46°-52°S;65°-70°W) and regions R1 (black 36°-39.5°S, east of 70°W), R2 (yellow, 40°-44°S, east of 70°W) and R4 (blue, 53°-55°S, east of 70°W). The nearest gridpoint to Rosario Aero Station (32°55'S;60°47'W) is marked with an x. b-e) 21-day mean time series of T' in SEPG (red curve) and Rosario, R1, R2 and R4 (black curves), respectively, centred on day 0 (d0), as defined for the 201 heat waves in SEPG. Continuous (dashed) curves correspond to the composite spatial mean (standard deviation) of the corresponding regions.*

sequence of z500' composites over the South Pacific Basin centred on *d0* (Fig. 3.4) shows on day -7 a negative height anomaly to the south of SE Australia and a positive anomaly to the SE of New Zealand. From that day on, we observe both features moving eastward with a phase speed of around 6-7°/day, embedded in a developing wave train pattern, extended along the South Atlantic, from Oceania across the South Atlantic. On day -4, the negative anomaly observed on day -7 to the south of SE Australia is located over the Southern Island of New Zealand and persists in that position over the next days while its intensity decays. At the easterly edge of the wave train, we observe a strengthening ridge over the southern tip of SA. On day -1, the positive centre is located to the east of SSA and reaches its peak intensity. By day +3, the anticyclonic anomaly is centred over the Southwest Atlantic and progressively weakens.

It is worth to comment that the anticyclonic anomaly that will induce the heat waves in SPEG progresses very slowly from its location to the west of the southern tip of the continent on day -5 to day +4, when it is found off the eastern coast of SSA. Essentially, a 2-wave packet is discernible all along the evolution of the large-scale pattern, although different waves determine it. Between day -1 and day 0, the upstream wave decays while a new wave develops downstream. This could be an evidence of *downstream baroclinic development*, a process that has been identified in previous works (Lee and Held 1993; Orlanski and Chang 1993).
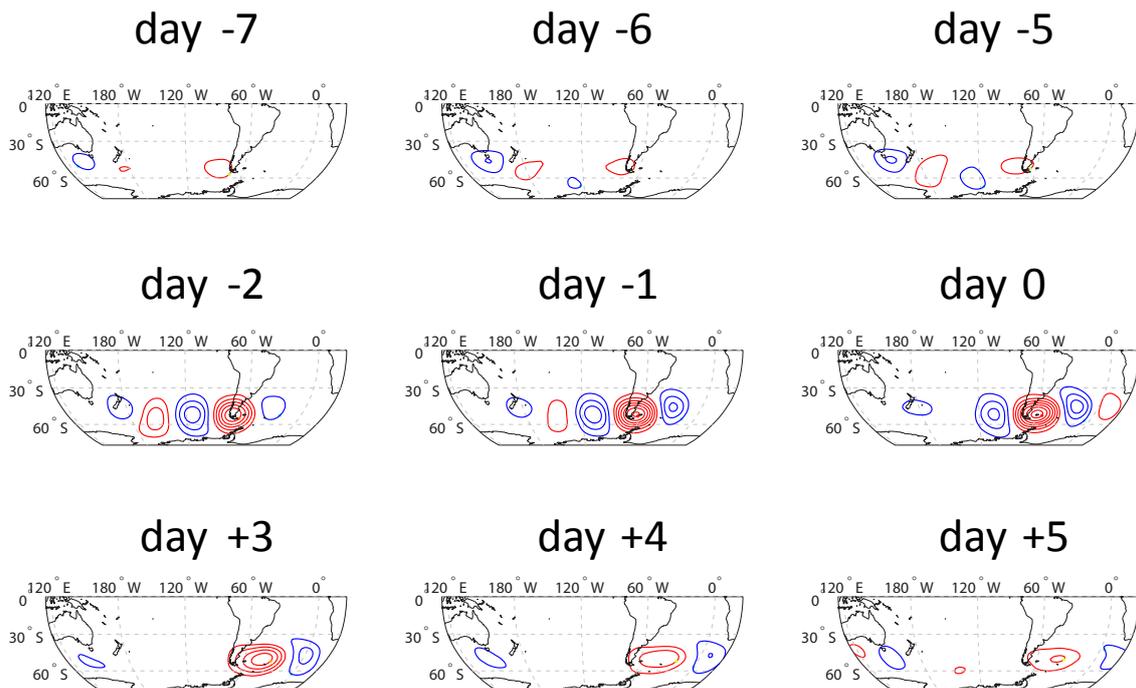
3.3.3 Circulation and precipitation anomalies in Oceania that precede heat waves in SEPG

The z500' composites suggest a relationship between the heat wave signal in SEPG and the circulation in the South Pacific and over Oceania. Similar wave trains linking climate variability over the western south Pacific region with that over South America have been previously identified on interannual timescales (e.g. Berman et al. 2013) and also on intraseasonal timescales (e.g. Liebmann et al. 2004). In this subsection we further explore the teleconnection specifically described by the anticorrelation pattern between temperature anomalies in SSA and precipitation anomalies in SE Australia on the interannual timescale (Jacques-Coper and Brönnimann 2014). A more profound understanding of this teleconnection might be useful as a further source of validation of the remote signals associated with the heat wave events in SEPG.

Figure 3.5 shows the slp' and prate' composites for Oceania based on the heat wave events identified at SEPG, displayed between day -6 and day 0. In correspondence with the eastward propagation of a slp' cyclonic anomaly over the Tasman Sea, we identify a dry (wet) pattern over SE Australia (South Island of New Zealand) that peaks around day -4. Positive prate' anomalies are observed over the North Island of New Zealand until day -5. These signals, showing dry conditions in SE Australia and wet conditions over New Zealand by day -5, are well captured in the time series of Fig. 3.1e. The dry anomaly in SE Australia during the first days of the evolution seems then to be caused by the cyclonic circulation over the Tasman Sea. Relatively dry air masses are transported
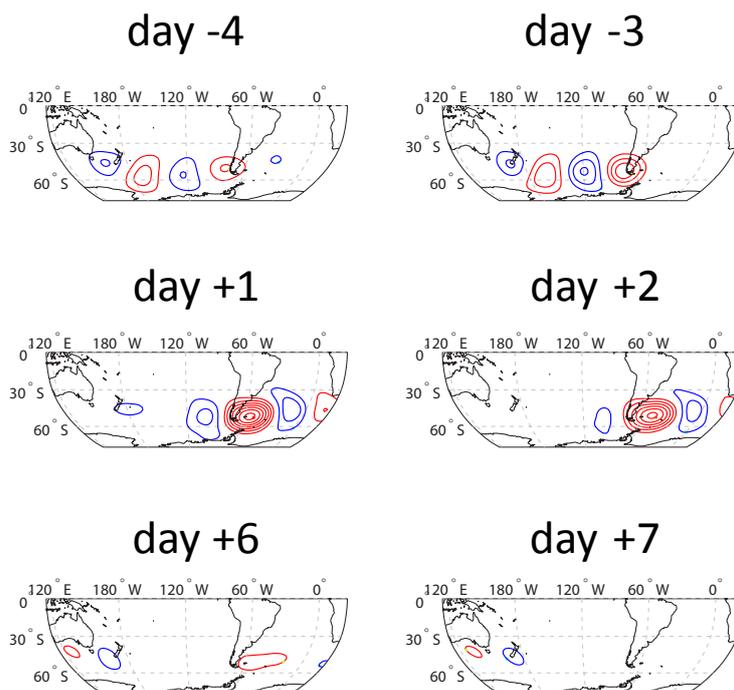
Fig. 3.4: *Composite fields of z500', considering the 201 heat wave events, centred on day 0 (d0), from day -10 until day 10. Red (blue) contours are drawn every 20 gpm and denote positive (negative) anomalies; zero contour omitted. Statistically significant anomalies at 95% are depicted by black dots.*

eastward from the Australian continent to the Sea, which is the opposite pattern of the easterly anomaly that typically leads to precipitation over that region (Rakich et al. 2008). Contrastingly, relatively moist air masses are advected by this system from the west towards New Zealand, inducing the local wet anomaly, in agreement with Ummenhofer and England (2007).

As a mean to validate our results, we use meteorological observations from SE Australia and New Zealand to analyse perturbations in rain probability related to the heat wave events identified for SEPG in 20CRv2. For that, we use composites of 21-day sequences of precipitation, centred on *d0*. The methodology followed for calculating the rain probability perturbations is described in the Appendix 1.

Figure 3.6 shows the probability perturbations of precipitation computed for SE Australia (Cataract Dam Station, upper panel) and the South Island of New Zealand (Hororata Station; lower panel) in association with heat wave events in SEPG. Black (white) bars represent the probability perturbations computed for each day of the sequence associated with precipitation in excess of 1 mm (10 mm). Blue (red) curves show the mean and 25% and 75% percentiles of the Monte Carlo distributions for those thresholds, calculated as described in the Appendix 1. In SE Australia (Fig. 3.6a), we observe almost only negative perturbations, i.e., less probability of rain in this area in connection with heat waves in SEPG. In particular, for events above 1 mm, we identify *dry conditions* between days -10 and 3, and 8 and 10 and a *wet cluster* in-between, from day 4 until day 7. The perturbation in rain probability related to events exceeding 10 mm follows a similar behaviour. Compared with the 1 mm events, in this case the probability differences are mostly lower due to the also lower frequency of these stronger events (Table 3.2). The fact that the mean distribution of the random sequences are negative points to the wet bias and the higher probability of rain exceeding the defined thresholds in this region during the reference period 1961-1990 in comparison with the whole period

a) slp'

b) prate'
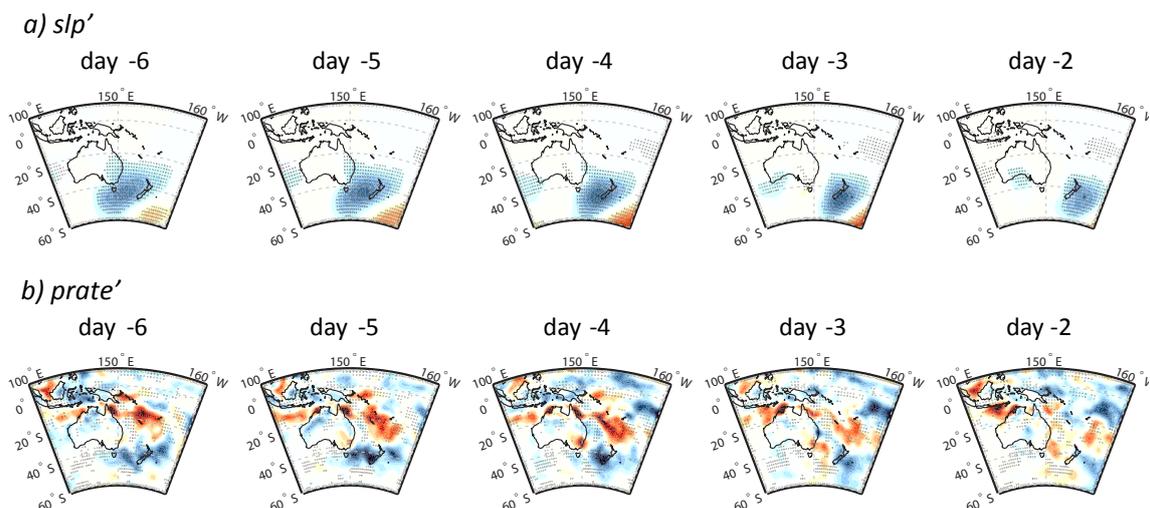
(Table 3.2).

In turn, the record from the South Island of New Zealand (Fig. 3.6b) exhibits positive probability perturbations of rain events above 1 mm, i.e. *wet conditions*, between days -10 and 0, with a peak on day -5, and again on day 7. Although the signal associated with rain events larger than 10 mm follows a similar pattern, it shows much lower amplitude, reflecting again the fact that these events are less frequent than those exceeding 1 mm (Table 3.2). The little positive departure from zero of the random 1 mm signal is not caused by a mean precipitation bias of the reference period 1961-1990 compared to the whole period but apparently by the fact that the rain probability associated with events exceeding this threshold is lower during 1961-1990 (Table 3.2).

We conclude that the precipitation probability perturbations in SE Australia and New Zealand, concurrent with the occurrence of heat wave events in SEPG detected in instrumental records from both regions, confirm the prate' signals found in reanalysis data (Fig. 3.1e, cyan and green curves). Therefore, they provide a means for a remote validation of the robustness of the heat wave and teleconnection signals detected in 20CRv2.

3.4 Intensity of the heat wave events and the SACZ

Cerne and Vera (2011) showed that summer heat waves in Rosario (Fig. 3.3) are strongly influenced by the SACZ dynamics. Enhanced convection in the SACZ (i.e. an active SACZ) induces subsidence over this region and thus reinforces the local temperature rise through adiabatic warming and diabatic processes. In the case of heat waves in Rosario (subtropical SA), convection in the SACZ (i.e. an active SACZ) induces
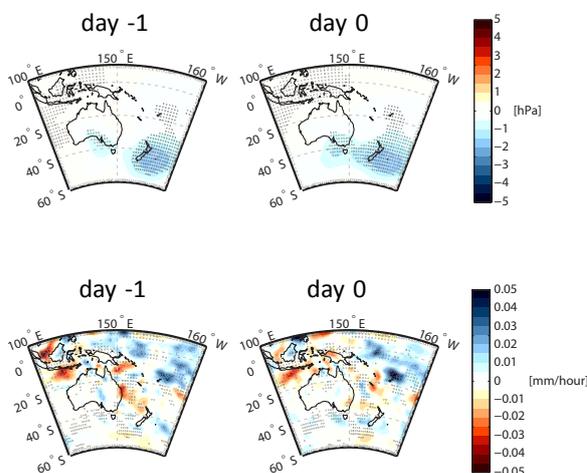

Fig. 3.5: *Composite fields over Oceania based the 201 heat wave events at SEPG, centred on day 0 (d0), and described from day -6 until day 0. Upper and lower panels show the sequences of a) slp' and b) prate'. Reddish (bluish) colors denote positive (negative) anomalies. Contours every 0.5 hPa and 0.005 mm/hour; zero contour omitted. Black dots denote values which are statistically significant at 95%; for prate' a Monte Carlo calculation was made with 500 composites of 201 members.*

subsidence over this region and thus reinforces the local temperature rise through adiabatic warming and diabatic processes (Cerne and Vera 2011). The sub-monthly (2-30-day range) variability of the SACZ is related to a nearly equivalent barotropic wave train circulation pattern over the South Pacific (Liebmann et al. 1999), a feature that resembles the results presented in this study. Moreover, Lima et al. (2010) found a well-defined wave train over the south Pacific and SA, with a strong ridge over Argentina and

a) Cataract Dam, Southeastern Australia
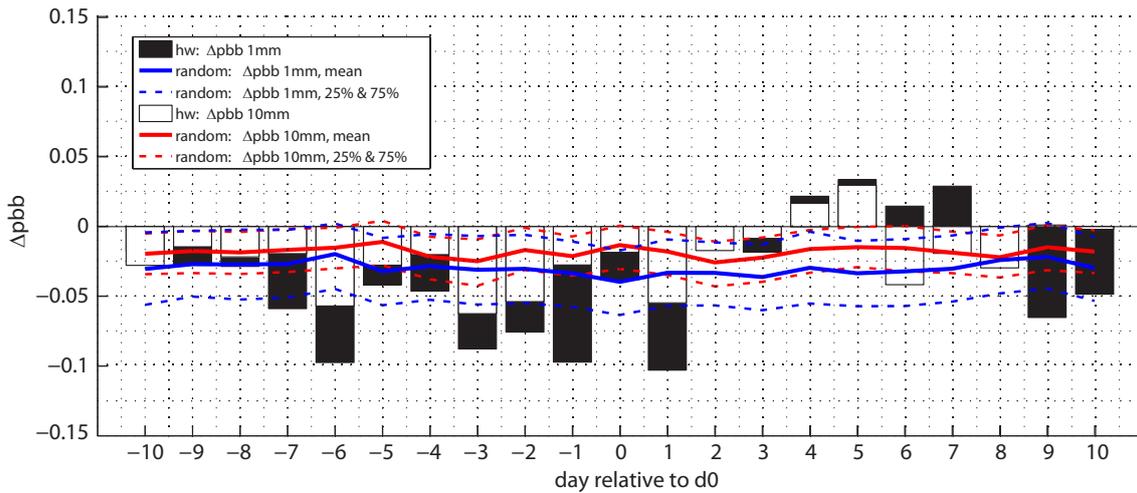
b) Hororata, Southern Island, New Zealand
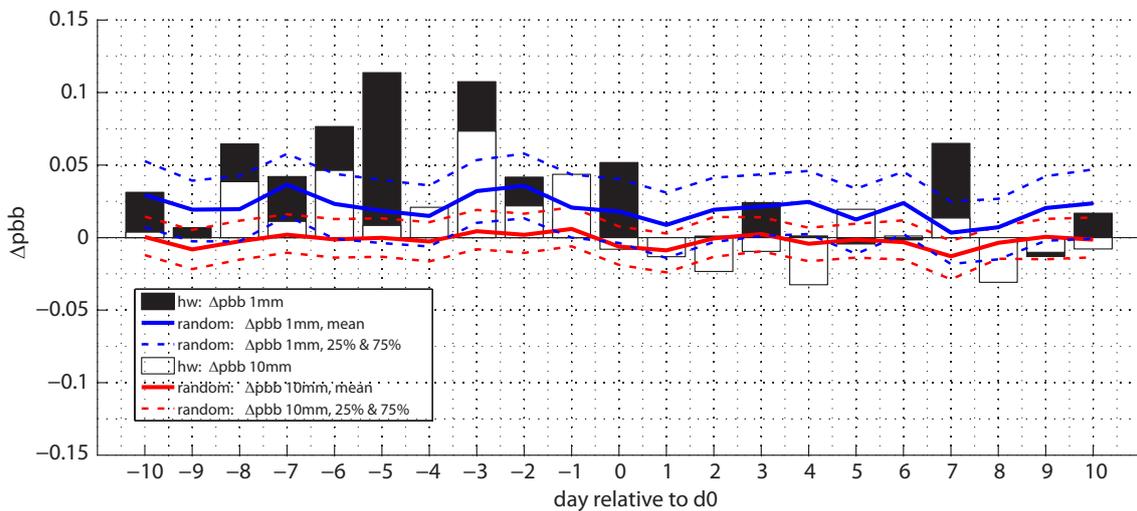
Fig. 3.6: *Changes in probability of rain exceeding 1 mm and 10 mm (black and white bars, respectively) during the 21-day sequence of days centred on day 0 (d0) for a) Cataract Dam Station (Southeastern Australia) and b) Hororata Station (South Island of New Zealand); see Table 3.2. The reference period is 1961-1990. Thick blue and red curves depict the mean values obtained for events above 1 mm and 10 mm, respectively, through a Monte Carlo approach of 1000 random realizations; thin curves represent the 25% and 75% percentiles of the corresponding distributions.*

active SACZ conditions in association with heavy rainfall episodes in southeast Brazil. Indeed, a remote manifestation observed in connection with the heat waves in SEPG is a wet anomaly signal in the SACZ from day -2 on (Fig. 3.2c). Because the SACZ, a quasi-stationary system, is related to several climate impacts in SA, as shown above, it is of interest to explore to which extent the intraseasonal variability of convection in that region is linked to the development of heat waves over SEPG.

To investigate the connection between the SACZ and the heat waves in SEPG, we define a SACZ index as the spatial mean value of ω500 anomalies within 18°-30°S; 20°-44°W (Fig. 3.1a). For this definition, as in Cerne and Vera (2011), we use anomalies that result from subtracting the seasonal cycle from the raw values but retaining the interannual anomalies. We classify the daily SACZ activity based on the area-mean sign of these local ω500 anomalies. Hence, an active (non-active) SACZ corresponds to abnormal ascent (descent) conditions determined by negative (positive) ω500 anomalies spatially averaged over the SACZ region (Fig. 3.1a), hereafter denoted as A_SACZ (NA_ SACZ).

The dynamical conditions associated with heat wave events in SEPG discriminated by the SACZ activity are displayed in Fig. 3.7. Our results show that 135 out of the 201 heat wave events (67.2%) occur during active SACZ periods. As shown in Fig. 3.7a, these cases exhibit an enhanced ascent band in the SACZ region and a subsidence area over SESA (at around 30°S), being both anomalies oriented in the NW-SE direction and extended well into the southwest Atlantic. Also weak ascent is observed over the southern tip of the continent. In contrast, non-active SACZ cases (Fig. 3.7d) imply very weak subsidence over the SACZ, suppressed subsidence over subtropical SA and the

Table 3.2: *November-March (NDJFM) precipitation statistics for two stations in Oceania*

| NDJFM precipitation	Cataract Dam Station (SE Australia) 34.26°S; 150.81°E, 340 m a.s.l., record length: 1905-2006		Hororata Station (South Island of New Zealand) 43.546°S; 171.898°E, 213 m a.s.l., record length: 1891-2010	
reference period	long-term (whole record)	1961-1990	long-term (whole record)	1961-1990
seasonal mean	445.4 mm	568 mm	356.1 mm	354.1 mm
daily mean	3.2 mm	3.8 mm	2.4 mm	2.4 mm
daily mean probability of precipitation >1 mm [>10 mm]	27% [9%]	30% [10.6%]	27.3% [7.5%]	26% [7.8%]

southwest Atlantic (spatially more restricted than in the previous case) and ascent again over southern Patagonia. As a consequence, the ω500' difference field (Fig. 3.7g), calculated as A_SACZ – NA_SACZ, shows a similar ascent-subsidence-ascent pattern as for the A_SACZ cases, although no signal is detected over SEPG. Thus, we can only infer that stronger heat waves are related to stronger ω500' anomalies over the southern half SA. No significant upstream effect of the SACZ on SEPG can be identified.

The corresponding z500' sequences (not shown) reveal stronger anomalies within the wave train pattern in the South Pacific in connection with A_SACZ events. In particular, the anticyclonic anomaly over SSA appears sooner and is more pronounced
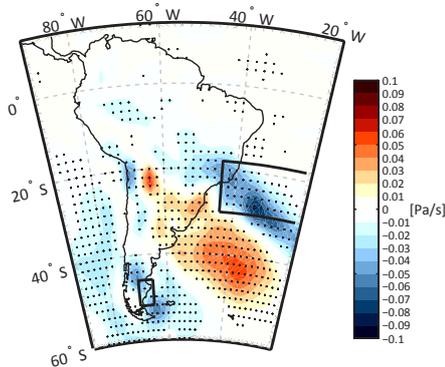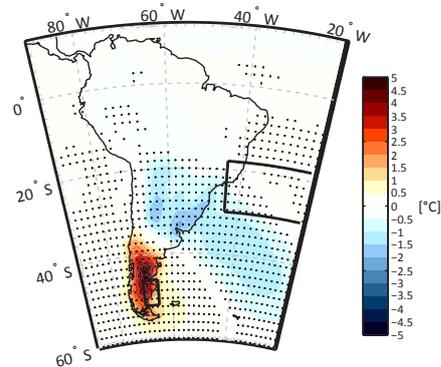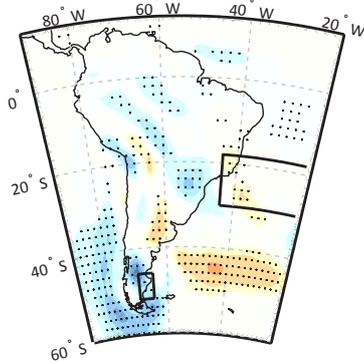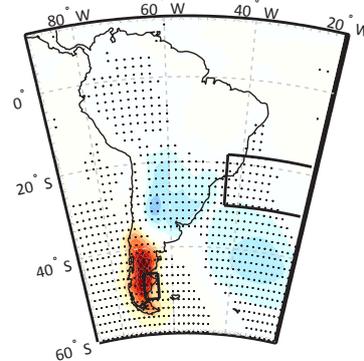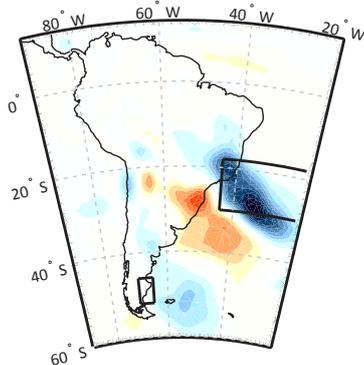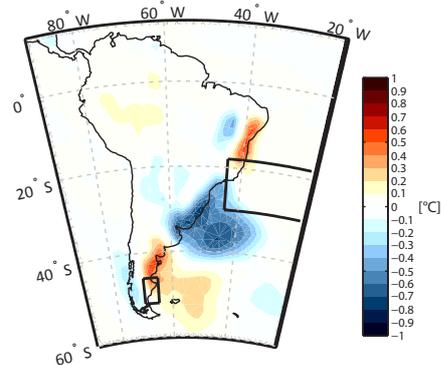
in the A_SACZ composite than in the NA_SACZ one. This feature seems to slightly enhance the warming observed before and at the peak of the heat wave (*d0*) for the A_SACZ composite with respect to the NA_SACZ composite (Fig. 3.7i; T' differences of +1.8°C on day -6 and +0.3°C on *d0*).

As a final step, we explore whether the T' signal of heat waves in SEPG is directly related to the intensity of the ascent/descent patterns over SA, depicted by the ω500 anomalies. For that, we select the upper and lower quartiles from the T' value at *d0* of all heat wave events in SEPG (named p75 and p25, respectively), as a way to compare *strong* and *weak* events. The corresponding composite fields of ω500' and T' (along with their differences), as well as the mean 21-day T' sequences around *d0* are shown in Fig. 3.S2. The mean T' on *d0* is ~6.4°C for p75 and ~2.9°C for p25 (Fig. 3.S2c,f). Furthermore, in association with the p75 composite, the positive anomaly after *d0* lasts until day 10, whereas that of the p25 composite just lasts until day 5 (Fig. 3.S2i). The spatial patterns of T' are comparable for these two composites (Fig. 3.S2b,d) and resemble the overall mean pattern shown in Fig. 3.2 for the whole dataset: warming over SSA and cooling in the subtropical region. However, the cooling signal in subtropical SA is more intense and oriented in a more meridional way in the p75 case, a fact that is reflected
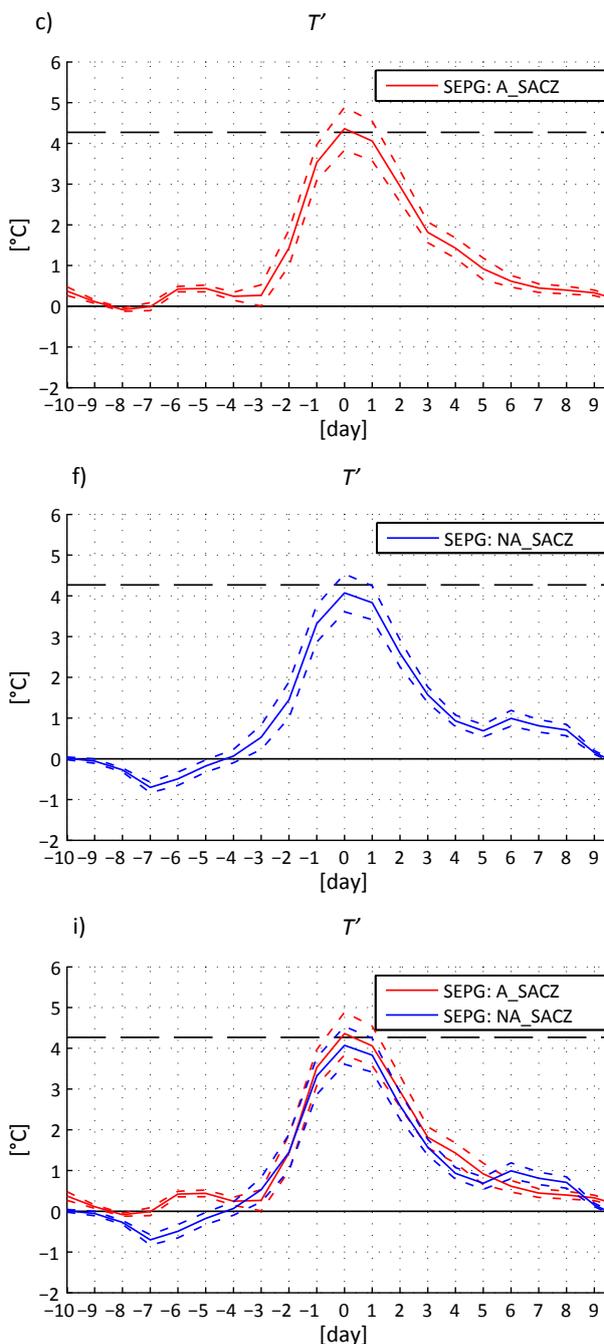
Fig. 3.7: *Composites of a,d,g) ω500' and b,e,h) T', and 21-day T' sequences centred on day 0 (d0) for: a,b,c) the 135 active SACZ (A_SACZ) cases and d,e,f) the 66 non-active SACZ (NA_SACZ) cases from the total of 201 heat wave events in SEPG;g,h,i) difference fields between A_SACZ and NA_SACZ. The panels in c,f,i) show the 21-day time series of T' for the corresponding composites. Interval units are 0.01 Pa/s for ω500' and 0.5 K for T'.*

in the spatial pattern of the T' difference (p75-p25). The ω500' spatial patterns exhibit ascent over the southern tip of SA, subsidence over the southwest Atlantic and to the north of SEPG, and ascent again over subtropical SA and in the SACZ region. As in the case of T', the features shown by ω500' are more pronounced for p75 than for p25. Therefore, we conclude that the magnitudes (but not the spatial patterns) of the regional T' and ω500' anomalies are directly related to the intensity of the heat waves.

3.5 The relationship between the intraseasonal and the interannual circulation anomalies

In this section, a possible link between the intraseasonal heat wave events in SEPG and the interannual variability of the DJF temperature means is analysed. For that, we use the DJF SAT anomaly time series over SEPG (1878-2004) described in Section 3.2. Extreme positive (negative) years are defined as those whose seasonal SAT mean exceeds one long-term standard deviation (0.63°C). We found that 21 heat waves occur in the 16 extreme positive years and 25 events in the 17 extreme negative years. This result means that the 16 (17) extreme positive (negative) years, which correspond to the 12.6% (13.4%) of the total record length of 127 years, account for 10.5% (12.4%) of the total 201 heat wave events. Therefore, this finding indicates that heat waves do not tend to concentrate in years with extreme seasonal means.

The relationship to be analysed between both timescales is the spatial structure
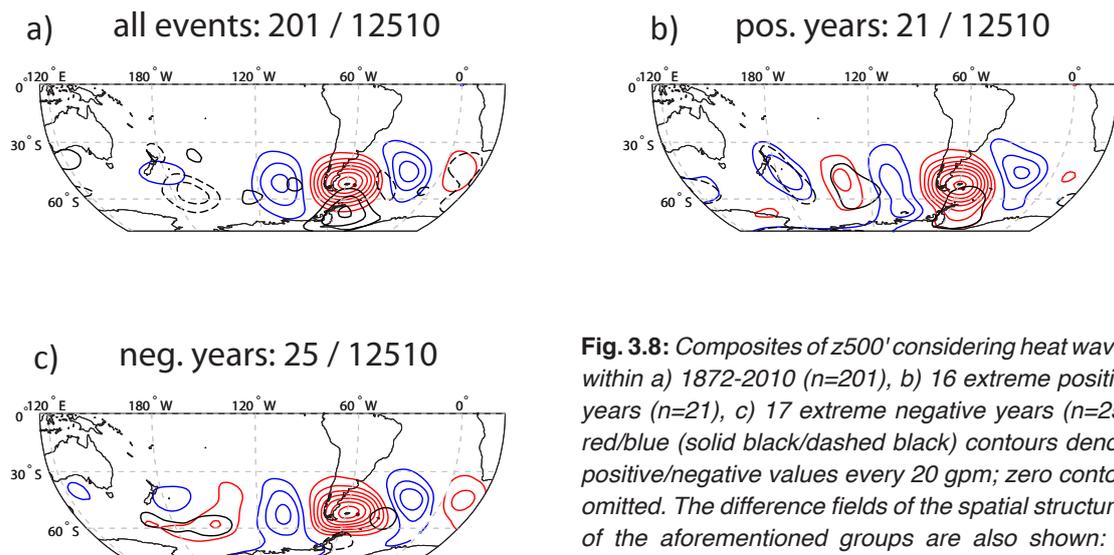
Fig. 3.8: *Composites of z500' considering heat waves within a) 1872-2010 (n=201), b) 16 extreme positive years (n=21), c) 17 extreme negative years (n=25); red/blue (solid black/dashed black) contours denote positive/negative values every 20 gpm; zero contour omitted. The difference fields of the spatial structures of the aforementioned groups are also shown: a) positive extreme years — negative extreme years, b) positive extreme years — all events and c) negative extreme years — all events; solid black/dashed black contours denote positive/negative values every 20 gpm; zero contour omitted.*

of the wave train patterns leading to heat waves in SEPG in positive and negative extreme years, respectively. Figure 3.8 shows the wave train pattern observed on *d0* for the composite of a) all 201 heat waves, b) 21 heat waves within extreme positive years, c) 25 heat waves within extreme negative years, and their respective difference fields. The anomaly of extreme positive years compared with all events (Fig. 3.8b, black contours) indicates that the wave train associated with this group bears stronger centres of action, which also extend further to the South. In contrast, the anticyclonic anomaly over SSA associated with extreme negative years (Fig. 3.8c) seems to be meridionally more restricted than that in the composite of all cases (Fig. 3.8a). Consequently, the difference between positive and negative extreme years (Fig. 3.8a, black contours) exhibits a positive anomaly to the south of SSA and a negative anomaly to the southeast of New Zealand. We conclude that the anomalies related to the action centres of the wave train pattern within extreme positive years tend to be stronger and spatially broader than those of the composites of extreme negative years and also than those of the composite of all events.

A complementary cluster analysis of z500' is presented in Appendix 2.

3.6 The decadal variation of the circulation anomaly waveguide

Given the availability of long-term reconstructions, an aspect worth of being investigated is the possible temporal variation of the spatial structure of the wave train pattern identified in z500' in association with heat wave events in SEPG. In SSA, the interdecadal summer SAT variability is dominated by a mode that is correlated to the PDO since the 1960s but appears to be out of phase with it during the first decades of the 20th century (Jacques-Coper and Brönnimann 2014). This main interdecadal variability mode defines warm decadal periods between early 1910s and early 1930s and between late 1970s and mid-1990s and a cold period amid them. Therefore, in this section we compute separate composites of z500' conditions associated with heat wave events in SEPG for the following sub-periods: 1911-1930, 1935-1975 and 1981-2000. The number of heat waves (n) occurred within each of these three periods are n=27 or 1.35 events/year; n=69 or 1.68 events/year; and n=49 or 2.45 events/year, respectively. The corresponding z500' composites, along with the composite computed for the whole period, 1872-2010, are shown in Fig. 3.9, spanning between day -2 and day +2 from *d0*.

It is worth to point out that geopotential heights at 500 hPa are derived in the 20CR dataset from observations of surface pressure only, which are combined with

background first-guess fields supplied by global model forecasts (Compo et al. 2011). Therefore, considering the important deficiencies in the observation spatial coverage in the SH, particularly during the early decades, the geopotential height fields are model dependent. Caution should be taken then in the conclusions that emerge from these composites. Figure 3.9 shows that wave-trains are evident in the composites of all the periods considered. In particular, the arch shape of the z500' wave-train pattern during 1872-2010 resembles more the composite of the cold multidecadal period 1935-1979 than those of the warm periods 1911-1930 and 1981-2000, which exhibit more zonal patterns. Besides, during 1935-1979, a higher frequency of events is registered and their associated z500' anomalies appear stronger than during the preceding period. A conclusive explanation to these observations lies beyond the scope of this study and modelling work should be done in order to address these aspects. However, we suggest some links to previous results that could be of interest for further research. A strong positive trend of the SAM index, observed since mid-1970s (Marshall 2003; Thompson and Solomon 2002), has been related to a southward shift of the mid-latitude storm track
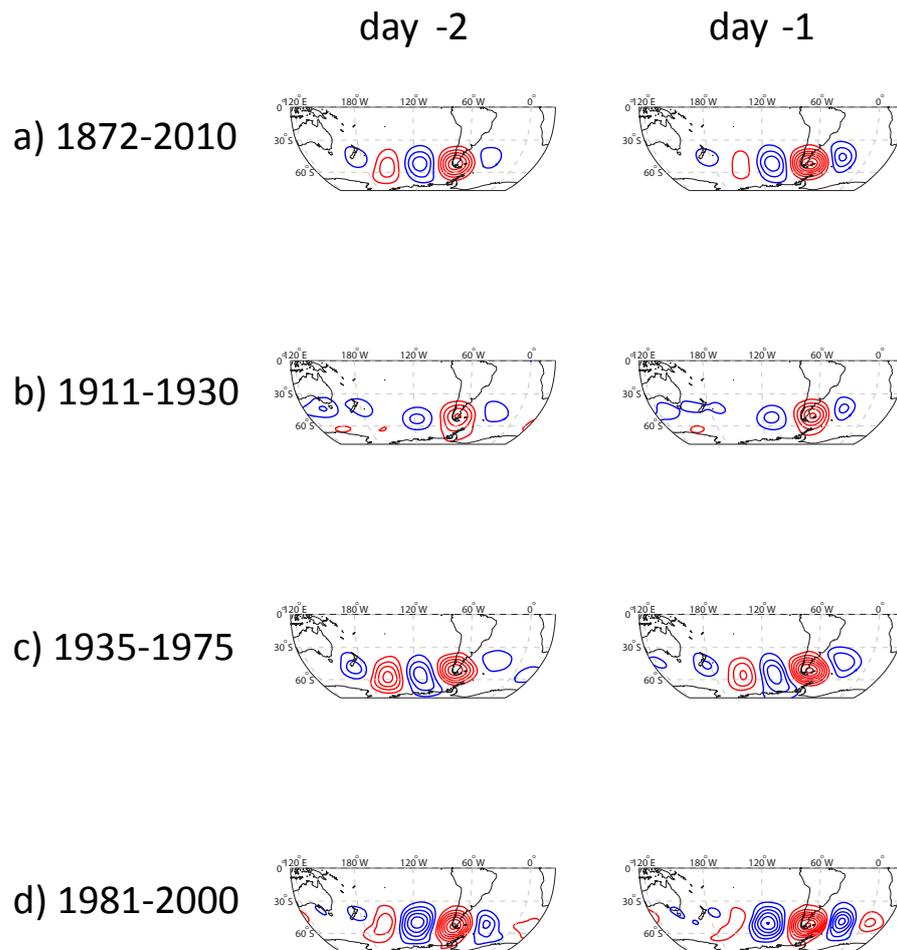
Fig. 3.9: *Sequence of composite fields of z500' between day -2 and day 2 considering heat wave event within a) 1872-2010 (201 events), b) 1911-1930 (27 events), c) 1935-1975 (69 events), and*

and in turn to the poleward shift of frontal activity in the Southern Hemisphere, mainly during the warm season (Solman and Orlanski 2013). These observations are consistent with the more zonal-shaped wave-train pattern observed during 1981-2000 in Fig. 3.9d, which does not clearly show the equatorward deflection over South America and the South Atlantic observed for the other periods. There are many possible implications of this change on the orientation of the waveguide since mid-1970s, including those related to disruptions of teleconnections between Oceania and South America (Jacques-Coper and Brönnimann 2014) and also between South America and South Africa (Compagnucci et al. 2002).
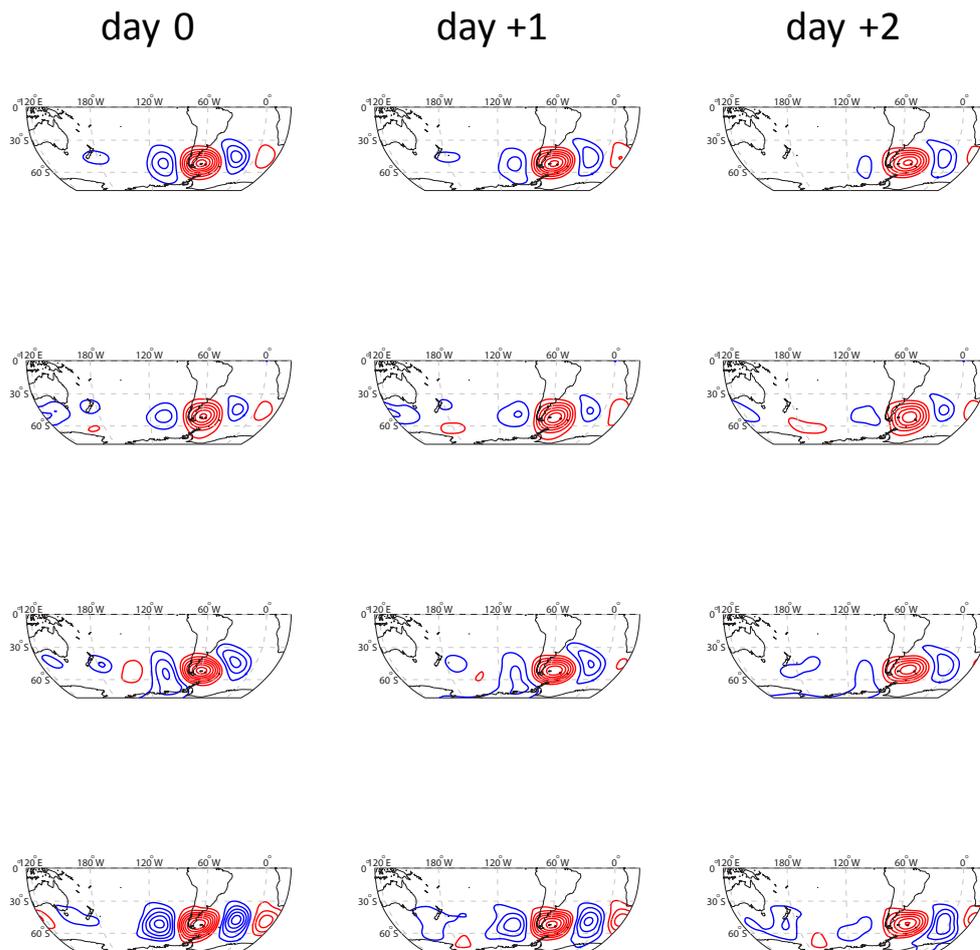
d) 1981-2010 (49 events). Red (blue) contours every 20 gpm denote positive (negative) anomalies; zero contour omitted. Statistically significant anomalies at 95% are depicted by black dots.

3.7 Summary and conclusions

We have analysed the occurrence of summertime heat wave events in Southeastern Patagonia (SEPG) since the late 19th century using the 20CRv2. A total of 201 heat wave events were identified for 1872-2010. The regional intraseasonal anomalies of temperature (T') affect a broad area in SSA on both sides of the Andes, which spans from the southern tip of the continent until around 36°S. As shown by local instrumental SAT records, this reanalysis dataset captures the timing and structure of intraseasonal heat waves in this region.

The evolution of a typical heat wave in SEPG is described showing the 21-day sequences of composites of various variables centred at *d0*. This day corresponds to the first day of a cluster of days that satisfy the conditions of intensity and persistence which define a heat wave. Moreover, *d0* coincides with the T' peak of 4.3°C. In SEPG, a temperature increase is observed from day -3 on, and the warm anomaly then typically lasts until day 10. The positive perturbation of slp' peaks at day -2 over SEPG and decays thereafter. Local warming is hence related to the eastward drift of a surface anticyclone, which is situated to the east of SEPG at *d0*. In agreement with the baroclinic structure of this perturbation on the eastern side of the Andes, z500' reaches its highest value over SEPG on day -1. As a consequence of these circulation anomalies, a dry anomaly is observed in SSA between days -4 and 1. In connection with the heat waves in SEPG and as revealed by regional composites of reanalysis data and also by instrumental records in SEPG, there is a northward propagation of the positive temperature anomaly along the Atlantic coast and an almost synchronous development of a cooling signal in subtropical SA. This cold perturbation emphasizes the resemblance between the sequence of fields presented here and the perturbations described for the intrusion of cold air over subtropical SA by Garreaud (2000). Thus, since our focus is on heat waves in SEPG and their signal in SSA, we have extended the results of that study into a subcontinental context and have complemented it with a perspective on the associated large-scale circulation anomalies.

Moreover, we explored climate signals in Oceania that co-occur with the heat wave events in SEPG. We found in 20CRv2 that the anticyclone that precedes a heat wave over SEPG is also related to a cyclonic anomaly over the Tasman Sea of Oceania. Both circulation anomalies are embedded in a quasi-stationary wavetrain-like pattern with negative (positive) action centres in New Zealand and to the west of SA (north of the Ross Sea and SSA). The cyclonic anomaly over the Tasman Sea propagates eastward from a position south of SE Australia on day -6 and reaches New Zealand on day -4, inducing dry conditions in the former region and a wet anomaly in the latter one.

The wave train pattern is evident from day -6 on and resembles the structure described for the interannual summertime SAT variability in Eastern SSA by Jacques-Coper and Brönnimann (2014), which leads to the teleconnection responsible for the anticorrelation between precipitation in southeastern Australia and SAT in Eastern SSA. Furthermore, we confirmed that the intraseasonal precipitation signal in Oceania is modulated by this atmospheric perturbation using century-long instrumental records from SE Australia and the South Island of New Zealand. Hence, this result provides an explanation for the origin of the precipitation-temperature teleconnection between Oceania and SSA observed at intraseasonal and interannual timescales.

We found that strong and weak heat wave events are associated with a pattern of ascent over the southern tip of SA, subsidence in SESA and ascent in the SACZ, with more pronounced anomalies in the first case. Moreover, two thirds of the heat wave events in SEPG are related to convective conditions in the SACZ, although no evident upstream effect of this anomaly can be identified in SEPG. Nevertheless, the summer sub-monthly activity of the SACZ, a quasi-stationary system, is related to circulation anomalies that are similar to those shown in this study (Liebmann et al. 1999; Lima et al. 2010). Moreover, Carvalho et al. (2002), in connection with a *weak-oceanic* pattern of OLR anomalies in the SACZ, found similar ascent conditions. This pattern induces extreme precipitation events in the coastal region of São Paulo in southeast Brazil, a result that is also consistent with the precipitation composites shown in the present study. Hence, our findings provide a continental context of the climate impacts related to wavetrain-like circulation anomalies over the South Pacific and SA.

Finally, we proposed a link between the wave train pattern anomalies on intraseasonal and on interannual (DJF seasonal means) timescales. We found that intraseasonal heat waves occurring in extreme positive years (i.e. in years with strong positive seasonal SAT means) are related to stronger and spatially broader intraseasonal anomalies of geopotential height at 500 hPa than those occurring in extreme negative years (i.e. in years with strong negative seasonal SAT means).

The findings presented in this paper unveil regional and large-scale processes related to intraseasonal SAT perturbations in SEPG. Besides, our results suggest a potential link between synoptic-to-intraseasonal phenomena and previous results on the main interannual and interdecadal SAT variability modes of SSA. The use of independent instrumental data adds robustness to our study and provides a means of validation of 20CRv2 in the Southern Hemisphere. In particular, the signal found in century-long daily precipitation records from Oceania confirms the teleconnection between this region and SEPG. Modelling studies could aim at exploring dynamical features related to open

issues raised by the present work, such as the origin of the wave train pattern linked to the heat waves in SEPG and its interdecadal modulation.

3.A1 Appendix 1: Calculation of precipitation probability perturbations in Oceania

In order to compute the precipitation probability perturbations for stations of SE Australia and New Zealand related to heat wave events in SEPG, we first define a mean precipitation *background probability* from the climatology. For each of the analysed precipitation records, we identify daily rainy events from November to March during the period 1961-1990 according to the thresholds 1 mm and 10 mm. Each day is assigned a 1 in case of precipitation excess of a given threshold and a 0 otherwise. Thus, for each threshold, the *background probability* of rain for every Julian day within this period corresponds to the 30-year average of this binary classification.

Then, we compute the local precipitation signal associated with heat wave events in SEPG. For every rainfall record and precipitation threshold, we form 21-day binary rainfall sequences associated with each heat wave event in SEPG that overlap the rainfall data (i.e., a total number of 201 or less) centred on *d0*. One should note that the heat wave events may partly fall within the reference period (1961-1990). The mean probability of rain for each day within this sequence is calculated again as an average, i.e., the number of rainy events on a certain date within the sequence composite divided by the total number of heat waves considered. For each precipitation record, this results in a rain probability sequence of 21 days associated with heat wave events, centred on *d0*, called hw_{rpbb}.

The next step is to calculate the probability of rain that a sequence of 21 days centred on the same Julian days as those of the heat waves (*d0*) would have if they were referenced to the norm, i.e. within the *background probability* of 1961-1990. This results in a sequence of mean probability of the composite calculated from the norm, which we denominate $norm_{rpbb}$.

Finally, the sequence of probability perturbations associated with heat wave events, compared to the climatological *background probability* is simply given by:

$$\Delta_{rpbb} = hw_{rpbb} - norm_{rpbb} \qquad (3.2)$$

So defined, Δ_{rpbb} represents the mean local change of rain probability for every

day of the sequence centred on *d0*, i.e., the mean heat wave, in comparison to the reference period 1961-1990.

We assess the robustness of this signal through Monte Carlo realizations. For each station, we select 1000 composites of 201 21-day sequences centred on random days from the whole precipitation record. We then repeat the aforementioned procedure to calculate the sequence of mean probability perturbations associated with these groups of random events. This results in a distribution of probability perturbation values for each one of the 21 days of the sequence. In the end, we compare Δ*rpbb* with the sequence of means of those distributions, and also with the sequences of the 25% and 75% percentiles. The results of this methodology are shown in Fig. 3.6.

3.A2 Appendix 2: Cluster analyisis of z500'

With the aim of studying the intraseasonal circulation regimes and their potential link to the interannual patterns, we perform a cluster analysis of the intraseasonal z500' fields, i.e. of all 12510 DJF days (139 years, 1872-2010). As in Cazes-Boezio et al. (2003), we select the region within 20°-70°S and 150°E-60°W. The algorithm used defines the centroids of each cluster so that minimum inner variance, measured as the inner squared distance, is reached. Four clusters (C1, C2, C3, and C4) represent separate groups in the dendrogram. They exhibit a frequency distribution of 13.7%, 36%, 27.9% and 22.4% of all days, respectively, and are characterized by the spatial mean patterns presented in Fig. 3.S3. All of them correspond to different phases of the eastward propagation of a wave train along the mid-latitudes. C1 shows positive centres to the south of New Zealand and the west of SSA and negative centres to the north of the Ross Sea (the most intense) and over SSA. C3 represents the roughly opposite pattern of C1. C4 corresponds to the eastward displacement of C1, in such a way that the centres of action of C2, which are weaker in this case, are located in the nodes observed for C1. C2, the most populated cluster, exhibits an opposite pattern as C4, and even much weaker anomalies.

3.A2.1 Cluster trajectories associated with heat waves in SEPG

For every day belonging to a certain cluster, we construct the 15-day sequence of cluster frequencies, spanning between one week before that day and one week after

it. The composites of all frequencies define mean cluster trajectories for each of our four categories. They reveal a strong persistence and the eastward propagation of each cluster (not shown). This observation means, for instance, that a C1 day is likely followed by one from the same group or from C4, but not from C3.

This subsection focuses on the 201 heat wave events (centred on *d0*). In this case, the frequency distributions of C1, C2, C3 and C4 change to 6.5%, 27.4%, 46.3% and 19.9%, respectively. This result clearly emphasizes our findings: heat waves in SEPG are associated with an anticyclonic anomaly over SSA, which belongs to a wave train pattern over the South Pacific with negative (positive) action centres over New Zealand and west of SSA (to the north of the Ross Sea and SSA).

Now, we aim at discerning between 15-day cluster trajectories centred on C3 days that lead to heat waves in SEPG (i.e. *d0* classified as C3) and those which do not. The method used is similar to that described in the Appendix 1 for precipitation probability perturbations. In the case of heat wave events, the probability that a certain day of the sequence belongs to a given cluster (C1-C4), named seq_{pbb_hw}, is just the number of such cases divided by the total amount of series (n=201). The *background probability*, named seq_{pbb_all}, is computed by selecting from the whole dataset all sequences of 15 days centred on C3 (n=3488; these cases not correspond necessarily to a heat wave). Note that cluster persistence has an effect in this result, since the selected sequences are clearly not independent groups and therefore exhibit autocorrelation. The changes of frequency probability between both sequences is given by:

$$\Delta seq_{pbb} = seq_{pbb\_hw} - seq_{pbb\_all} \tag{3.3}$$

We plot Δseq_{pbb} in Fig. 3.S4. We observe that sequences centred on *d0* corresponding to C3 show higher persistence of this cluster in the previous days, as far back as day -6 (+7.6%) and its highest perturbation on day -3 (+13.2%). On the other hand, C2 is less frequent since day -6 (-10.6%), with the greatest probability change in day -3 (-14.7%). During the days following *d0*, the highest opposite perturbations are found on day 2 within C2 (+13.7%) and C3 (-9.4%). These results stress the fact that the onset of typical heat waves in SEPG follows a persistent mid-level ridge over the region which is already noticeable with higher probability even back to day -6 in the mean sequence of all C3 days. In the case of heat waves in SEPG, there is a tendency of the action centres of the wave-train pattern (in particular of the anticyclone over SSA) for propagating eastward rather than persisting in their locations. These aspects are reflected by the typical evolution of z500' within a heat wave in SEPG (Fig. 3.1c).

Cluster trajectories could offer a potential for predicting heat waves in SEPG. This aspect is assessed by computing a conditional probability. In the whole dataset (n=12510) and in the subset of heat wave events (n=201), the conditional probability of classifying day 0 as C3 given that day -3 was classified as C3 is 48.4% and 63.1%, respectively. This result means that heat wave events in SEPG are related to more persistent C3 clusters. A more interesting result, however, is the conditional probability of identifying a heat wave on a *d0* classified as C3, given that day -3 was also classified as C3. The modest result, 2%, points in part to the low frequency of these cases and suggests also that cluster trajectories are not enough as a tool for forecasting purposes. Hence, more factors should be considered for a potential predictor base.

3.A2.2 Relationships between intraseasonal circulation regimes and interannual temperature anomalies in SEPG

In this subsection, a possible link between intraseasonal circulation regimes over the South Pacific and the interannual summer SAT anomaly in SEPG are analysed. For that, we use the interannual DJF SAT anomalies defined in Section 3.5.

One relationship consists in the mean frequency distribution of daily DJF clusters. We compare each group of extreme years against a random distribution of years from the whole period. For that, we form 50 groups of 16 (17) random years, without excluding extreme years, for the cases of positive (negative) extreme years. As shown in Fig. 3.S5a, the frequencies of C2 and C4 within extreme years fall very close to the 5% percentile, a result that indicates a relative reduction in the frequency of these clusters. This decrease is compensated by the increment in frequency observed for C1, virtually matching the 95% percentile, and for C3, whose frequencies for extreme years are higher than the 95% percentile of the random distribution. Our conclusion is that a higher frequency of C3 , the cluster associated with an anticyclonic anomaly over SSA, takes place during extreme years. This fact could be related to more favourable conditions for the development of persistent heat waves within both warm and cold extreme years.

The second relationship we explore here relates to the mean duration of heat wave events according to each category of extreme years and to the all interannual DJF means. The length of a heat wave is defined here as the number of consecutive days that satisfy the conditions presented in Section 3.2, i.e., those days starting on *d0*. Figure 3.S5b shows the mean length for all heat wave events (2.28 days), for extreme

positive years (2.47) and for extreme negative years (2.24), as well as the corresponding minimum and maximum duration for each category. These results do not exhibit statistical significance, but may suggest that the duration of the heat waves within extreme positive years is slightly longer than within extreme negative years.

Acknowledgments

References

Berbery EH, Nogués-Paegle J (1993) Intraseasonal Interactions between the Tropics and Extratropics in the Southern Hemisphere. J Atmos Sci 50:1950–1965. doi: 10.1175/1520-0469(1993)050<1950:IIBTTA>2.0.CO;2

Berbery EH, Nogués-Paegle J, Horel JD (1992) Wavelike Southern Hemisphere Extratropical Teleconnections. J Atmos Sci 49:155–177. doi: 10.1175/1520-0469(1992)049<0155:WSHET>2.0.CO;2

Berman A, Silvestri G, Compagnucci R (2013) On the variability of seasonal temperature in southern South America. Clim Dyn 40:1863–1878. doi: 10.1007/s00382-012-1596-5

Berman AL, Silvestri G, Compagnucci R (2012) Eastern Patagonia Seasonal Precipitation: Influence of Southern Hemisphere Circulation and Links with Subtropical South American Precipitation. J Clim 25:6781–6795. doi: 10.1175/JCLI-D-11-00514.1

Carrasco J, Casassa G, Rivera A (2002) Meteorological and Climatological Aspects of the Southern Patagonia Icefield. In: Casassa G, Sepúlveda F, Sinclair R (eds) Patagon. Icefields SE - 4. Springer US, pp 29–41

Carvalho LM V, Jones C, Liebmann B (2002) Extreme Precipitation Events in Southeastern South America and Large-Scale Convective Patterns in the South Atlantic Convergence Zone. J Clim 15:2377–2394. doi: 10.1175/1520-0442(2002)015<2377:EPEISS>2.0.CO;2

Cazes-Boezio G, Robertson AW, Mechoso CR (2003) Seasonal Dependence of ENSO Teleconnections over South America and Relationships with Precipitation in Uruguay. J Clim 16:1159–1176. doi: 10.1175/1520-0442(2003)16<1159:SDOETO>2.0.CO;2

Cerne SB, Vera CS (2011) Influence of the intraseasonal variability on heat waves in subtropical South America. Clim Dyn 36:2265–2277. doi: 10.1007/s00382-010-0812-4

Compagnucci RH, Agosta EA, Vargas WM (2002) Climatic change and quasi-oscillations in central-west Argentina summer precipitation: main features and coherent behaviour with southern African region. Clim Dyn 18:421–435. doi: 10.1007/s003820100183

Compo GP, Whitaker JS, Sardeshmukh PD, et al. (2011) The Twentieth Century Reanalysis Project. Q J R Meteorol Soc 137:1–28. doi: 10.1002/qj.776

Garreaud R (2000) Cold Air Incursions over Subtropical South America: Mean Structure and Dynamics. Mon Weather Rev 128:2544–2559. doi: 10.1175/1520-0493(2000)128<2544:CAIOSS>2.0.CO;2

Garreaud R, Lopez P, Minvielle M, Rojas M (2012) Large-Scale Control on the Patagonian Climate. J Clim 26:215–230. doi: 10.1175/JCLI-D-12-00001.1

Gonzalez PM, Vera C (2013) Summer precipitation variability over South America on long and short intraseasonal timescales. Clim Dyn 1–15. doi: 10.1007/s00382-013-2023-2

Hertel D, Therburg A, Villalba R (2008) Above- and below-ground response by Nothofagus pumilio to climatic conditions at the transition from the steppe–forest boundary to the alpine treeline in southern Patagonia, Argentina. Plant Ecol Divers 1:21–33. doi: 10.1080/17550870802257026

Hoskins BJ, Simmons AJ, Andrews DG (1977) Energy dispersion in a barotropic atmosphere. Q J R Meteorol Soc 103:553–567. doi: 10.1002/qj.49710343802

Jacques M (2009) Caracterización del salto climático de mediados de los 1970s en Sudamérica. 147.

Jacques-Coper M, Brönnimann S (2014) Summer temperature in the eastern part of southern South America: its variability in the twentieth century and a teleconnection with Oceania. Clim Dyn 1–20. doi: 10.1007/s00382-013-2038-8

Jacques-Coper M, Garreaud RD (2014) Characterization of the 1970s climate shift in South America. Int J Climatol 1–16. doi: 10.1002/joc.4120

Jin F, Hoskins BJ (1995) The Direct Response to Tropical Heating in a Baroclinic Atmosphere. J Atmos Sci 52:307–319. doi: 10.1175/1520-0469(1995)052<0307:TDRTTH>2.0.CO;2

Lara A, Villalba R, Wolodarsky-Franke A, et al. (2005) Spatial and temporal variation in Nothofagus pumilio growth at tree line along its latitudinal range (35°40′–55° S) in the Chilean Andes. J Biogeogr 32:879–893. doi: 10.1111/j.1365-2699.2005.01191.x

Lee S, Held IM (1993) Baroclinic Wave Packets in Models and Observations. J Atmos Sci 50:1413–1428. doi: 10.1175/1520-0469(1993)050<1413:BWPIMA>2.0.CO;2

Liebmann B, Kiladis GN, Marengo J, et al. (1999) Submonthly Convective Variability over South America and the South Atlantic Convergence Zone. J Clim 12:1877–1891. doi: 10.1175/1520-0442(1999)012<1877:SCVOSA>2.0.CO;2

Lima K, Satyamurty P, Fernández J (2010) Large-scale atmospheric conditions associated with heavy rainfall episodes in Southeast Brazil. Theor Appl Climatol 101:121–135. doi: 10.1007/s00704-009-0207-9

Marshall GJ (2003) Trends in the Southern Annular Mode from Observations and Reanalyses.

J Clim 16:4134–4143. doi: 10.1175/1520-0442(2003)016<4134:TITSAM>2.0.CO;2

Mo KC, Higgins RW (1998) The Pacific–South American Modes and Tropical Convection during the Southern Hemisphere Winter. Mon Weather Rev 126:1581–1596. doi: 10.1175/1520-0493(1998)126<1581:TPSAMA>2.0.CO;2

Mo KC, Paegle JN (2001) The Pacific–South American modes and their downstream effects. Int J Climatol 21:1211–1229. doi: 10.1002/joc.685

Müller G, Ambrizzi T (2007) Teleconnection patterns and Rossby wave propagation associated with generalized frosts over southern South America. Clim Dyn 29:633–645. doi: 10.1007/s00382-007-0253-x

Müller G V, Berri GJ (2007) Atmospheric Circulation Associated with Persistent Generalized Frosts in Central-Southern South America. Mon Weather Rev 135:1268–1289. doi: 10.1175/MWR3344.1

Orlanski I, Chang EKM (1993) Ageostrophic Geopotential Fluxes in Downstream and Upstream Development of Baroclinic Waves. J Atmos Sci 50:212–225. doi: 10.1175/1520-0469(1993)050<0212:AGFIDA>2.0.CO;2

Paruelo JM, Beltran A, Jobbagy E, et al. (1998) The climate of Patagonia: general patterns and controls on biotic. Ecol Austral 8:85–101.

Prohaska F (1976) The climate of Argentina, Paraguay, and Uruguay, Vol. 12, W. 57–69.

Rakich CS, Holbrook NJ, Timbal B (2008) A pressure gradient metric capturing planetary-scale influences on eastern Australian rainfall. Geophys Res Lett 35:L08713. doi: 10.1029/2007GL032970

Rasmussen LA, Conway H, Raymond CF (2007) Influence of upper air conditions on the Patagonia icefields. Glob Planet Change 59:203–216. doi: http://dx.doi.org/10.1016/j.gloplacha.2006.11.025

Rignot E, Rivera A, Casassa G (2003) Contribution of the Patagonia Icefields of South America to Sea Level Rise. Sci 302:434–437. doi: 10.1126/science.1087393

Robertson AW, Mechoso CR (2003) Circulation Regimes and Low-Frequency Oscillations in the South Pacific Sector. Mon Weather Rev 131:1566–1576. doi: 10.1175//2548.1

Solman SA, Orlanski I (2013) Poleward Shift and Change of Frontal Activity in the Southern Hemisphere over the Last 40 Years. J Atmos Sci 71:539–552. doi: 10.1175/JAS-D-13-0105.1

Sprenger M, Martius O, Arnold J (2013) Cold surge episodes over southeastern Brazil – a potential vorticity perspective. Int J Climatol 33:2758–2767. doi: 10.1002/joc.3618

Thompson DWJ, Solomon S (2002) Interpretation of Recent Southern Hemisphere Climate Change. Sci 296 :895–899. doi: 10.1126/science.1069270

Ummenhofer CC, England MH (2007) Interannual Extremes in New Zealand Precipitation Linked to Modes of Southern Hemisphere Climate Variability. J Clim 20:5418–5440. doi: 10.1175/2007JCLI1430.1

Del Valle HF, Elissalde NO, Gagliardini DA, Milovich J (1998) Status of desertification in the Patagonian region: Assessment and mapping from satellite imagery. Arid Soil Res Rehabil 12:95–121. doi: 10.1080/15324989809381502

Zamboni L, Kucharski F, Mechoso CR (2012) Seasonal variations of the links between the interannual variability of South America and the South Pacific. Clim Dyn 38:2115–2129. doi: 10.1007/s00382-011-1116-z

row) difference fields between p75 and p25. The panels on the right show the 21-day time series of T' for the corresponding composites. Interval units are 0.01 Pa/s for ω500' and 0.5 K for T'

3.S Supplementary material
Figures
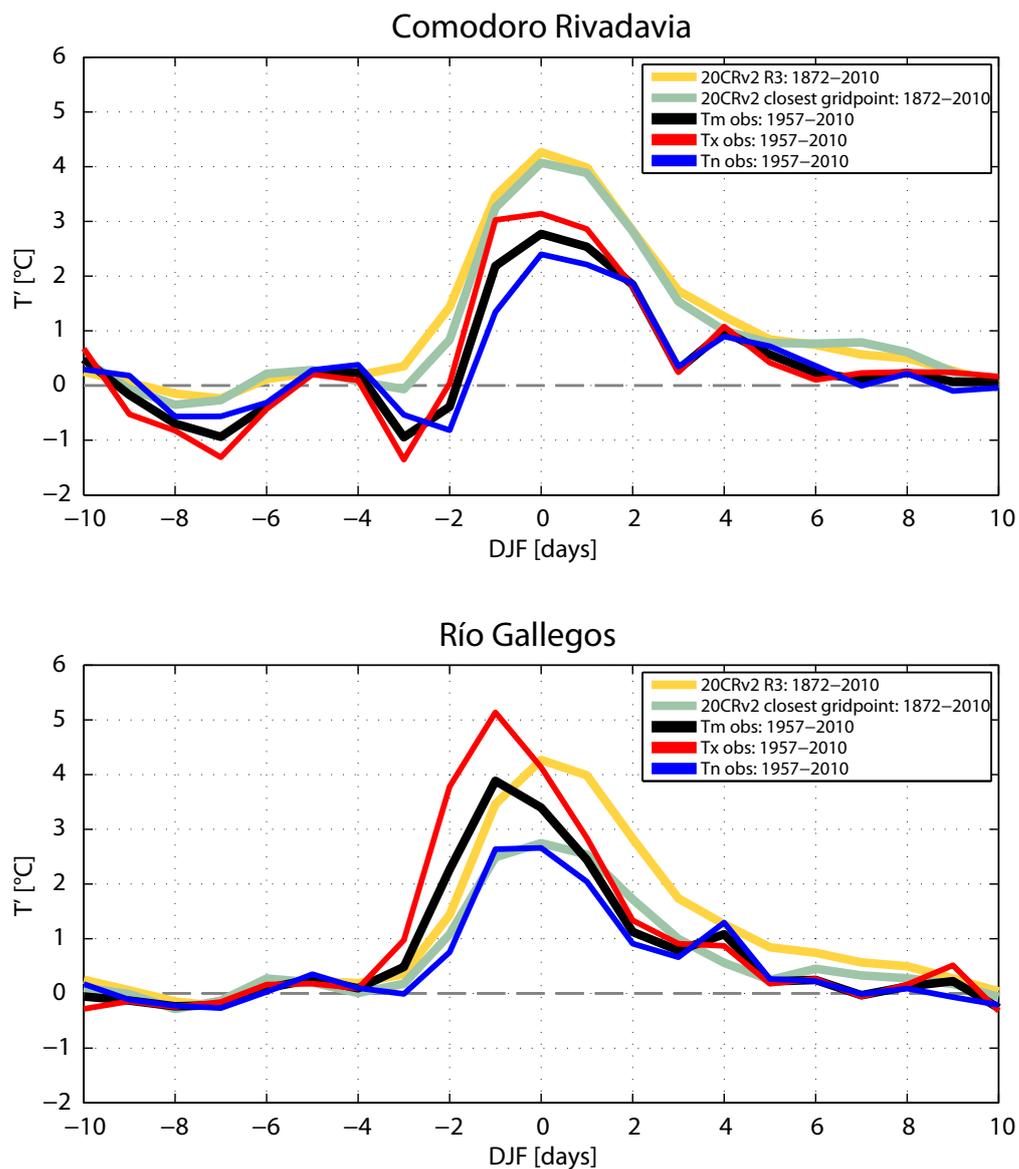
Fig. 3.S1: *21-day composite sequences of T' from 20CRv2 and instrumental records, associated with the 201 heat wave events in SEPG identified in 20CRv2, centred on day 0 (d0): SEPG mean (gray curve, 20CRv2, 1872-2010, same as in Fig. 3.1a), closest gridpoint to the station (green curve, 20CRv2, 1872-2010), and instrumental time series of minimum temperature (Tn', blue curve, 1957-2010), maximum temperature (Tx', red curve, 1957-2010) and mean temperature (Tm', black curve, 1957-2010). Stations correspond to a) Comodoro Rivadavia and b) Río Gallegos.*
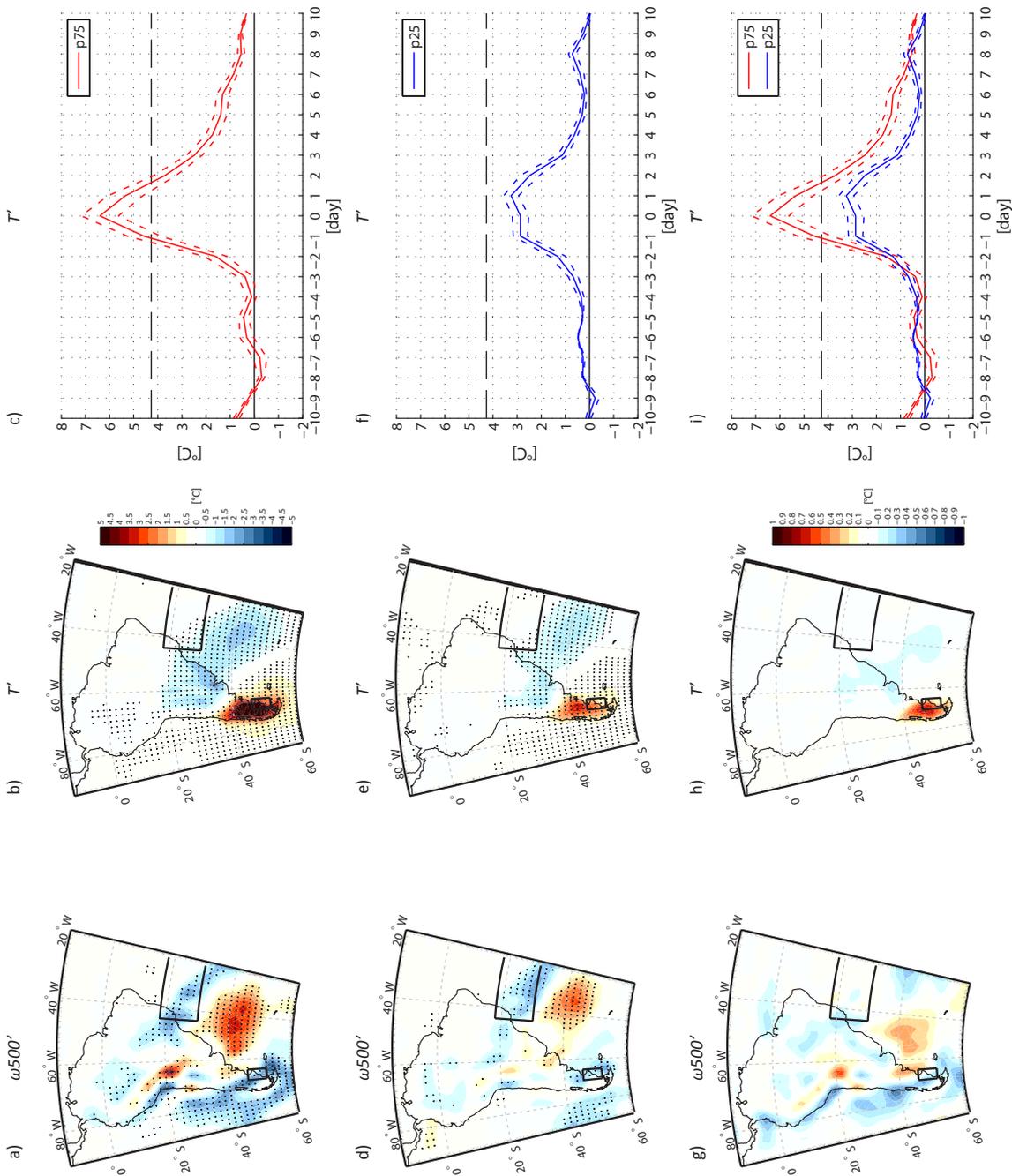
Fig. 3.S2: *Composites of ω500' (left panels) and T' (central panels) and 21-day T' sequences centred on d0 for: (upper row) the upper quartile of T' on d0 (p75) and (middle row) the lower quartile of T' on d0 (p25) from the total of 201 heat wave events; (lower row) difference fields between p75 and p25. The panels on the right show the 21-day time series of T' for the corresponding composites. Interval units are 0.01 Pa/s for ω500' and 0.5 K for T'.*

a) C1: 13.7% (6.2%)

b) C2: 36% (26.2%)

c) C3: 27.9% (44.3%)

d) C4: 22.4% (19%)
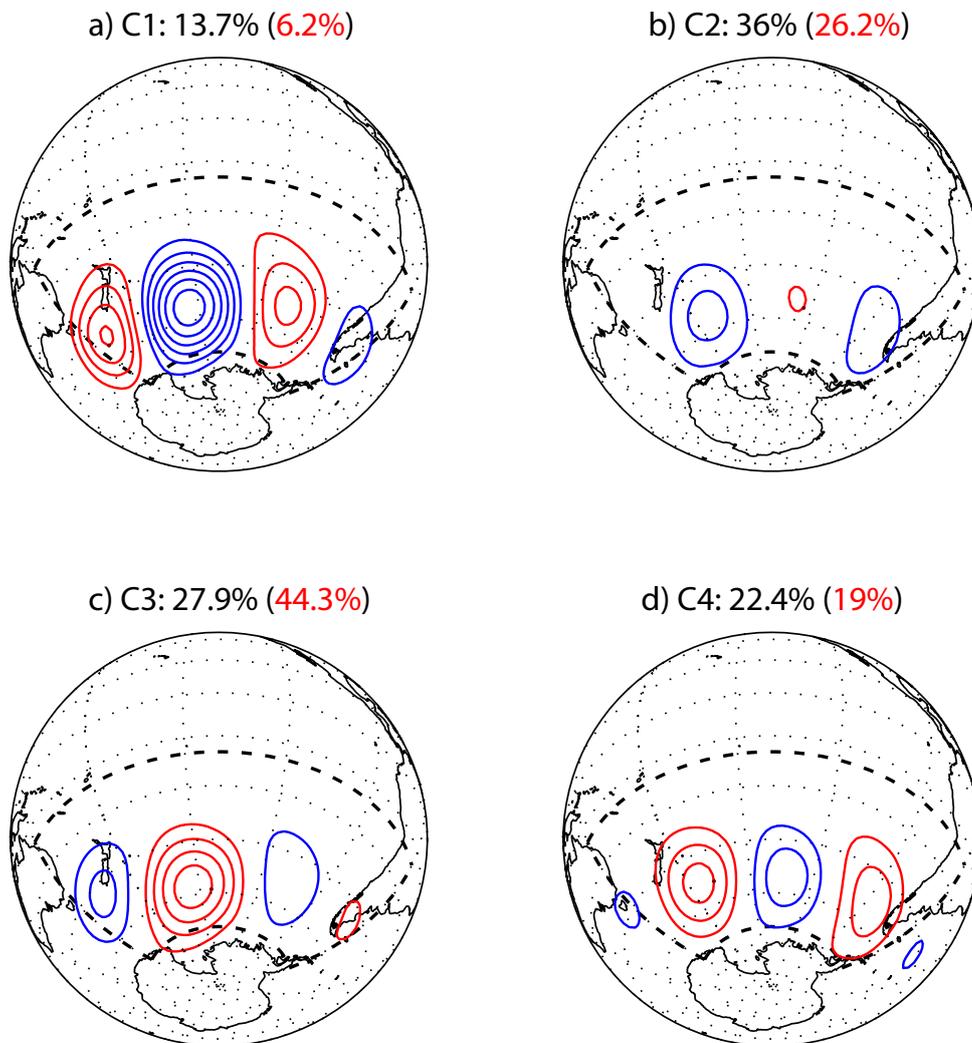
Fig. 3.S3: *Spatial patterns of the four clusters (C1-C4) defined from the whole DJF dataset (n=12510). Red (blue) contours every 20 gpm denote positive (negative) values; zero contour omitted. The legends indicate the total amount of days within each cluster for all days (n=12510, black) and heat wave events (n=201, red). The dashed lines enclose the domain used for the calculation of the clusters (20°-70°S and 150°E-60°W).*
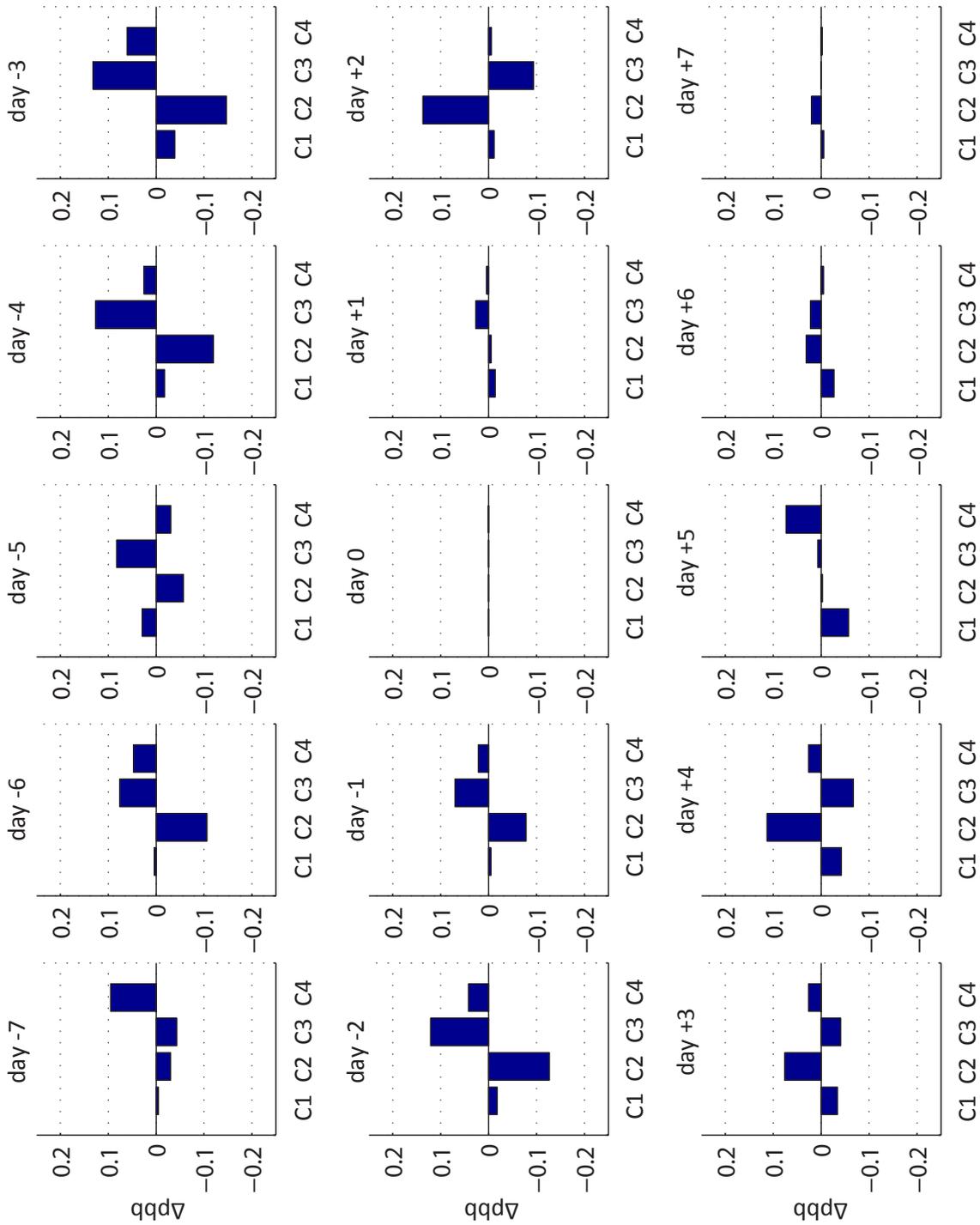
Fig. 3.S4: *Differentials of probability of cluster frequencies between the mean 15-day sequence of heat wave events with day 0 (d0) classified as C3 and the mean sequence of 15 days centred on every C3 day. A value of 0.1 represents an increment of 10% in the chances of observing a given cluster on a certain day.*

a) cluster frequencies

b) heat wave length
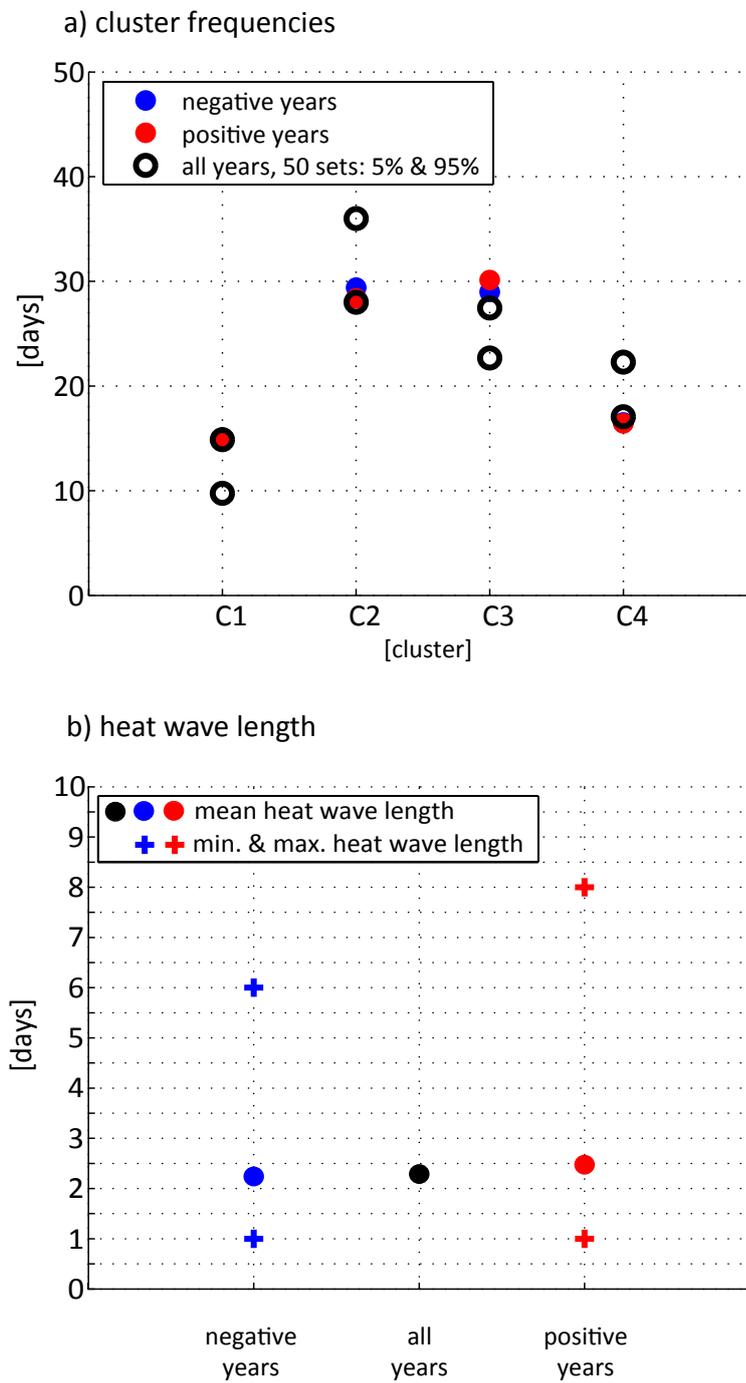
Fig. 3.S5: *a) Mean frequency distribution of clusters associated with the 90 DJF days from extreme negative years (n=17, blue), extreme positive years (n=16, red), and the 5% and 95% percentiles of 50 random realizations, of similar size as the previous group, from the period 1872-2010. b) Mean length of the heat waves considering all events (black), those events within extreme positive years (red), and those events within extreme negative years (blue). Crosses denote the minimum and maximum length of the composites of extreme years.*

Chapter 4

Evidence for a tropical modulation of the intraseasonal summer temperature in Eastern Patagonia

Martín Jacques-Coper[1], Stefan Brönnimann[1], Olivia Martius[1],
Carolina Vera[2], and Bibiana Cerne[2]
[1]*Oeschger Centre for Climate Change Research and Institute of Geography, University of Bern, Bern, Switzerland*
[2]*Centro de Investigaciones del Mar y la Atmósfera, CIMA/CONICET-UBA, DCAO/FCEN, UMI-IFAECI/CNRS, Buenos Aires, Argentina*

In preparation

Abstract

We describe the relationship between the intraseasonal component of air surface temperature variability in Eastern Patagonia in South America (south of ~40°S and East of the Andes) and the Madden-Julian Oscillation (MJO) during austral summer based on ~50 years of daily instrumental records, the Twentieth Century Reanalysis (20CR), and a century-long reconstruction of the MJO index of Wheeler and Hendon. Our results show that the variability of surface temperature in Patagonia during summer is highly driven by the intraseasonal activity and particularly by that associated with the MJO. The active MJO phases modulate the spatial mean intraseasonal temperature signal in Eastern Patagonia with an amplitude of ~1.5°C. In most of the region, the warmest conditions are found during active phase 8 and the coldest conditions during active phase 4. These opposite states of the temperature perturbations are related to almost inverse mid-level

circulation anomalies over Southern South America and the southwest Atlantic, namely anticyclonic and a cyclonic anomaly centres. Each of them is part of a large-scale Rossby-like wave train of alternating circulation anomalies extended along the South Pacific. The corresponding outgoing longwave radiation (OLR) anomalies suggest that these structures may be triggered by anomalous convection in the tropics. Furthermore, we show that intraseasonal heat wave events detected in southeastern Patagonia tend to occur also during phase 8 when these events are stratified according to the active MJO phases. Previous work showed that these heat waves are also induced by a wave train pattern over the South Pacific, associated with other intraseasonal variability sources. Hence, circulation anomalies over the South Pacific caused in general by tropical convection variability and in particular by MJO activity may constructively interact with circulation patterns resulting from the extratropical dynamics, eventually leading to an intraseasonal heat wave in southeastern Patagonia. We briefly discuss this possibility based on a case study.

4.1 Introduction

Eastern Patagonia is the region of Southern South America located south of 40°S and to the East of the Andes cordillera. At the western side of this mountain range, the forced ascent of the westerlies that blow from the Pacific leads to orographic rain; in contrast, the lee side is characterised by extremely windy conditions and high aridity, a phenomenon known as rain shadow effect. Eastern Patagonia exhibits a high annual thermal amplitude, which is characteristic of a rather continental climate (Garreaud et al. 2012).

During austral summer (December to February, DJF), the continental heating is higher in the northern part of Eastern Patagonia than in the more austral zones, a fact that causes a meridional temperature gradient and hence a north-south pattern of temperature variability (Prohaska 1976). Berman et al. (2013) studied the year-to-year seasonal variability of surface air temperature (SAT) in this part of the world for 1979-2009 based on instrumental records and reanalysis. The authors found that in summer, anticyclonic (cyclonic) anomalies extending over Southern South America and the adjacent oceans advect warm (cold) conditions to the northern part of Eastern Patagonia (ca. 40°S-44°S) (Berman et al. 2013). That study also showed that during austral summer, local anticyclonic (cyclonic) anomalies result in increased (reduced) incoming solar radiation in the southern part of Eastern Patagonia (ca. 50°S-56°S), thus contributing to local warm (cold) conditions. These SAT anomalies were found to be

negatively correlated with those over the central-southern region of Brazil, more than 3000 km to the north; a pattern identified as a temperature dipole between the southern tip and subtropical areas of the continent.

With a broader spatial and temporal perspective, Jacques-Coper and Brönnimann (2014) described the summer variability of SAT in Eastern Patagonia at interdecadal and interannual scales during the 20th century. The main interannual mode exhibits a period of ~3.4 years and is associated with a wave train circulation pattern over the South Pacific, with alternating action centres in New Zealand, to the north of the Ross Sea, to the west of South America, and over Southern South America. This pattern, which resembles the Pacific-South American mode 2 (Mo and Paegle 2001), presumably originates (at least partially) in the tropical West Pacific and its circulation anomalies induce a teleconnection between the climates of Oceania and Eastern Patagonia.

Further own work (Jacques-Coper et al., in prep.) has been devoted to understanding the role played by the intraseasonal variability on the modulation of strong and persistent warm conditions in southeastern Patagonia (SEPG, 46°-52°S; 65°-70°W). These events, identified as local heat waves, exhibit a mean temperature anomaly larger than 4°C and typically last for several days. A finding of that study was that the large-scale circulation pattern that triggers these intraseasonal heat waves resembles the wave train found for the summer seasonal scale. Moreover, that work also addressed the temporal development of that circulation pattern, which gives rise to the teleconnection between Eastern Patagonia and Oceania. In addition, the temperature dipole pattern between Eastern Patagonia and subtropical regions of the continent, which was observed for the seasonal means, was also found for the intraseasonal temperature anomalies. Nevertheless, the possible tropical influence on the atmospheric circulation leading to warm conditions in Southern South America and, in particular, in Eastern Patagonia has remained an open aspect to explore. This is one of the main points addressed in the present study.

The intraseasonal variability range has been reported to exhibit a notorious impact in temperature (especially in minimum temperature) in southeastern South America during winter (Naumann and Vargas 2012). For this region and season, Naumann and Vargas (2010) showed consistent covariability of temperature and precipitation with the Madden-Julian Oscillation (MJO) (Madden and Julian 1971). The MJO is the dominant mode of intraseasonal variability of the tropical coupled ocean-atmosphere system. It consists of a planetary-scale eastward-propagating pattern of atmospheric circulation and deep convection, associated with anomalies in various variables in both tropical and subtropical regions (Zhang 2005). The modulation of regional weather and climate systems by the MJO, especially in subtropical latitudes, has been extensively studied,

regarding both precipitation [e.g. Sperber (2003), Donald et al. (2006), Kanamori et al. (2013), and Matthews et al. (2013)] and temperature [e.g. Salby and Hendon (1994) and Maloney and Kiehl (2002), Zhou et al. (2011), and Oliver (2014)]. Large-scale impacts associated with this mode have been also described for climates of higher latitudes, both in the Northern Hemisphere (Cassou 2008; Vecchi and Bond 2004) and in the Southern Hemisphere, in particular South America [e.g. Moore et al. (2010), Naumann and Vargas (2010), Barrett et al. (2011), and Juliá et al. (2012)]. Recently, Alvarez et al. (2014, submitted to *Climate Dynamics*) have described the seasonal variations of the MJO influence on both rainfall and surface temperature anomalies in South America, based on reanalysis for 1979-2012. In particular they show a significant MJO signal on positive (negative) temperature anomalies in Southern South America during MJO phases 7-8 (3-4) during summer.

Nevertheless, to the best knowledge of the authors, the relationship between intraseasonal temperature and the MJO during summer in Eastern Patagonia has so far not been deeply studied. Therefore, this paper explores this subject with a long-term perspective on the 20th century and with emphasis on the possible role played by the MJO in the triggering of intraseasonal heat waves in SEPG. The present work is structured as follows: section 4.2 introduces the data and methods used in this work; section 4.3.1 explains the decomposition of the SAT field to obtain the intraseasonal variability range of this variable; the modulation of intraseasonal summer SAT in Eastern Patagonia by the MJO is presented in section 4.3.2; section 4.3.3 shows the large-scale fields associated with the active phases of the MJO that lead to the greatest SAT departures in Eastern Patagonia; section 4.3.4 describes the connection found between intraseasonal heat waves in SEPG and the MJO; a case study illustrating the previous results is offered in section 4.3.5; and finally, section 4.4 discusses and summarizes our findings.

4.2 Data and methods

4.2.1 Instrumental and reanalysis data

In this study we focus on austral summer, i.e. DJF (December 1st to February 28, ignoring leap years; seasons are assigned to the corresponding JF year). Non-detrended daily fields of the reanalysis ensemble means of SAT at 2 m and geopotential height at 500 hPa (z500) were accessed from the Twentieth Century Reanalysis version 2 (20CR, available for DJF 1872-2010) (Compo et al. 2011). The interpolated outgoing longwave radiation (OLR) dataset obtained from the National Center for Atmospheric Research (NCAR) spans DJF 1975-2013 (Liebmann and Smith 1996). The observational temperature

datasets used in this study contain information on minimum temperature (*Tn*) and maximum temperature (*Tx*) recorded by 16 stations (in most cases for DJF 1957-2010; see Table 4.1) and were supplied by the Argentinean National Weather Service. The mean instrumental SAT (*Tm*) was calculated as the arithmetic average of *Tx* and *Tn*.

The intraseasonal anomalies of each variable are defined in this paper after Cerne and Vera (2011), as the result of subtracting from the daily values their corresponding climatological daily means (a term which accounts for the annual cycle) and the seasonal departures of each particular year from the climatology (i.e., the DJF mean of each year minus the long-term seasonal mean). That is, the intraseasonal anomaly of a given variable for day *d* and year *y* is calculated as:

$$intraseasonal\ anomaly_{d,y}$$
$$= daily\ value_{d,y} - climatological\ daily\ mean_d \qquad (4.1)$$
$$- (DJF\ seasonal\ mean_y - long\text{--}term\ DJF\ seasonal\ mean)$$

The reference period for defining long-term statistics (mean, standard deviation, seasonal cycle, etc.) and anomalies is 1961-1990. For simplicity, in the rest of the paper, an apostroph will denote the intraseasonal variables (e.g. SAT', z500', etc.).

In section 4.3.4, we analyse the signal of the MJO in association with the occurrence of intraseasonal heat waves in SEPG. For that purpose, we first calculate the daily spatial SAT' mean of the five 20CR gridpoints within SEPG. Then, we use that time series to detect local intraseasonal heat waves according to criteria of heat wave persistence and intensity after Cerne and Vera (2011): i) SAT'>0 for at least 5 consecutive days, and ii) SAT' larger than its own standard deviation for at least 3 days.

4.2.2 The reconstructed MJO index

The Wheeler and Hendon real-time multivariate MJO index, available from 1974 on, is formed by two principal components (RMM1 and RMM2) extracted from near-equatorially-averaged zonal wind at 850 and 200 hPa and satellite-observed OLR data. Hence, this index can be plotted on a two-dimensional phase space defined by these orthogonal axes and characterized by values of amplitude and phase, which describe the intensity and position of the convection centres in the tropical band, respectively. Wheeler and

Hendon (2004) divided that phase space into 8 equal segments, and stated that the nominal time of transition between each of them is 6 days, but with variations from event to event. In this study, we use the 1905-2008 reconstruction of the MJO index of Wheeler and Hendon (2004) by Oliver and Thompson (2011). This product is based on daily fields of sea level pressure from the 20CR and was validated against several variables for three different subperiods. Days with *active MJO phases* were defined as those exhibiting the amplitude of their MJO index in the upper tercile of the total distribution of DJF MJO amplitudes within 1906-2008, i.e. after the exceedance of a threshold of 1.65 (dimensionless units).

4.3 Results

4.3.1 The intraseasonal signal of SAT in Southern South America

The decomposition of SAT into the different temporal variability portions described in section 4.2.1 is illustrated for the temperature conditions of 22nd of January of 1992 (Fig.1). The full SAT field depicted from 20CR shows warm conditions in the northeastern and central-eastern parts of Argentina, exceeding 32°C at around 38°S (Fig. 4.1a). That region is located slightly to the west of the area of highest mean SAT variability (standard deviation of ~4°C). These regional warm conditions result from the superposition of the following terms: a high SAT value expected for that day of the year from the mean climatology (>28°C, Fig. 4.1b), a relatively cold seasonal anomaly for the summer of 1992 (~-1.2°C, Fig. 4.1c), and a warm intraseasonal anomaly detected for that particular day (>4°C) mainly over eastern Patagonia. The standard deviation fields of both the DJF seasonal cycle (Fig. 4.1b) and the DJF seasonal anomalies (Fig. 4.1c) reach their maxima in the same region as that of the full SAT field for that particular day (Fig. 4.1a), with values of the order of 1.5°C and 2°C, respectively. However, it is noteworthy that the standard deviation field of full SAT resembles that of SAT' (Fig. 4.1d). Indeed, the maximum of the positive SAT' observed on our selected day (~9°C) lies within the region of highest intraseasonal variability (>3.5°C). Therefore, this temporal decomposition of the full SAT field allows us to conclude that the largest part of the positive temperature anomaly of this particular day arises from the intraseasonal range. Moreover, the region enclosed by the 2°C-contour of intraseasonal standard deviation (Fig. 4.1d) comprises an extensive area spanning from the subtropics to the mid-latitudes, including vast zones of Patagonia, at both sides of the Andes. This result reflects the fact that the temperature regimes in Southern South America are not strongly divided by the Andes (Coronato and

Bisigato 1998).

Fig. 4.S1 in the Supplementary Material shows SAT time series for DJF 1992. They correspond to instrumental *Tn'* (blue curve), *Tx'* (red curve), and *Tm'* (black curve) of the station Comodoro Rivadavia Aero in southeastern Patagonia (see Table 4.1


a) raw SAT, 22 Jan 1992

b) SAT climatology (1961-1990), 22 Jan

c) DJF seasonal anomaly (1961-1990), 1992

d) intraseasonal SAT, 22 Jan 1992
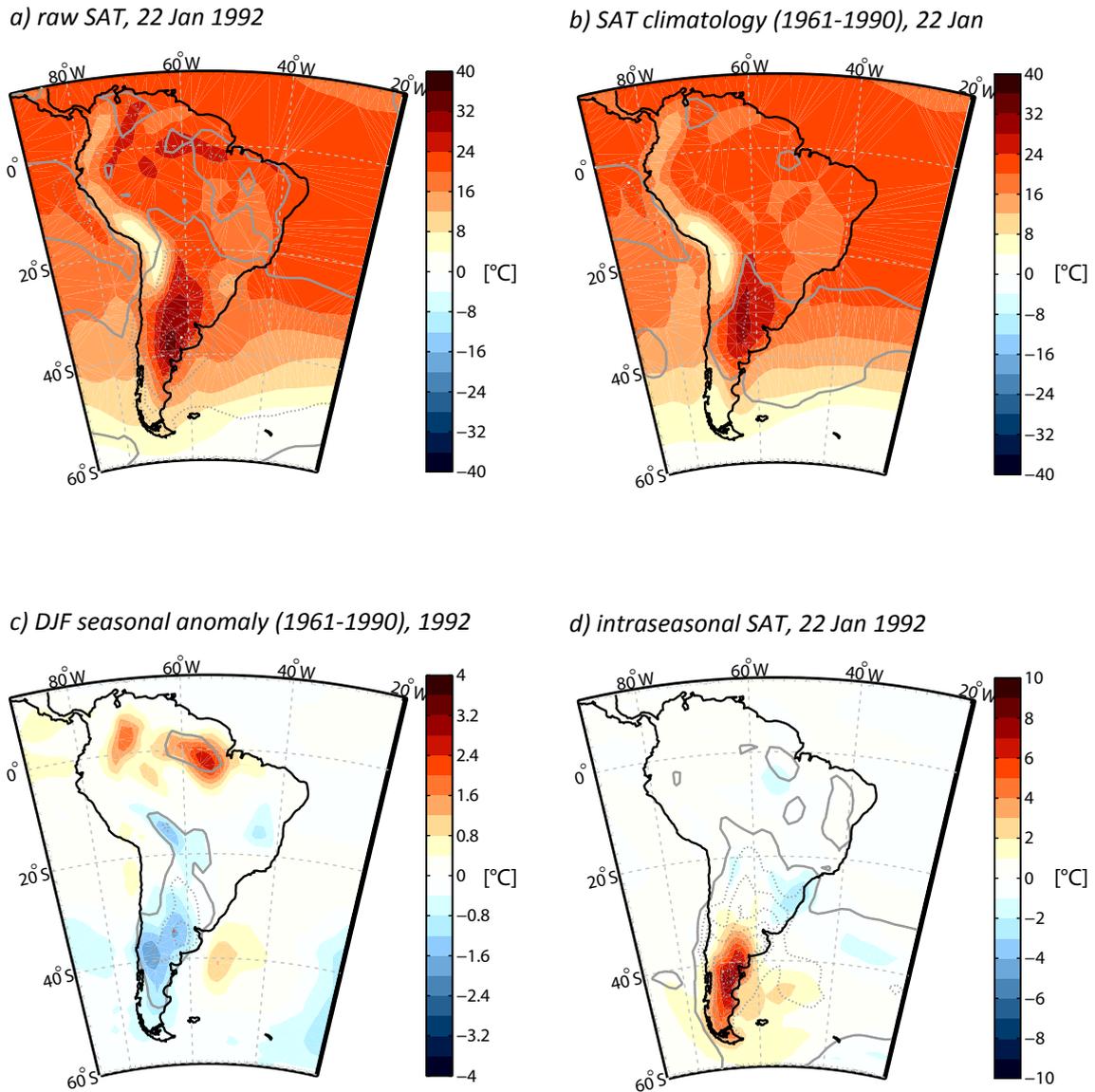
Fig. 4.1: *Decomposition of a) the full SAT field over South America for the 22nd of January of 1992 into b) the DJF SAT climatology for that day (1961-1990), c) the DJF SAT seasonal anomaly of 1992 with respect to 1961-1990, and d) the (residual) intraseasonal SAT field for that day. The grey contours depict the 1961-1990 standard deviation of each field every 0.5°C (thin contours), starting from 1°C (thick contour). All fields correspond to 20CR.*

and Fig. 4.2a), as well to *Tm'* from 20CR, extracted from the closest gridpoint to that station (grey curve). The maximum instrumental value of *Tx* during DJF 1992, 37.4°C, was registered on January 21st 1992 (*Tn*=21.4°C), followed by *Tx*=30.3°C (*Tn*=19.8°C) on January 22nd 1992, our selected day. The instrumental anomaly *Tm'* for that day reached 7.4°C, which means that the intraseasonal anomaly accounted for 29.6% of the measured *Tm* (25.1°C). The series extracted from 20CR shows a good overall agreement with the instrumental records, considering both trends and disturbances of synoptic character. However, 20CR tends to show less amplitude than the observations and thus to underestimate extreme daily values, which may be also influenced by local factors not resolved by the reanalysis.

4.3.2 The modulation of summer SAT by the MJO in Eastern Patagonia

To assess the impact of the MJO on SAT' in Eastern Patagonia, we use *Tm'* from 16 stations (Fig. 4.2a and Table 4.1). For each station time series, we categorize each of the DJF days in terms of both amplitude and phase of the MJO. In the following analyses, we

a) location of stations

Fig. 4.2a *Location of temperature stations used in this study; the red rectangle encloses southeastern Patagonia (SEPG, 46°-52°S; 65°-70°W). The yellow/red/green/cyan stars indicate the location of Bahía Blanca/Viedma/Esquel/Comodoro Rivadavia (see Table 4.1).*
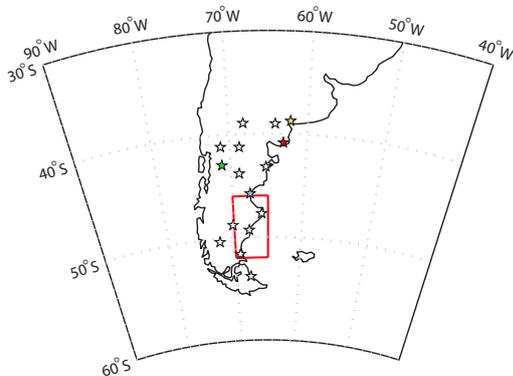
**Fig. 4.2b** *Composites of mean intraseasonal surface air temperature anomalies calculated for each station time series in association with active MJO phases (thin black curves), station composite mean (thick black curve), and composite mean of the 5 20CR gridpoints within SEPG (red curve). Black circles denote statistical significance at 95% (see text); red circles show the 95% confidence intervals for the SEPG mean signal.*

b) MJO signal

Table 4.1: *Stations from the Argentinean National Weather Service used in this study*

station code	station name	latitude	longitude	altitude [m a.s.l.]	period covered	Tx: data availability [%]	Tn: data availability [%]	active MJO phase with lowest Tm	active MJO phase with highest Tm
87715	Neuquén Aero	-38°57'	-68°08'	271	1957-2010	95.9	97.8	4	8
87736	Río Colorado	-39°01'	-64°05'	79	1957-2010	74.2	77.9	4	8
87750	Bahía Blanca Aero	-38°44'	-62°10'	83	1957-2010	99.1	99.1	5	7
87765	Bariloche Aero	-41°09'	-71°10'	840	1957-2010	95.2	99.4	4	8
87774	Maquinchao	-41°15'	-68°44'	888	1957-2010	94.4	95.8	4	8
87791	Viedma Aero	-40°51'	-63°01'	7	1968-2010	95.9	96.0	4	2
87803	Esquel Aero	-42°56'	-71°09'	797	1962-2010	91.0	91.7	3	8
87814	Paso de Indios	-43°49'	-68°53'	460	1969-2010	84.9	85.7	4	8
87828	Trelew Aero	-43°12'	-65°16'	43	1957-2010	99.8	99.8	4	8
87860	Comodoro Rivadavia Aero	-45°47'	-67°30'	46	1957-2010	98.5	98.5	4	8
87880	Gobernador Gregores Aero	-48°47'	-70°10'	358	1957-2010	62.8	70.6	4	8
87896	Puerto Deseado Aero	-47°44'	-65°55'	80	1957-2010	78.6	82.1	4	8
87903	Lago Argentino Aero	-50°20'	-72°18'	220	1957-2010	75.1	75.0	4	8
87909	San Julián Aero	-49°19'	-67°47'	62	1937-2010	61.8	65.3	4	8
87925	Río Gallegos Aero	-51°37'	-69°17'	19	1957-2010	94.4	96.8	4	8
87934	Río Grande B.A.	-53°48'	-67°45'	22	1960-2010	86.0	82.1	4	8

just consider days classified as *active* according to their MJO amplitude. Fig. 4.2b shows a clear modulation of SAT' by the MJO (amplitude of ~1.5°C), revealed by both the mean SAT' magnitudes obtained for each station time series and the composite mean. For each station and phase, we assessed the statistical significance at 95% (two-tailed) of the mean SAT' signal against the distribution of 1000 means calculated from random samples of the same size as that of the original group of days considered. Significant values correspond mainly to phases 3 and 4 (negative anomalies) and to 7 and 8 (positive anomalies), in agreement with the results of Alvarez et al. (2014, submitted to *Climate Dynamics*). Indeed, from the 16 analysed stations, 13 (depicted by white stars in Fig. 4.2b) exhibit their highest (lowest) SAT' mean in phase 8 (4). The exceptions are Bahía Blanca (yellow star), Viedma (red star), and Esquel (green star), with their maxima in phases 7/2/8 and their minima in phases 5/4/3, respectively.

The evolution of the MJO modulation observed in the instrumental SAT' records agrees with that revealed from the mean SAT' signal of SEPG (the area enclosed by the red rectangle in Fig. 4.2a) extracted from 20CR for 1906-2008 (red curve in Fig. 4.2b). This region was selected in order to make the present results comparable to those of our study about intraseasonal heat waves in the same area (Jacques-Coper et al., in prep.). Although the amplitude of the signal from this region next to the Atlantic coast is lower in the reanalysis than that in the instrumental records, a robust result is that the maximum (0.67°C) and minimum (-0.32°C) SAT' perturbations are again detected in phases 8 and 4, respectively, giving rise to a signal amplitude of 1°C.

4.3.3 Large-scale circulation anomalies associated with the extreme signatures of the MJO on intraseasonal SAT in Eastern Patagonia

In this section, we explore the imprint of the MJO on the SAT' field of South America revealed by 20CR for 1906-2008. We focus on the active phases of the MJO that induce the lowest and the highest SAT' signals in Eastern Patagonia, i.e. MJO phase 4 and 8, respectively. The figures corresponding to this section, extended to all phases, can be found in the supplementary material as Figs. 4.S2-S4. Because the active phases of the MJO tend to exhibit persistence, often a cluster of neighbouring days that correspond to a particular active phase is observed (see Table 4.2 and Fig. 4.S1). In the following compositing analyses, we account for the autocorrelation effect caused by this fact by selecting just the first days of each cluster. This means that we retain just 104 (102) out of 364 (394) days for the active phase 4 (8).

Table 4.2: *Statistics of clusters of days classified as active MJO phases during DJF 1906-2008*

	phase 1	phase 2	phase 3	phase 4	phase 5	phase 6	phase 7	phase 8
total days	332	341	473	364	308	424	453	394
number of clusters (i.e., *first days*)	94	93	112	104	96	112	115	102
length (median) [days]	3	4	4	3	3	4	4	3
length (mean) [days]	3.52	3.66	4.21	3.49	3.20	3.78	3.92	3.85
length (std. dev.) [days]	1.84	1.63	2.54	1.67	1.86	1.88	2.22	2.24

active phase 4

a)

SC

b)

c)

SAT' anomaly [°C]

days relative to MJO active phase 4

active phase 8

d)

EC

e)

f)

SAT' anomaly [°C]

days relative to MJO active phase 8

SEPG: SAT'
Monte Carlo mean
MC normfit: 90%, 95%, 99%

[°C]
1
0.8
0.6
0.4
0.2
0
-0.2
-0.4
-0.6
-0.8
-1
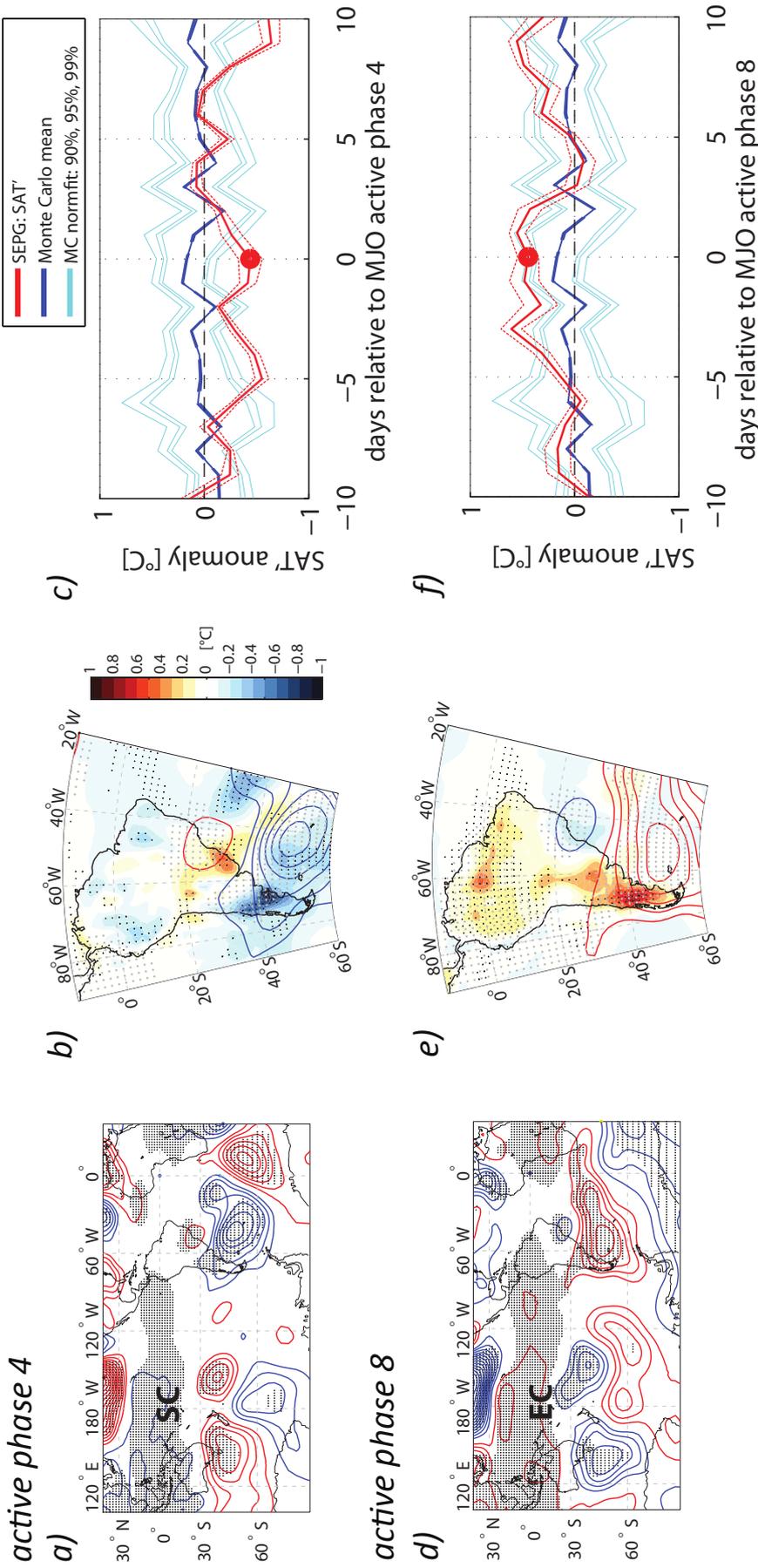
Fig. 4.3: (a,d) Mean intraseasonal anomaly of geopotential height at 500 hPa; red/blue contours every 7.5 gpm denote positive/negative anomalies and black dots show statistically significant values at 95%. (b,e) Same fields as in the left panels, superimposed on the mean intraseasonal anomaly of temperature (see color scale); black/grey dots show statistically significant temperature/geopotential height values at 95%. (c,f) Mean intraseasonal temperature anomaly (thick red curve) and its spatial standard anomaly (thin red curve), centred on the first day of the cluster composite of the active MJO phase; light blue lines denote the 90%, 95% and 99% percentiles of the normal distributions adjusted to 1000 random realizations of the same size of the original sample. The panels correspond to composites of (upper row) active phase 4 and (lower row) active phase 8. In panels a and d, the acronyms "SC" and "EC" stand for "suppressed convection" and "enhanced convection" and denote the location of these features with respect to the climatology for the composites of active MJO phases 4 and 8, respectively.

The left panels of Fig. 4.3 show the mid-level intraseasonal circulation anomalies, depicted by the geopotential height at the level of 500 hPa (z500'), calculated as the composite mean of the days selected as explained above. In the active phase 4 (Fig. 4.3a), a cyclonic perturbation extends over the southern half of South America with a centre that exceeds -45 hPa in magnitude and is located over the southwest Atlantic. A downstream anticyclonic anomaly of similar amplitude is noticeable to its east, between southern Africa and Antarctica. Upstream, over the South Pacific, a weak anticyclonic anomaly appears at ca. 70°S; 120°W, and, further to the West, we observe a stronger cyclonic anomaly around 60°S; 180°. To the north of this perturbation, two anticyclonic centres are distinguished according to the contour interval used (7.5 hPa): one to the northwest (with its centre located to the south of Tasmania) and the other to the northeast (centred at ca. 40°S; 150°W). These alternating anomalies suggest that the cyclone over the southwest Atlantic and the south of South America is part of a mid-latitude wave train that extends over the South Pacific with at least partly tropical origin. Fig. 4.3b shows that the mid-level cyclone over Southern South America is linked to a negative temperature anomaly that extends from the western coast at around 30°S until the southern tip of the continent and exceeds -1°C around the mid-latitudes. To its northeast, a warm anomaly centre is evident over Uruguay and southeastern Brazil, located to the southwest of a weaker anticyclonic circulation. Fig. 4.3c exhibits the evolution of the mean SAT' signal over SEPG (see Fig. 4.2a) between the 10 days preceding the first day of the cluster of active phase 4 (denoted as day 0) and the 10 days after it. We note that, in general, cold conditions are found over SEPG in this composite. This result agrees with the cold anomalies over Southern South America during active MJO phases 3, 4 and 5 (Fig. 4.S3c-e). In particular, a negative temperature anomaly is observed around the first cluster day of active phase 4. That anomaly is statistically significant at 99% after a Monte Carlo simulation of 1000 random realizations of the same size as that of the original sample.

A similar analysis was made for the active phase 8 and the resulting mean anomalies (Fig. 4.3d) are to a great extent of opposite sign to those obtained for phase 4. In particular, over the South Pacific a pattern of alternating z500' of opposite sign as those of phase 4 is detected, with a more evident arch-shaped wavetrain-like structure extended from the date line towards South America. For both phases 4 and 8, the circulation patterns described here show good agreement with those obtained by Alvarez et al. (2014, submitted to *Climate Dynamics*). The signature for phase 8 might be evidence of a stronger contribution of the tropical forcing to the development of these circulation anomalies. As discussed in next section, this hypothesis is consistent with the location of maximum convection for this MJO phase, shown by OLR, 850-hPa winds and cloud cover anomaly fields (Cassou 2008; Oliver and Thompson 2011; Wheeler and Hendon 2004). The downstream effect of this alternation of z500' is an anticyclonic centre

located slightly to the east of SEPG. As a consequence, warm conditions are observed over the region, with a maximum of 0.7°C at ca. 42°S in the interior of the continent (Fig. 4.3e). To the northeast, over southeastern Brazil, a cold anomaly appears in connection with a cyclonic centre located above it. This feature suggests some resemblance to the SAT dipole described for the DJF seasonal means by Jacques-Coper and Brönnimann (2014). In a symmetrical way to what was observed for active phase 4, the composite sequence centred on the first day of the clusters corresponding to active phase 8 (day 0, Fig. 4.3f) bears a statistically significant positive SAT' anomaly, in particular for day 0. In this case, the general warm conditions around day 0 agree with the composite anomaly fields of temperature for active MJO phases 7, 8, and 1 (Fig. 4.S3g, h, and a).

4.3.4 The signal of the MJO in the intraseasonal heat waves in Southeastern Patagonia

The 22nd of January of 1992, the day presented as an example in section 4.3.1, was classified as a day with an active MJO phase 8. On that day, a heat wave was detected over the SEPG region using SAT' from 20CR (see Fig. 4.S1). In total, 201 intraseasonal heat waves were detected in SEPG after the criteria presented in section 4.2 within the

a) day −18, ~phase 4

b) day −13, ~phases 1 & 5
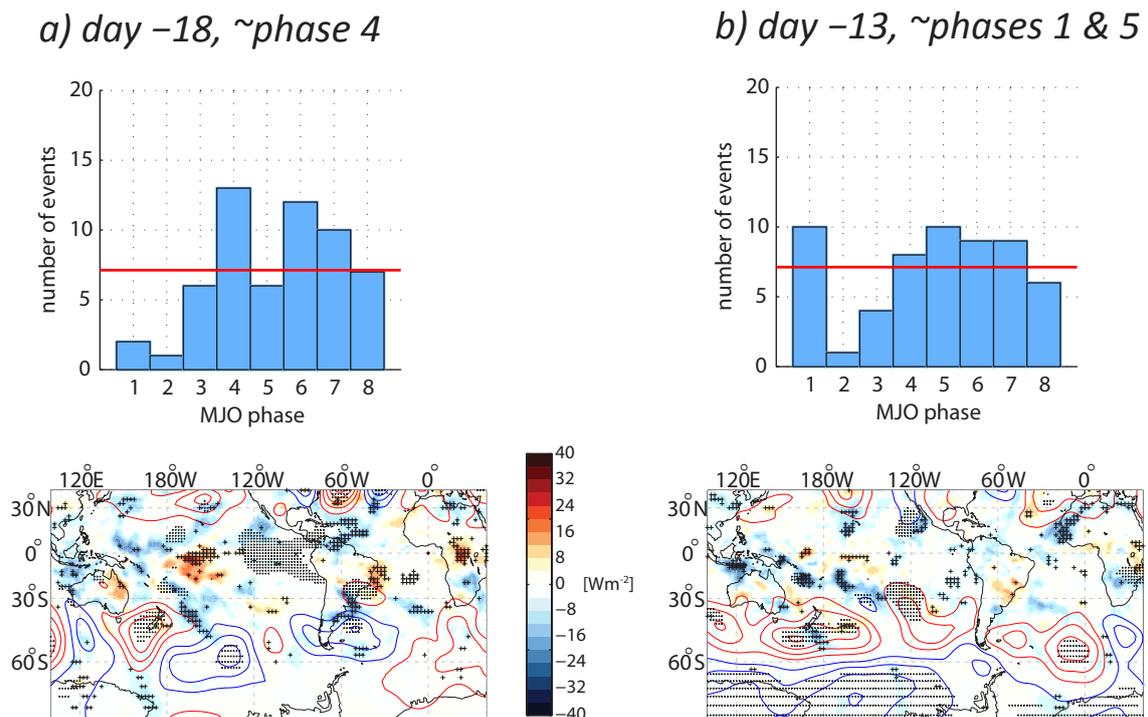
period DJF 1872-2010. As for the active MJO phases, the days that fulfil the conditions defining a heat wave also tend to occur within clusters. Therefore, we characterise here a *heat wave event* just by the first day of such a cluster, which we name *d0*. The mean warm perturbation over SEPG extracted from those events lasts approximately two weeks and exhibits a SAT' peak of 4.3°C on *d0*. From those 201 heat waves, 166 events correspond to the period overlapping with that of the reconstructed MJO index, DJF 1906-2008. Within this group, we selected those events that occurred during active MJO phases (Table 4.3). The spatial patterns of the mean warm anomaly induced over Southern South America by the active MJO phase 8 (n=394-16=378, excluding heat wave events) and by heat waves classified also as active MJO phase 8 (n=16) are comparable (Fig. 4.S5). However, we note that, by definition, the heat wave events are associated with much warmer conditions.

Considering the composite of heat wave events that are also active MJO days (i.e., on *d0*, Fig. 4.4e), its distribution after their MJO phases (valid for 1906-2008) reveals that the majority of them (16 out of 57, 28.1%) belongs to active phase 8, followed by active phase 7 (10 out of 57, 17.5%). One should note that the expected frequency for every phase in case of a random distribution would be 7.13 events. Below the histogram, we show the corresponding composite fields for these events, constructed from the subset of cases that occur within 1981-2008 (Table 4.3). The restriction of the events to the last decades is due to the limited availability of the OLR dataset, which starts only in 1974. The z500' composite of Fig. 4.4e features a wavetrain-like pattern over

c) day −9, ~phase 6
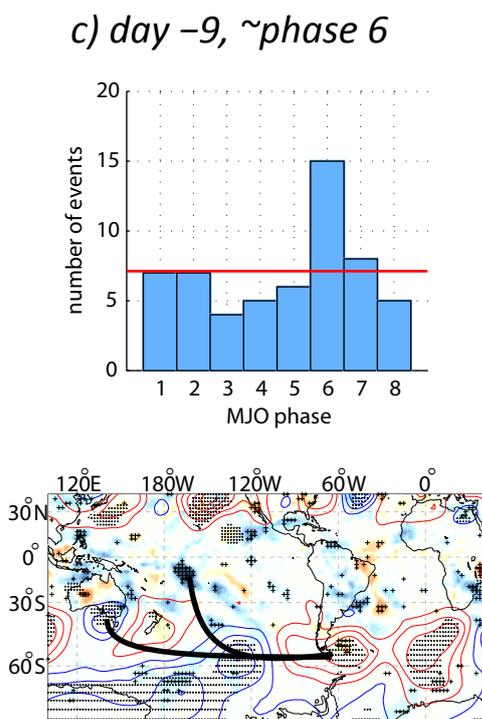
Fig. 4.4: *(upper panels) Histograms of days related to intraseasonal heat waves that occurred in southeastern Patagonia on active MJO phases, sorted according to them. (lower panels) Composite mean fields of the intraseasonal anomalies of geopotential height at 500 hPa (z500', contours every 5 gpm, red/blue for positive/negative values) and outgoing longwave radiation (OLR', see colour scale). Panels are relative to the composite of the first days of each heat wave, named day 0 (d0, panel e) and correspond to: a) day -18, b) day -13, c) day -9, d) day -5, e) day 0, and f) day 5. Above each panel, the most frequent phase is indicated. In panel e), all MJO phases are active. Histograms show all intraseasonal heat wave events whose d0 are classified as MJO active within 1906-2008 (see Table 4.3); the red line denotes the expected value from a random distribution (7.13 events/phase). The spatial composite fields are constructed with the corresponding subset of data for 1981-2008 (see Table 4.3). Statistical significance at 95% is indicated for z500'/OLR' by black dots/crosses. In panels c and d, the thick black lines indicate the wave guides inferred for the tropical and extratropical patterns.*

the South Pacific, which starts in Oceania, crosses South America and reaches South Africa. Again, as exhibited by the composite of the active MJO phase 8 in section 4.3.2, we observe an anticyclonic anomaly extending over the southern part of South America, whose centre exceeds 40 hPa and is located at the southwest Atlantic. Moreover, the OLR' field exhibits an area of significant positive anomalies over Patagonia, which may be related to enhanced solar radiation to the ground and thus may constitute a warming factor that contributes to the occurrence of a heat wave event.

Besides, in the tropical region, the OLR' field also features significant negative anomalies around 10°S; 160°W, a pattern that is characteristic of MJO phases 7 and 8 (Cassou 2008; Wheeler and Hendon 2004). We hypothesize that the convective signal observed in the tropics is linked to the wavetrain-like circulation anomalies observed poleward and further to the East. As described by Moore et al. (2010), tropical convection can induce the formation of poleward-propagating, planetary-scale Rossby waves in both hemispheres, a phenomenon that is called the Matsuno-Gill response (Barlow et al. 2007; Gill 1980; Matsuno 1966).

To explore this feature, we also show the composite fields of the days preceding d0. Note that although all days corresponding to d0 are classified by definition as active MJO phases, this is not necessarily the case for the days around them. However, the MJO reconstruction still provides a classification according to MJO phases for all available days. The histogram of day -5 (Fig. 4.4d) shows its highest frequency of events in phase

d) day −5, ~phase 7

e) day 0, ~phase 8
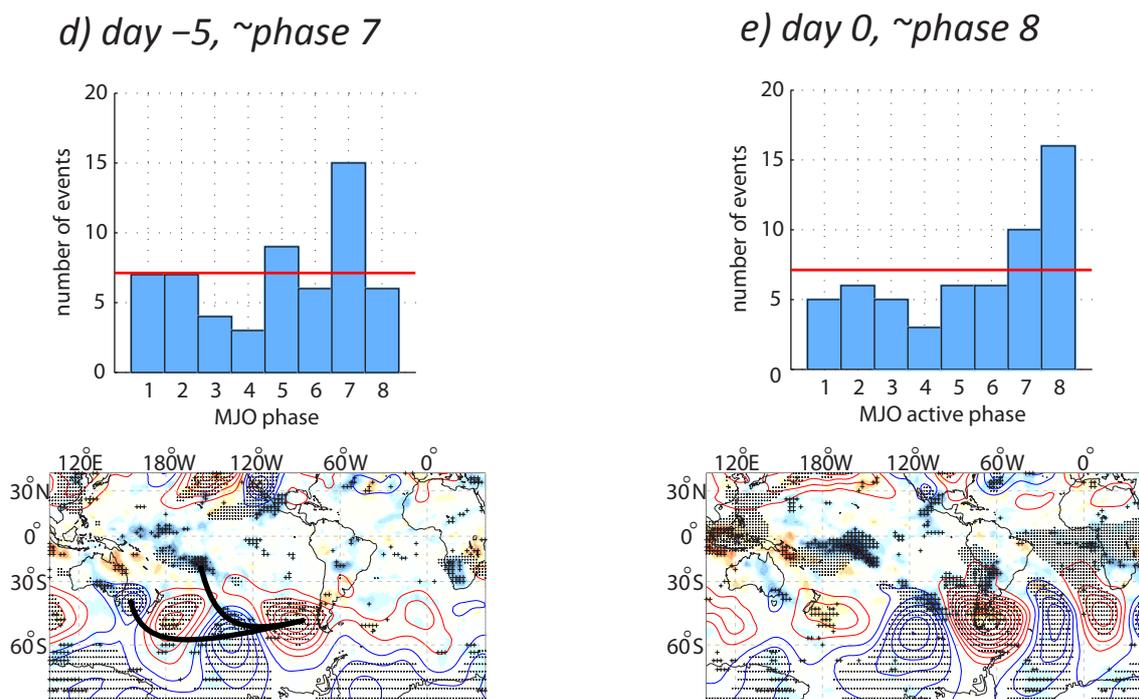
7 (15 out of 57, 26.3%, valid for 1906-2008), a value that doubles again the one expected from a random distribution. Considering that the nominal duration of each MJO phase is 6 days (Wheeler and Hendon 2004), this result seems to be a natural consequence of the distribution of the *d0* composite. In the corresponding z500' composite (valid for 1981-2008), shown below, an arch-shaped alternation of negative and positive anomaly centres is observed over the South Pacific. The connection between this anomalous circulation pattern and the negative OLR' anomaly located around 15°S; 160°W appears evident in this panel, in such a way that deep tropical convection seems to trigger, at least partly, the wave train observed downstream. However, the cyclone located over the Tasman Sea, between Australia and New Zealand, suggests that the wave train pattern also extends further to the southwest of the tropical convective anomaly. Thus, this pattern seems to bear also the signal of a mid-latitude disturbance. Therefore, these anomalies lead us to hypothesize that the observed wave train pattern may arise from a constructive tropical-extratropical interaction, as indicated by the wave guides drawn in Fig. 4.4c-d (thick black lines).

In the composite of day -9 relative to *d0* (Fig. 4.4c), again 15 out of 57 days (26.3%, valid for 1906-2008) correspond to MJO phase 6. In this case, the tropical convective anomaly mentioned above is located closer to the date line. The corresponding anomalies of the z500' field, which are weaker than in the composites discussed previously, still resemble the wavetrain-like structure over the South Pacific. On day -13 (Fig. 4.4b), despite the fact that the frequency distribution looks more uniform, phases 1 and 5 are

f) day 5, ~phase 8 and 1
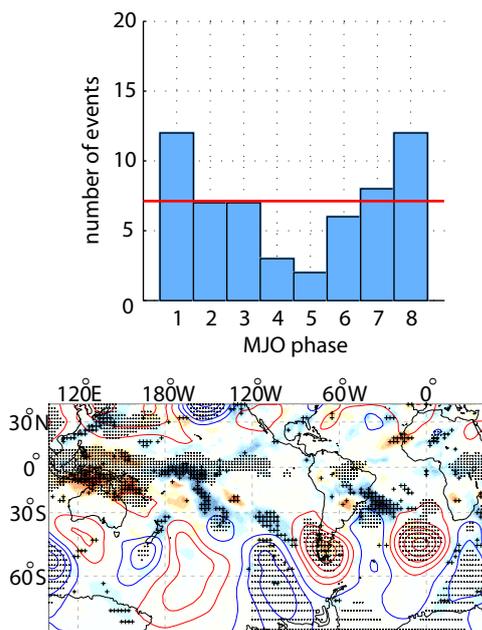
Fig. 4.4: *(continuation).*

Table 4.3: *Number of intraseasonal heat waves identified in southeastern Patagonia on days classified also as active MJO phases*

Phase	1	2	3	4	5	6	7	8	total (total divided by 8)
DJF 1906-2008	5	6	5	3	6	6	10	16	57 (7.13)
DJF 1981-2008	1	2	1	0	0	2	4	4	14 (1.75)

more populated than the others, both with 10 out of 57 events (17.5%, valid for 1906-2008). On day -18 (Fig. 4.4a), most of the events are classified as phase 4 (13 out of 57, 22.8%, valid for 1906-2008). In this case, the cyclonic anomaly over the southwest Pacific and Southern South America corresponds to that discussed in section 4.3.2 for cold conditions in Patagonia. For both composites of day -13 and day -18, tropical convection is mainly found over the Maritime Continent, a result which is consistent with predominating MJO phases 5 and 4, respectively.

The sequence suggested by these composites indicates that the occurrence of the selected heat wave events tend to follow the development of the MJO. This fact means that there is a time lag for the large-scale wave propagation before the occurrence of a heat wave in SEPG. This result is clearly depicted by the 21-day-long trajectories of these heat wave events, drawn on the phase space diagrams also for the rest of the active MJO phases (Fig. 4.S6). The present result suggests that this intraseasonal tropical mode may induce considerable temperature perturbations on the summer climate of Patagonia.

The eastward propagation of the circulation patterns observed in the sequence of composites of Fig. 4.4 is further supported by the frequency of phases of day +5 (Fig. 4.4f), where most members are found in phases 8 and 1, each of them with 12 occurrences out of 57 (21.1%, valid for 1906-2008). Although by this day the large-scale pattern over the South Pacific has already weakened, a positive OLR' signal is still observed over Patagonia. A further feature of this composite, which we also relate to the wave train pattern of z500', is the enhanced convective activity observed in the South Atlantic Convergence Zone (SACZ) in southeastern Brazil, a phenomenon observed in our previous work on intraseasonal heat waves in SEPG and also at the seasonal scale

for summer (Jacques-Coper and Brönnimann 2014).

Fig. 4.S7 in the Supplementary Material shows analogous composites of Fig. 4.4, but considering the intraseasonal anomalies of the wind at 200 hPa and of the streamfunction at 200 hPa. The corresponding panels essentially reveal that the wave train pattern found in z500', leading to the heat wave in SEPG on *d0*, can also be identified in upper levels, especially in the composites of days -5 and 0 relative to *d0* (panels d and e). Thus, the large-scale circulation anomalies causing heat waves in SEPG are present throughout the troposphere. In particular, for day -5, a noteworthy anticyclonic anomaly is found to the south of the main tropical convection centre in the western Pacific.

4.3.5 An example of tropical-extratropical interaction: the case study of the 22nd of January 1992

To better understand the interaction between tropical convection and the extratropical dynamics we analyse in detail selected stages of the 6-hourly large-scale circulation anomaly development leading to the heat wave in SEPG on the 22nd of January 1992, as depicted in 20CR. We are aware that only by means of a modelling study it would be possible to discern between tropical and extratropical waves. However, following descriptions can shed light on the subject under analysis.

Ten days before the event, on the 12th of January (classified as *active MJO phase 7*, Fig. 4.5a), an alternation of z500' centres is observed around 50°S, with cyclones to the south of Australia and at 60°S; 160°W, and anticyclones to the south of New Zealand (around the date line), also at 40°S; 130°W, and over Southern South America. This structure, noticeable also in the intraseasonal wind anomalies at 200 hPa (wnd200') and their streamfunction (sf200'), resembles a *mid-latitude wave train pattern*. In the tropical Pacific, the main convective activity is located to the north and to the east of Australia, at ca.15°N; 150°E and 20°S; 170°E, respectively. Anticyclonic anomalies are observed directly poleward of these convective centres, and thereafter they are called *tropical anomalies*.

Nine days before the event, on the 13th of January (classified as *active MJO phase 7*, Fig. 4.5b), the mid-latitude wave train has propagated eastward with respect to the preceding day. The tropical convective activity is more restricted to the east of Australia and the associated upper-level anticyclonic centre appears to its southeast, centred at ~30°S; 170°E. In Fig. 4.5c, the streamfunction contours connect this anticyclone with

a) 12 January 1992, 00 UTC

b) 13 January 1992, 12 UTC

c) 15 January 1992, 12 UTC
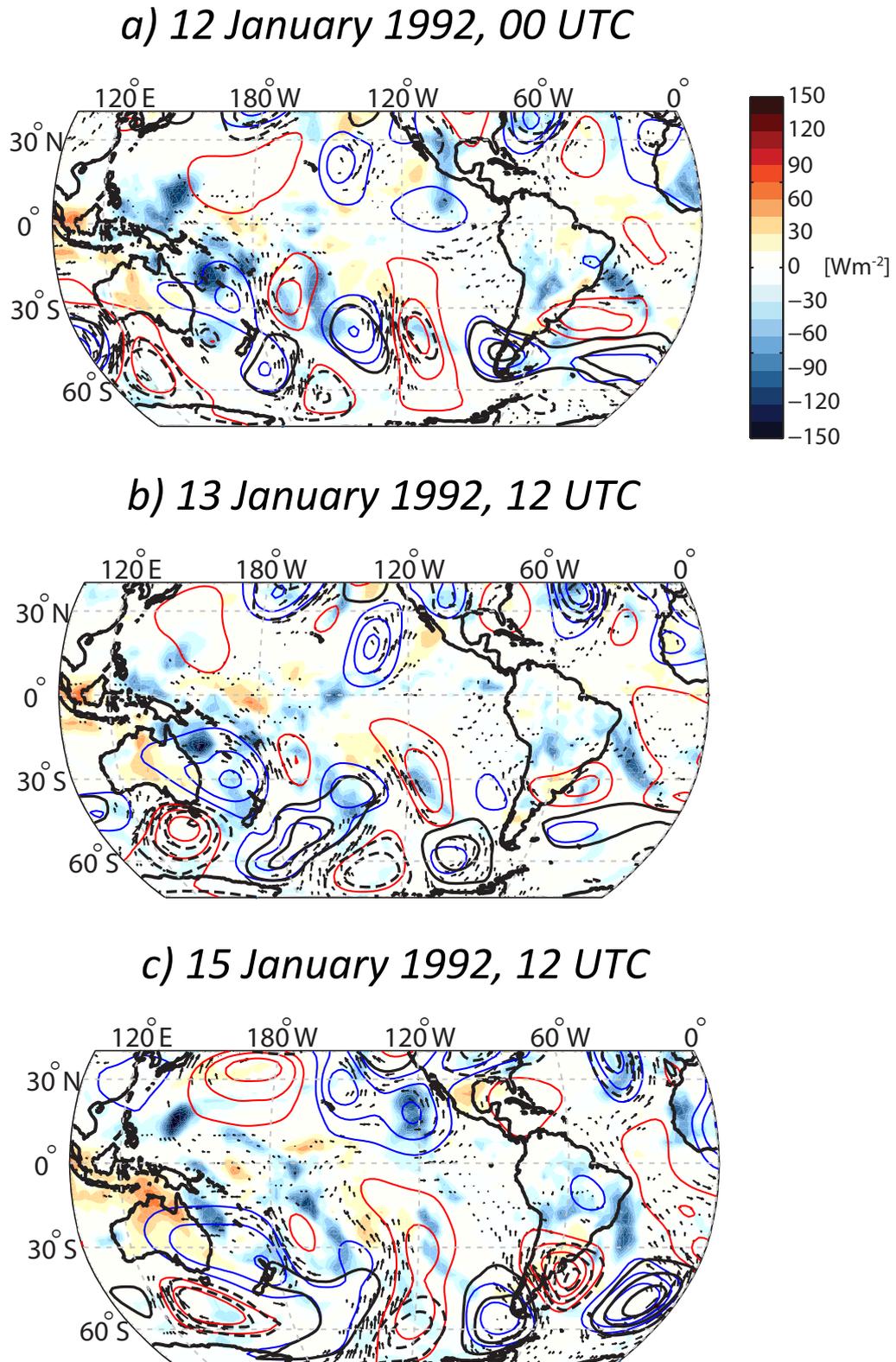
Fig. 4.5: *Case study of the heat wave of 22nd of January 1992. Selected fields of the 6-hourly sequence within the 10 days preceding the event are shown: a) 12th of January 1992, 00 UTC; b) 13th of January 1992, 12 UTC; c) 15th of January 1992, 12 UTC; d) 17th of January 1992, 12 UTC; e) 19th of January 1992, 06 UTC; and f) 21st of January 1992, 18 UTC. Fields correspond to the intraseasonal anomalies of outgoing longwave radiation (shaded, see color scale), geopotential height at 500 hPa (continuous/dashed contours every*

d) 17 January 1992, 12 UTC
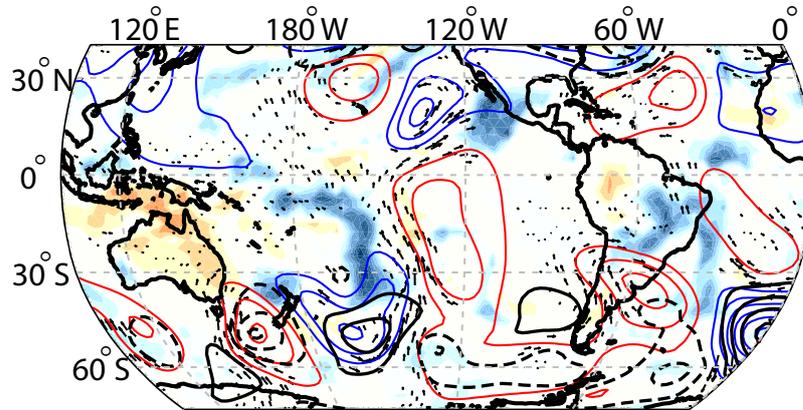
e) 19 January 1992, 06 UTC
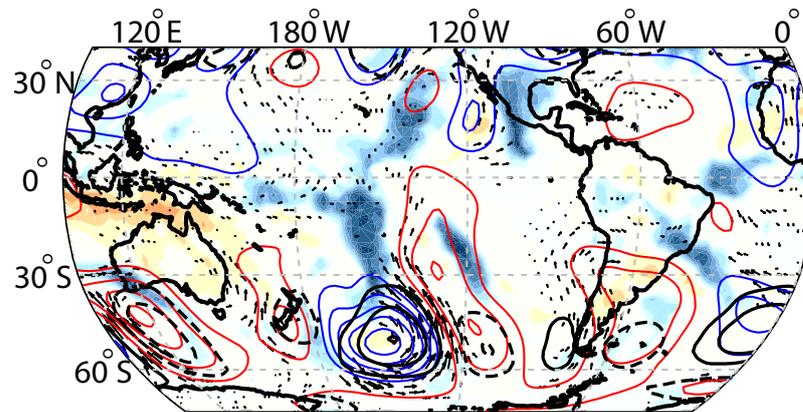
f) 21 January 1992, 18 UTC
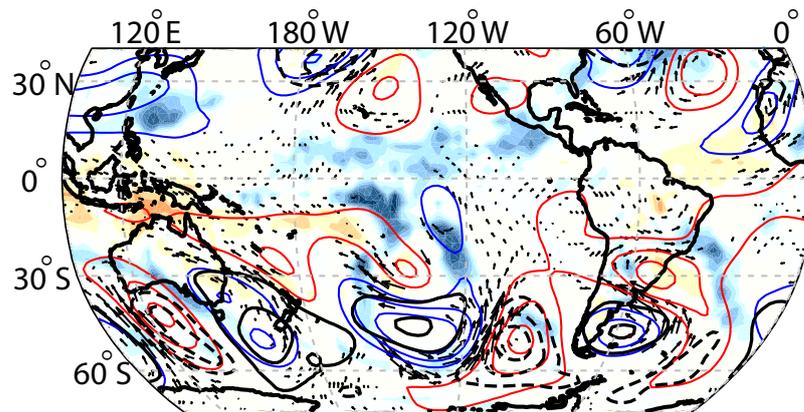
100 m for positive/negative values) and wind at 200 hPa. Wind vectors are only shown where the upper tercile of the intensity distribution of the zonal or the meridional component of the wind at 200 hPa during January 1992 is exceeded. The streamfunction at 200 hPa (red/blue contours every 10^7 m²/s for positive/ negative values) was calculated from the corresponding intraseasonal anomalies of the wind components. Zero contours omitted.

that of the mid-latitude wave train. From this fact, we speculate that there may be a constructive superposition of tropical and extratropical circulation anomalies.

One week before the event, on the 15th of January (classified as *active MJO phase 8,* Fig. 4.5c), the main tropical convective centre is located around 15°S; 170°W. The sf200' reveal anticyclonic circulation patterns at this longitude in the extratropics of both hemispheres. The alternation of negative and positive anomalies in the mid-latitude wave train of the Southern Hemisphere is evident in this panel. In particular, an anticyclone is identified west of the southern tip of South America.

On day -5, the 17th of January (classified as *active MJO phase 8*, Fig. 4.5d), the convective activity in the central-western Pacific has intensified. Apparently in association with this large-scale convection centre, southerly wind anomalies at 200 hPa are observed in the south Pacific along 140°W. The action centres of the mid-latitude wave train have propagated eastward with respect to the last composite. On this day, a cyclonic circulation over the Tasman Sea appears to be related to a positive (negative) OLR' anomaly over eastern Australia (the North Island of New Zealand). The anticyclonic anomaly south of the tropical convective centre, however, remains quite stationary, centred at ~45°S; 160°W.

Three days before the event, on the 19th of January (classified as *active MJO phase 8*, Fig. 4.5e), both the main convection centre in the subtropics and the associated mid-latitude anticyclone have strengthened, along with southerly wnd200' at ca. 140°W. To the east of that anticyclone, a cyclone-anticyclone-cyclone alternation can be observed, with the last feature approaching the southern tip of South America.

On the day previous to the event, the 21st of January (classified as *active MJO phase 8*, Fig. 4.5f), the convective cell, by then in the central Pacific, is spatially more restricted. By then, this convective anomaly, along with the mid-latitude wave train, have shifted to the east. In this way, a strengthened cyclone is located to the west of Southern South America and an anticyclone is evident over Patagonia. As discussed in previous sections, this anticyclonic circulation is related to the warm anomaly in SEPG.

It is interesting to note that the day-to-day development of the circulation anomalies over the southern Pacific strongly resembles the composite pattern shown in this study (Figs. 4.4 and 4.S7). Moreover, in particular the mid-latitude disturbances show good agreement in time and space with the pattern proposed by our previous work on intraseasonal heat waves in SEPG (Jacques-Coper et al., in prep.), and with that associated with the MJO influence (e.g. Alvarez et al. 2014, submitted to *Climate Dynamics*). The case study described above provides then good insight about the way

in which the circulation anomalies related to tropical convective activity can influence the mid-latitude wave train by interacting constructively.

4.4 Discussions and conclusions

In this work, we have explored the modulation of intraseasonal SAT in Eastern Patagonia by the Madden-Julian Oscillation (MJO). The study is based on long-term climate reconstructions, namely the Twentieth Century Reanalysis (20CR) and the reconstruction provided by Oliver and Thompson (2011) of the MJO index defined by Wheeler and Hendon (2004) for 1905-2008, based on the SLP fields from 20CR. We complement our analysis with instrumental daily records of surface air temperature (SAT) from Eastern Patagonia, from which the majority starts in DJF 1957. Hence, an effort has been made to use the longest datasets available in order to extract robust relationship between them.

We found that the intraseasonal component of instrumental SAT in Eastern Patagonia exhibits a signal induced by the active phases of the MJO. In particular, for most of the stations, warm (cold) conditions are statistically significant at 95% during active phases 7 and 8 (3 and 4). A robust result is that most instrumental records show their warmest departure (ranging mostly between 0.5°C and 1°C) for active phase 8 and their coldest anomaly (mostly between -0.5°C and -1°C) for active phase 4. Therefore, we present here an intraseasonal modulation of ~1.5°C of amplitude. In 20CR, the modulation of SAT in southeastern Patagonia (SEPG) features a lower amplitude of the signal, of around 1°C, but also shows its extreme values in active MJO phases 4 and 8. Therefore, we restricted our analysis to those two specific MJO phases. The corresponding SAT anomalies induced by them in SEPG seem to last for a couple of days around the first day of each cluster of active MJO phases.

The consistency of the present results suggests that there may be an enhanced predictability of summer intraseasonal SAT in Eastern Patagonia, subject to a skilful MJO forecasting capability, which is estimated to be up to 15-17 days (Seo et al. 2009). Indeed, the geographical distribution and temporal evolution of tropical moist deep convection determines the prediction of mid-latitude weather at lead times longer than 4 or 5 days [Lau et al. (2012) and references therein]. In this sense, the present results provide an alternative perspective on the predictability of the intraseasonal component of summer SAT in Patagonia. This conclusion stands out, in agreement with the recent

results of Alvarez et al. (2014, submitted to *Climate Dynamics*), and in spite of previous related findings, which showed that the mutual information between SAT and the MJO is highest not in Patagonia but in southeastern Brazil and northeastern Argentina and features its maximum in autumn and winter and its minimum in summer (Naumann and Vargas 2010).

Concerning the regional and large-scale circulation patterns associated with the MJO signal in Eastern Patagonia, we found that positive (negative) SAT anomalies are linked to a mid-level anticyclonic (cyclonic) circulation anomaly centred over the southwest Atlantic and extending over Southern South America, in agreement with previous work on regional summer SAT means (Jacques-Coper and Brönnimann 2014). Moreover, these circulation anomalies appear to be part of patterns of alternating polarities of the intraseasonal component of geopotential height in 500 hPa over the South Pacific. Furthermore, for active phases 4 and 8, the patterns show almost opposite anomalies.

The exploration of the links between the development of heat waves in SEPG and the active MJO allows us to conclude that heat waves that are also classified as active MJO phases tend to culminate in phase 8 (Fig. 4.4e). This result is consistent with the maximum SAT' anomaly detected for active phase 8 in the analysed instrumental network. A direct comparison of the evolution of the circulation anomalies with those of convective activity in the tropics suggests a possible role of the MJO in the triggering of heat waves in SEPG. Our findings insinuate that the arched wave-train pattern over the South Pacific observed for the active phase 8 is associated with an area of enhanced convection in the tropics, located around 10°S; 160°W, which is characteristic of that phase (Cassou 2008; Wheeler and Hendon 2004). The proposed association between tropical convection and the downstream development of an alternation of circulation anomalies is supported by the fields of composites corresponding to 6 and 9 days preceding a heat wave in SEPG, identified as MJO phases 7 and 6, respectively (Figs. 4.4c-d).

To illustrate our results, we selected DJF 1992. The MJO modulation of the spatial mean intraseasonal temperature in Eastern Patagonia is clearly observed in the intraseasonal development of the measured and reconstructed temperature in Comodoro Rivadavia Aero (45°47'S; 67°30'W; Fig. S1). This series reaches its maximum around the 22nd of January, with a positive (negative) trend before (after) it. The 22nd of January 1992 was classified as active MJO phase 8 and also identified as the first day of a heat wave in SEPG. We showed that the largest part of the temperature anomaly for that maximum value was consequence of the intraseasonal variability. The description of the development of the large-scale intraseasonal circulation anomalies for the ten days preceding that event provided an insight to the possible constructive interaction between

tropical convective activity and the mid-latitude wave train.

Therefore, a main conclusion of the present work, which may be used as a hypothesis for further research, is that mid-latitude disturbances resulting from extratropical dynamics leading to SAT impacts in Patagonia may interact with tropical activity in a way of constructive interference in order to enhance the probability of occurrence of a heat wave, in particular in SEPG. In other words, we suggest that this is a case of a profound association between a tropical intraseasonal oscillation and the disturbances embedded in the midlatitudes, as described in Lau et al. (2012). This suggestion is based on the fact that heat waves may occur in all active MJO phases but clearly tend to be favoured by the conditions set up mainly by active phase 8.

Using long-term observations and reconstructions, we have presented strong evidence for tropical influence behind the evolution of the observed circulation patterns leading to strong temperature perturbations in Eastern Patagonia. Further efforts are needed to investigate this subject through modelling experiments. In fact, an atmospheric response comparable to that observed for the composite of day -9 with respect to the occurrence of a heat wave in SEPG (classified as mostly MJO phase 6, Fig. 4.4c), although of different phasing, was simulated by Ding et al. (2011) for austral winter as a consequence of an anomalous warm sea surface temperature pattern in the central Pacific.

Acknowledgments

References

Barlow M, Hoell A, Colby F (2007) Examining the wintertime response to tropical convection over the Indian Ocean by modifying convective heating in a full atmospheric model. Geophys Res Lett 34:L19702. doi: 10.1029/2007GL030043

Barrett BS, Carrasco JF, Testino AP (2011) Madden–Julian Oscillation (MJO) Modulation of Atmospheric Circulation and Chilean Winter Precipitation. J Clim 25:1678–1688. doi: 10.1175/JCLI-D-11-00216.1

Berman A, Silvestri G, Compagnucci R (2013) On the variability of seasonal temperature in southern South America. Clim Dyn 40:1863–1878. doi: 10.1007/s00382-012-1596-5

Cassou C (2008) Intraseasonal interaction between the Madden-Julian Oscillation and the North Atlantic Oscillation. Nature 455:523–527.

Cerne SB, Vera CS (2011) Influence of the intraseasonal variability on heat waves in subtropical South America. Clim Dyn 36:2265–2277. doi: 10.1007/s00382-010-0812-4

Compo GP, Whitaker JS, Sardeshmukh PD, et al. (2011) The Twentieth Century Reanalysis Project. Q J R Meteorol Soc 137:1–28. doi: 10.1002/qj.776

Coronato F, Bisigato A (1998) A temperature pattern classification in Patagonia. Int J Climatol 18:765–773. doi: 10.1002/(SICI)1097-0088(19980615)18:7<765::AID-JOC282>3.0.CO;2-H

Ding Q, Steig EJ, Battisti DS, Kuttel M (2011) Winter warming in West Antarctica caused by central tropical Pacific warming. Nat Geosci 4:398–403.

Donald A, Meinke H, Power B, et al. (2006) Near-global impact of the Madden-Julian Oscillation on rainfall. Geophys Res Lett 33:L09704. doi: 10.1029/2005GL025155

Garreaud R, Lopez P, Minvielle M, Rojas M (2012) Large-Scale Control on the Patagonian Climate. J Clim 26:215–230. doi: 10.1175/JCLI-D-12-00001.1

Gill AE (1980) Some simple solutions for heat-induced tropical circulation. Q J R Meteorol Soc 106:447–462. doi: 10.1002/qj.49710644905

Jacques-Coper M, Brönnimann S (2014) Summer temperature in the eastern part of southern South America: its variability in the twentieth century and a teleconnection with Oceania. Clim Dyn 1–20. doi: 10.1007/s00382-013-2038-8

Juliá C, Rahn DA, Rutllant JA (2012) Assessing the Influence of the MJO on Strong Precipitation Events in Subtropical, Semi-Arid North-Central Chile (30°S). J Clim 25:7003–7013. doi: 10.1175/JCLI-D-11-00679.1

Kanamori H, Yasunari T, Kuraji K (2013) Modulation of the Diurnal Cycle of Rainfall Associated with the MJO Observed by a Dense Hourly Rain Gauge Network at Sarawak, Borneo. J Clim 26:4858–4875. doi: 10.1175/JCLI-D-12-00158.1

Lau WM, Waliser D, Roundy P (2012) Tropical–extratropical interactions. Intraseasonal Var. Atmos. Clim. Syst. SE - 14. Springer Berlin Heidelberg, pp 497–512

Liebmann B, Smith CA (1996) Description of a complete (interpolated) outgoing longwave radiation dataset. Bull Amer Met Soc 77:1275–1277.

Madden RA, Julian PR (1971) Detection of a 40–50 Day Oscillation in the Zonal Wind in the Tropical Pacific. J Atmos Sci 28:702–708. doi: 10.1175/1520-0469(1971)028<0702:DOADOI>2.0.CO;2

Maloney ED, Kiehl JT (2002) MJO-Related SST Variations over the Tropical Eastern Pacific during Northern Hemisphere Summer. J Clim 15:675–689. doi: 10.1175/1520-0442(2002)015<0675:MRSVOT>2.0.CO;2

Matsuno T (1966) Quasi-Geostrophic Motions in the Equatorial Area. J Meteorol Soc Japan Ser II 44:25–43.

Matthews AJ, Pickup G, Peatman SC, et al. (2013) The effect of the Madden-Julian Oscillation on station rainfall and river level in the Fly River system, Papua New Guinea. J Geophys Res Atmos 118:10,910–926,935. doi: 10.1002/jgrd.50865

Mo KC, Paegle JN (2001) The Pacific–South American modes and their downstream effects. Int J Climatol 21:1211–1229. doi: 10.1002/joc.685

Moore RW, Martius O, Spengler T (2010) The Modulation of the Subtropical and Extratropical Atmosphere in the Pacific Basin in Response to the Madden–Julian Oscillation. Mon Weather Rev 138:2761–2779. doi: 10.1175/2010MWR3194.1

Naumann G, Vargas WM (2012) A Study of Intraseasonal Temperature Variability in Southeastern South America. J Clim 25:5892–5903. doi: 10.1175/JCLI-D-11-00482.1

Naumann G, Vargas WM (2010) Joint Diagnostic of the Surface Air Temperature in Southern South America and the Madden–Julian Oscillation. Weather Forecast 25:1275–1280. doi: 10.1175/2010WAF2222418.1

Oliver ECJ, Thompson KR (2011) A Reconstruction of Madden–Julian Oscillation

Variability from 1905 to 2008. J Clim 25:1996–2019. doi: 10.1175/JCLI-D-11-00154.1

Oliver EJ (2014) Multidecadal variations in the modulation of Alaska wintertime air temperature by the Madden–Julian Oscillation. Theor Appl Climatol 1–11. doi: 10.1007/s00704-014-1215-y

Prohaska F (1976) The climate of Argentina, Paraguay, and Uruguay, Vol. 12, W. 57–69.

Salby ML, Hendon HH (1994) Intraseasonal Behavior of Clouds, Temperature, and Motion in the Tropics. J Atmos Sci 51:2207–2224. doi: 10.1175/1520-0469(1994)051<2207:IBOCTA>2.0.CO;2

Seo K-H, Wang W, Gottschalck J, et al. (2009) Evaluation of MJO Forecast Skill from Several Statistical and Dynamical Forecast Models. J Clim 22:2372–2388. doi: 10.1175/2008JCLI2421.1

Sperber KR (2003) Propagation and the Vertical Structure of the Madden–Julian Oscillation. Mon Weather Rev 131:3018–3037. doi: 10.1175/1520-0493(2003)131<3018:PATVSO>2.0.CO;2

Vecchi GA, Bond NA (2004) The Madden-Julian Oscillation (MJO) and northern high latitude wintertime surface air temperatures. Geophys Res Lett 31:L04104. doi: 10.1029/2003GL018645

Wheeler MC, Hendon HH (2004) An All-Season Real-Time Multivariate MJO Index: Development of an Index for Monitoring and Prediction. Mon Weather Rev 132:1917–1932. doi: 10.1175/1520-0493(2004)132<1917:AARMMI>2.0.CO;2

Zhang C (2005) Madden-Julian Oscillation. Rev Geophys 43:RG2003. doi: 10.1029/2004RG000158

Zhou Y, Thompson KR, Lu Y (2011) Mapping the Relationship between Northern Hemisphere Winter Surface Air Temperature and the Madden–Julian Oscillation. Mon Weather Rev 139:2439–2454. doi: 10.1175/2011MWR3587.1

4.S Supplementary material

Figures
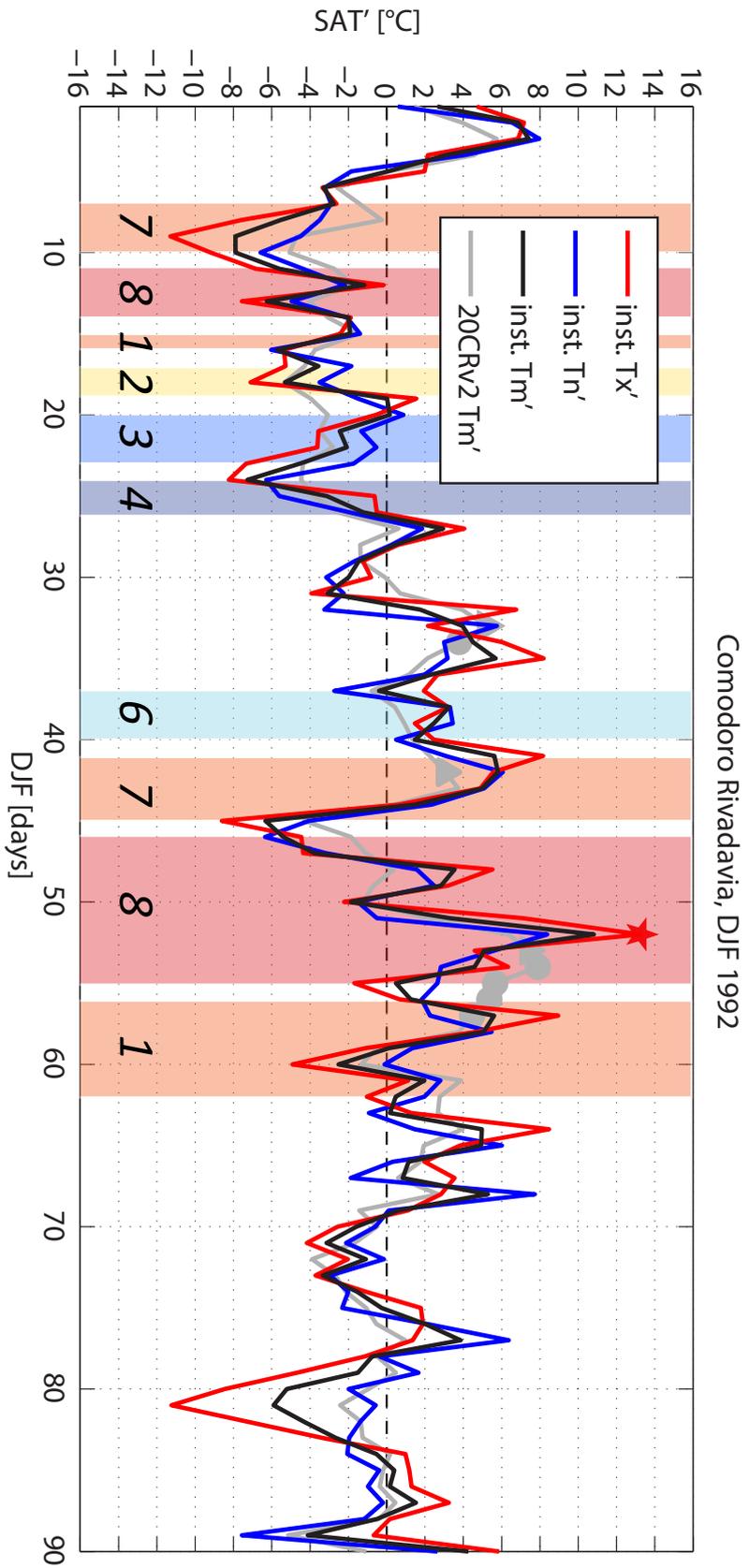
Fig. 4.S1: *Measured and reconstructed temperature for DJF 1992. The time series correspond to the station Comodoro Rivadavia Aero (see Table 4.1 and Fig. 2a): minimum temperature (Tn', blue curve), maximum temperature (Tx', red curve) and mean temperature (Tm', black curve), and to the reconstructed 20CR mean temperature (grey curve). For the 20CR record, days fulfilling the conditions for a heat wave are depicted by grey circles; the first day of each heat wave cluster is denoted by a grey triangle. The numbered shaded areas in the background depict the days classified as MJO active phases.*

a) phase 1
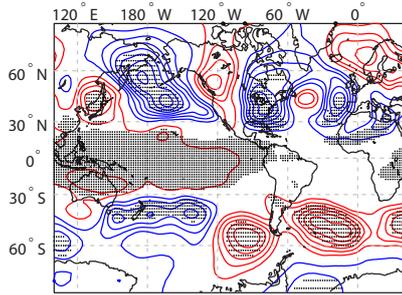
b) phase 2
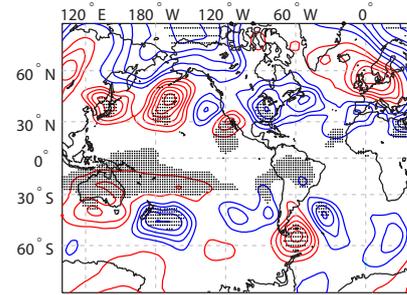
c) phase 3
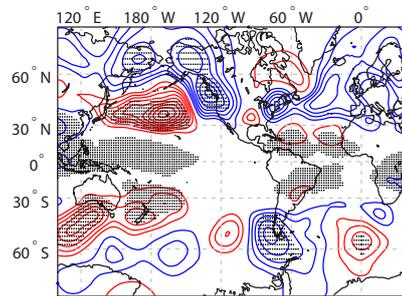
d) phase 4
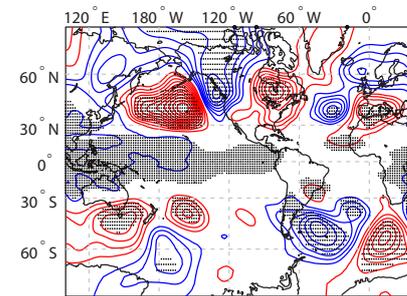
e) phase 5
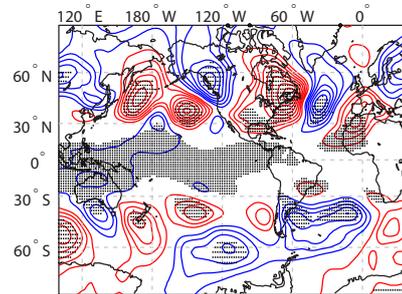
f) phase 6
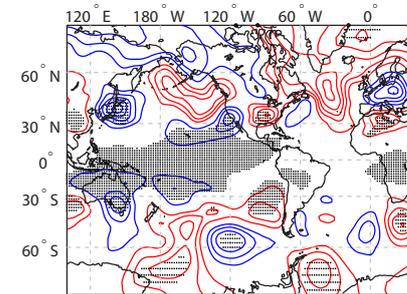
g) phase 7
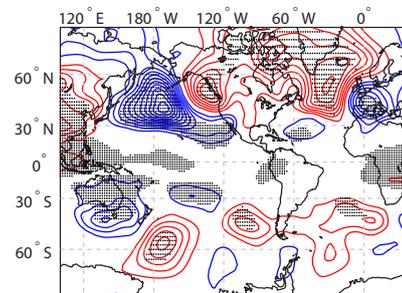
h) phase 8
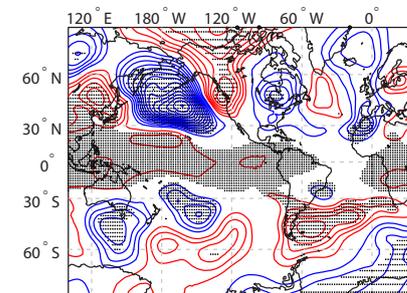
Fig. 4.S2: Analogous to the left panels of Fig. 4.2: mean intraseasonal anomaly of geopotential height at 500 hPa; red/blue contours every 7.5 gpm denote positive/negative anomalies and black dotes show statistically significant values at 95%. The panels correspond to composites of active phases of the MJO, as defined in the text.
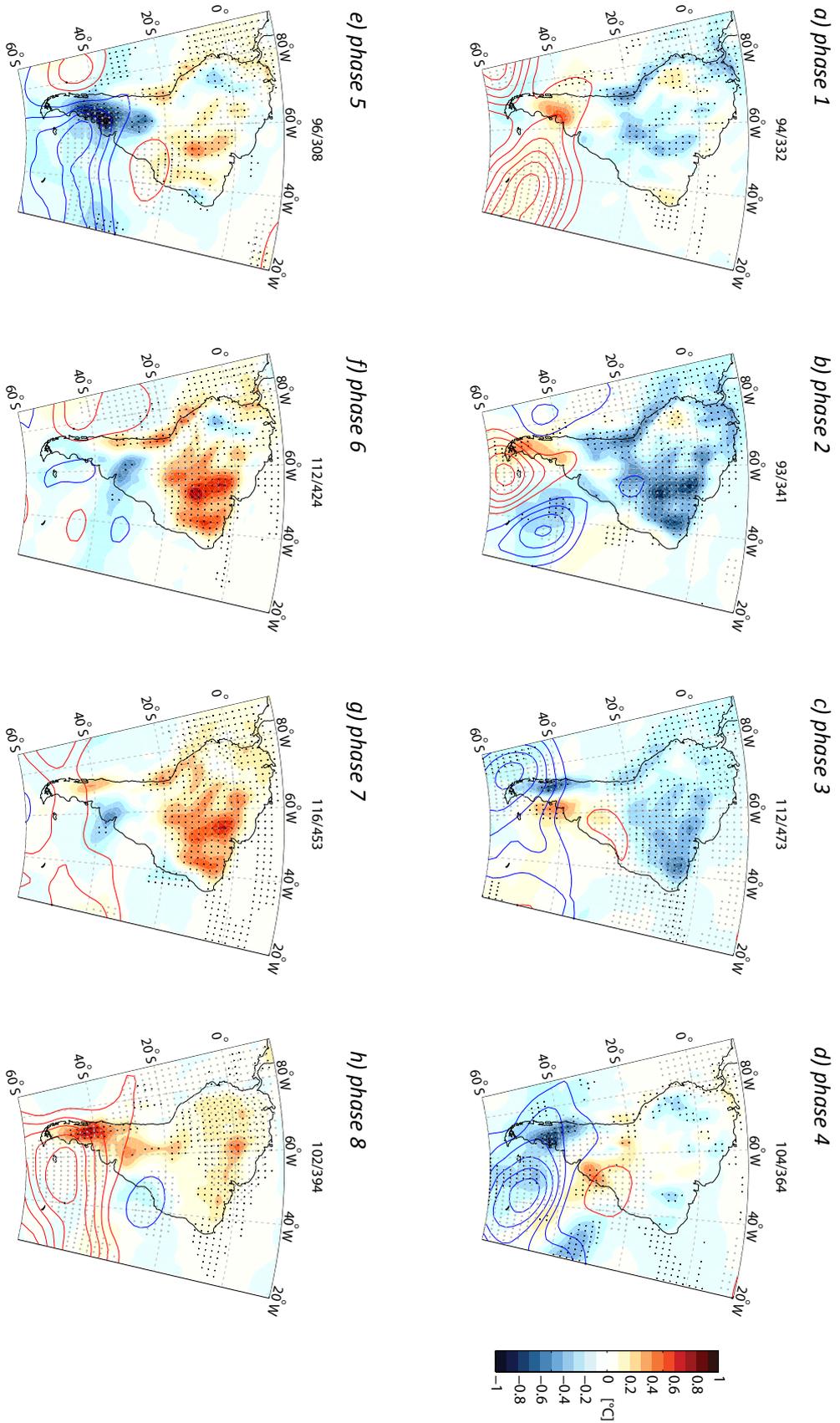
Fig. 4.S3: *Analogous to the middle panels of Fig. 4.2: mean intraseasonal anomaly of geopotential height in 500 hPa (red/blue contours every 7.5 gpm denote positive/negative anomalies), superimposed on the mean intraseasonal anomaly of temperature (see color scale); black/grey dots show statistically significant temperature/geopotential height values at 95%. The panels correspond to composites of active phases of the MJO, as defined in the text.*
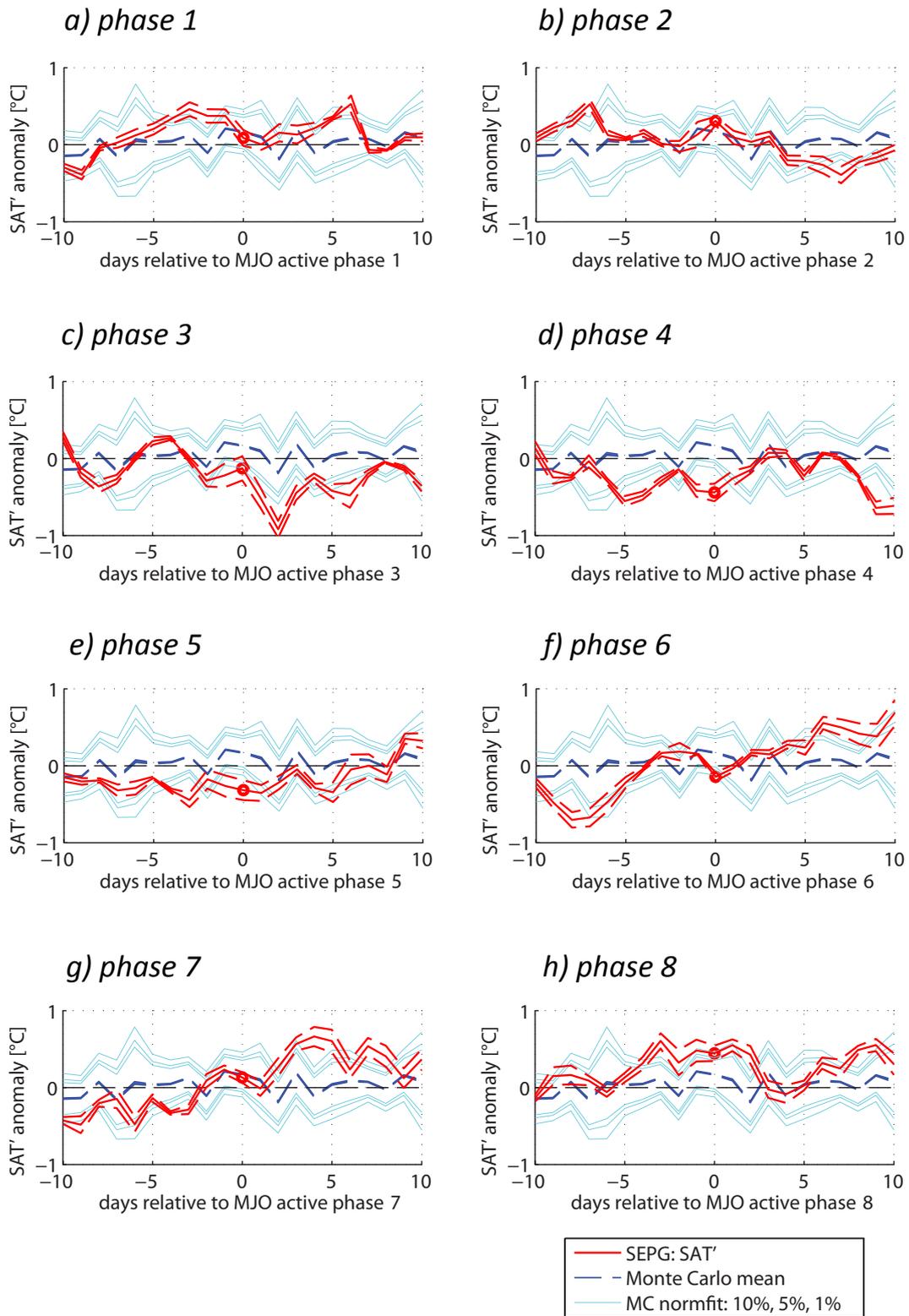
Fig. 4.S4: *Analogous to the right panels of Fig. 4.2: Mean temperature anomaly (red thick curve) centred on the first day of a cluster of each active MJO phase with its spatial standard anomaly (thin red curves); light blue lines denote the 90%, 95% and 99% percentiles of the normal distributions adjusted to 1000 random realizations of the same size as that of the original sample. The panels correspond to composites of active phases of the MJO, as defined in the text.*

a) MJO active phase 8: all days, no heat waves
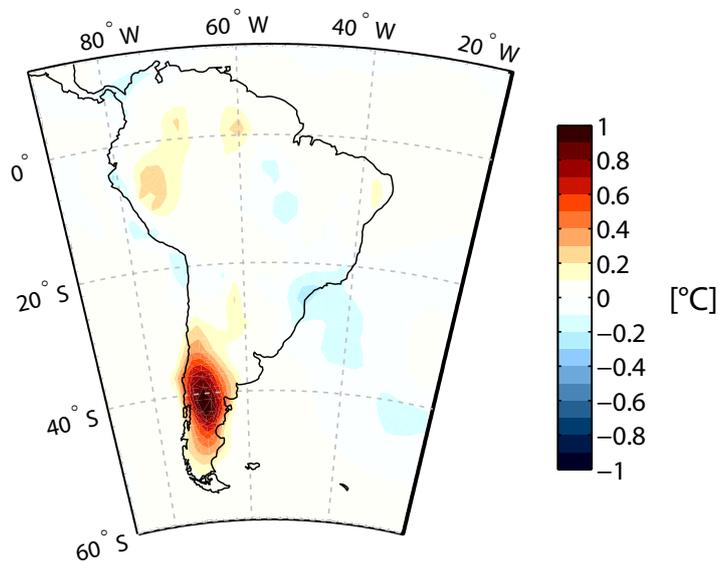
b) MJO active phase 8: heat waves
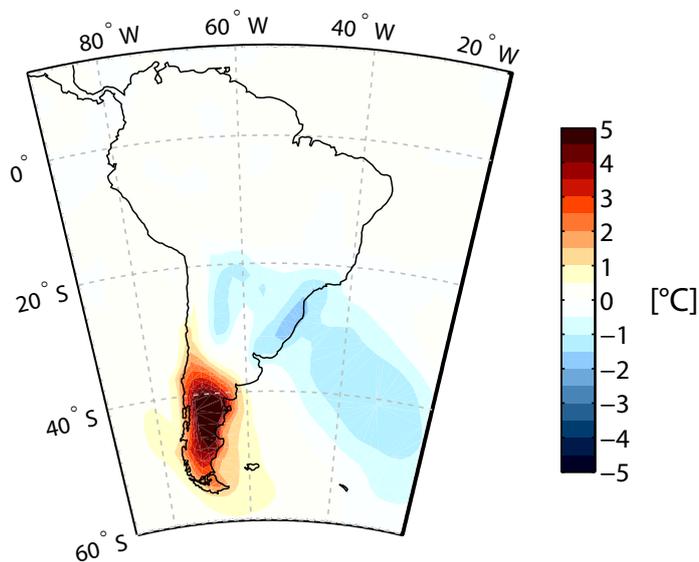
Fig. 4.S5*: Composites of intraseasonal mean surface air temperature from 20CR for summer days within 1906-2008 classified as: a) MJO active phase 8 and not corresponding to a heat wave event (n=378) and b) heat wave events (d0, see text for definition) occurring on active MJO phase 8 (n=16).*
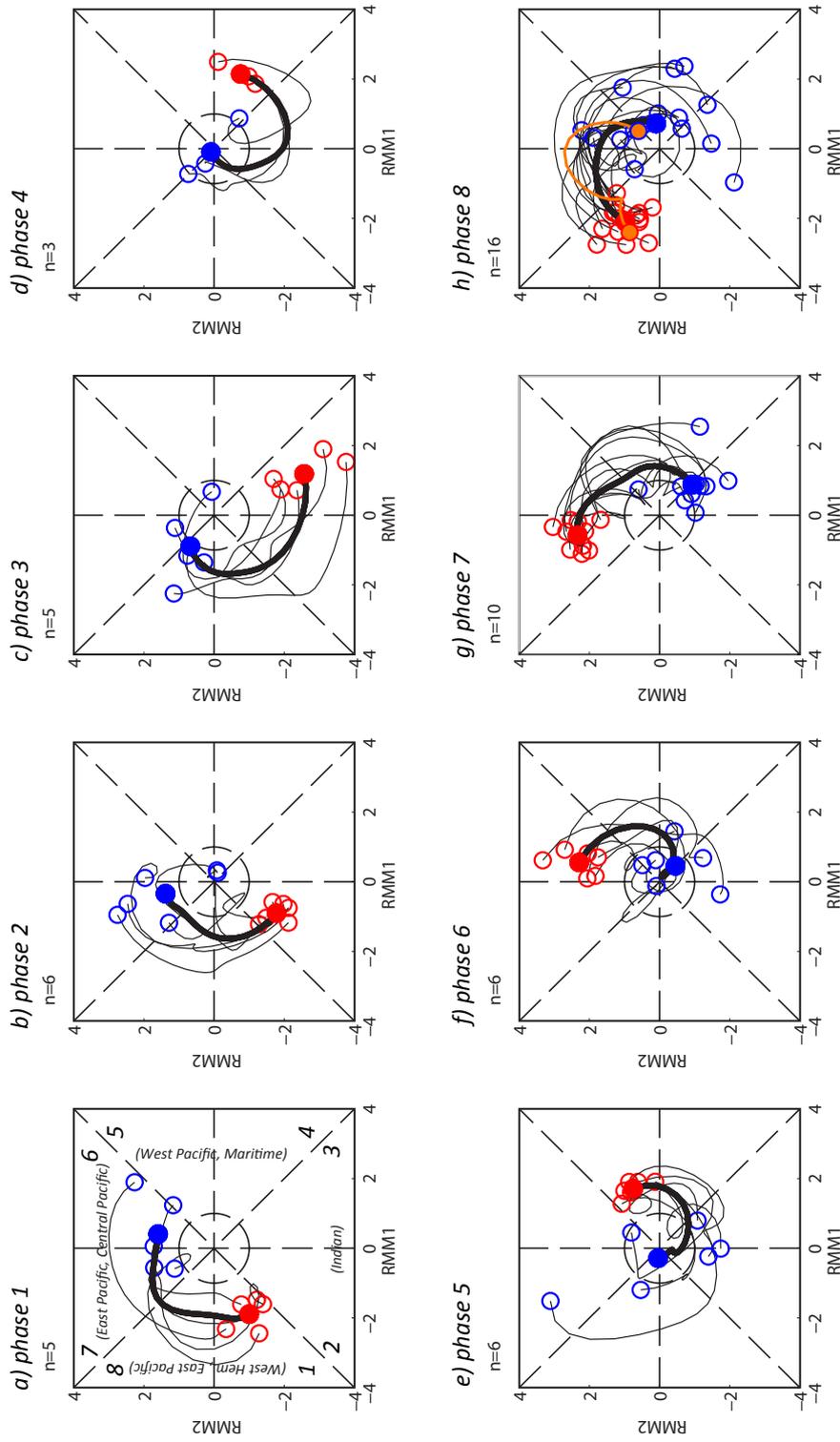
Fig. 4.S6: *Trajectories in the MJO phase space diagram of the heat waves in southeastern Patagonia occurring on days classified also as active MJO phases for 1906-2008 (see Table 4.3). For each trajectory, the red circle at its end denotes the first day of the heat wave cluster, d0 (see text for definition), and the blue circle at its beginning indicates the state 20 days before d0. The bold curves represent the mean trajectory for each group and the orange trajectory in panel h corresponds to the event of the 22nd of January of 1992. The number of cases of each group (n) is specified above each panel. In panel a), the eight phases of the diagram are indicated, as well as the rough geographical locations of the strongest convective cells associated with them. The inner dashed circle denotes an amplitude of 1.*

a) day −18, ~phase 4

b) day −13, ~phases 1 & 5

c) day −9, ~phase 6

d) day −5, ~phase 7

e) day 0, ~phase 8

f) day 5, ~phase 8 and 1
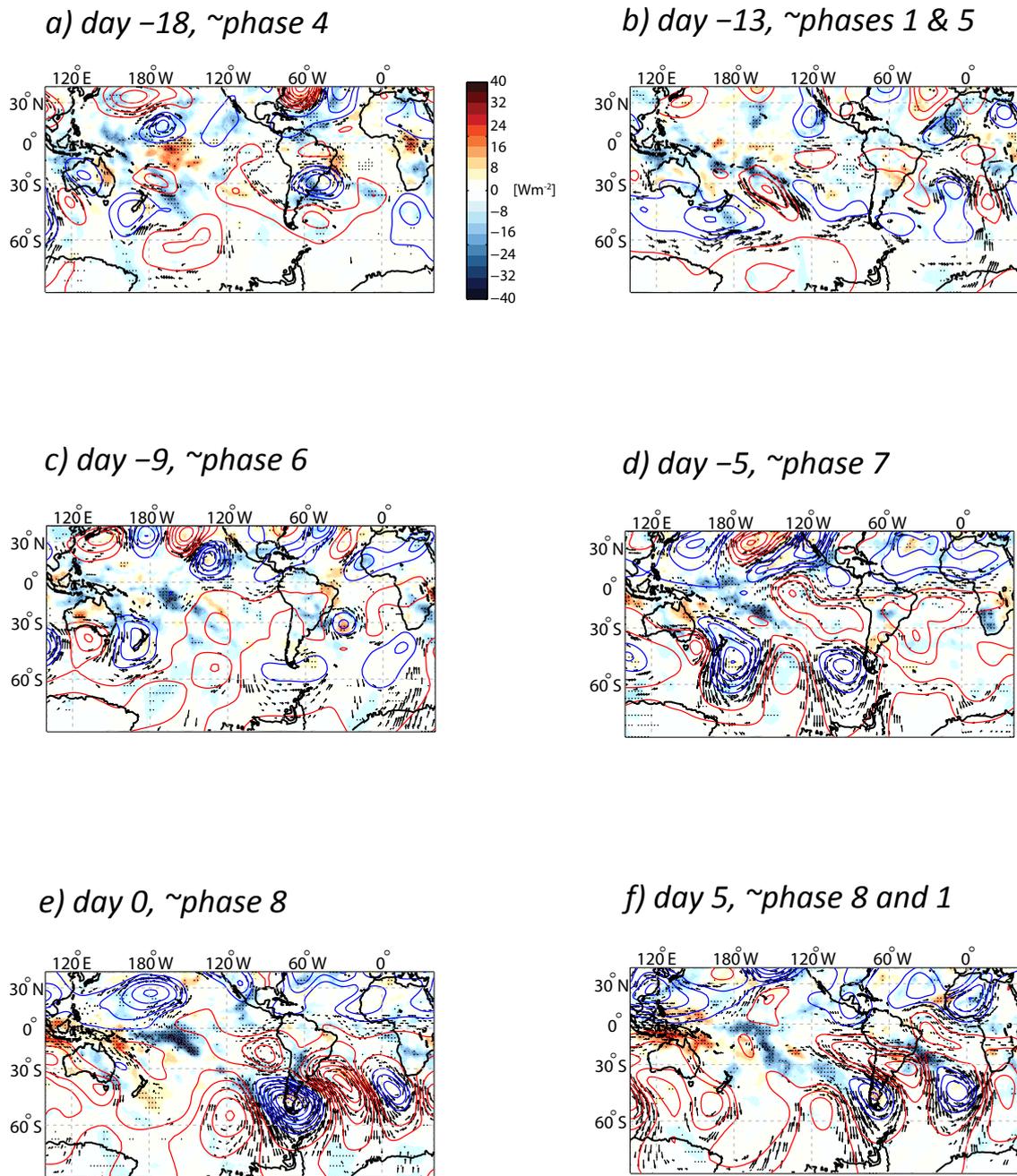
Fig. 4.S7*: Same as the composite fields of Fig. 4.4, but showing the intraseasonal anomalies of wind at 200 hPa (wnd200', only where the zonal or the meridional anomaly is significant at 95%), its streamfunction at 200 hPa (sf200', contours every 2.5*10⁶ m²/s, red/blue for positive/negative values), and outgoing longwave radiation (OLR', see colour scale); zero contours omitted. For each panel, the streamfunction was calculated for each member and then composited.*

Chapter 5

Conclusions and outlook

Throughout the chapters of this thesis, we have provided a novel long-term perspective on the summer air surface temperature (SAT) variability in Southern South America (SSA) with special emphasis on Patagonia. We have presented a valuable contribution to the understanding of the climate variability during the 20th century in a region where most of the previous studies were strongly restricted by the temporal and spatial availability of meteorological observations. To partially overcome this issue, we have based the present work on long-term instrumental measurements and the Twentieth Century Reanalysis (20CR), which are independent datasets. The 20CR is a global climate reconstruction whose employment on our study region, to our best knowledge, has not been reported before. To support the robustness of our main findings, additional climate measurements and reconstructions have also been taken into account.

Taking advantage of the potential offered by the 20CR, we have aimed at exploring the summer SAT variability considering different timescales. This approach, which was defined with the purpose of gaining a *multiscale* insight into our research subject, resulted in a study (Chapter 2) focused on phenomena taking place within comparatively *lower frequencies*, i.e. interannual and interdecadal timescales, and two studies (Chapters 3 and 4) on processes occurring within a *higher frequency*, namely in the intraseasonal range. The chapters follow a logical sequence. The analysis presented in Chapter 2, centred on the *summer-to-summer* SAT variability in SSA, yielded the motivation for Chapter 3: the exploration of the occurrence of *intraseasonal heat waves* in Southeastern Patagonia. These events may be interpreted as an analogue to the *warm summers* in the seasonal SAT means. Finally, Chapter 4 was outlined as an investigation to deepen the understanding of the dynamical mechanisms derived from the precedent chapters, as a means to highlight the potential applications of the climatological knowledge gained previously.

Specifically, we have drawn novel conclusions concerning the variability of summer SAT in our study region:

- The combination of long-term instrumental information and the 20CR has supplied an auspicious way to analyse the climate of SSA and its remote relationships during the 20th century.

- In particular, conclusions derived from signals extracted from 20CR for different timescales have been validated using instrumental records and thus represent *robust* results.

- The main interdecadal mode of summer SAT variability in SSA exhibits a *shifty* evolution. Besides the well-known cold-to-warm transition of late 1970s, we identified an opposite but more subtle one in the early 1930s. Moreover, in the 20th century, the in-phase behaviour between this mode and the PDO appears to be restricted to the period starting in the 1960s.

- The main interannual summer SAT variability mode is representative for almost the whole southern half of South America and has a frequency peak at ~3.4 years. Its large-scale correlation fields revealed a wave-train circulation pattern in the South Pacific that induces teleconnections between or study region and remote areas, in particular Oceania (specifically: the anticorrelation between SAT in SSA and precipitation in southeastern Australia). This teleconnection, along with the relationship between the main interannual mode and the Niño3.4 and the SAM indices, are non-stationary within the 20th century.

- In the intraseasonal timescale, we described the occurrence of heat waves in Southeastern Patagonia. We validated our results using local observations at daily resolution. These heat waves, whose mean signal lasts for ca. two weeks and reaches a mean peak anomaly that exceeds +4°C, are associated with regional dynamics in Patagonia and a large-scale circulation pattern in the South Pacific that resembles the wave-train pattern found for the interannual timescale.

- Specifically, we identified in the intraseasonal timescale a teleconnection between temperature in SSA and precipitation in Oceania that is comparable to the one described for the interannual timescale. Besides, the signatures in other variables (precipitation, SLP) over South America, associated with the heat waves in SEPG, are similar to the imprints found for the seasonal means. Hence, we observe the *similarity* of the mean patterns extracted from the seasonal averages (the interannual variability) and those derived from the synoptic-to-intraseasonal anomalies. Although the possible *climate intermodulation of these different frequency bands* was addressed in Chapter 3, our results concerning this aspect are still not conclusive.

- The identification of teleconnection mechanisms associated with the intraseasonal

and interannual SAT signals studied enables an *indirect* validation of these signals (and of the 20CR) by means of instrumental observations from remote places, in particular of precipitation and SLP in Australia and New Zealand.

- The MJO modulates the intraseasonal SAT in our study region during summer with an amplitude of ~1.5°C. Eventually, the MJO also favours the occurrence of heat waves in Patagonia via a tropical-extratropical interaction mechanism.

In summary, the objectives of the present PhD thesis were achieved. The studies have contributed to demonstrate some aspects of the usefulness of long-term observations and reconstructions for the analysis of the climate of the 20th century in SSA.

The results from this work can stimulate further possible studies. Among those, the following ones may be envisioned:

- The global warming signal was not explicitly considered in the present thesis. The incidence of this phenomenon on present results is an open area of research.

- The instrumental SAT signals were extracted from stations located mostly to the east of the Andes. However, we learnt that the mean SAT fields associated with their variability extend beyond that region and that most of our conclusions also apply for neighbouring areas. Thus, further observational data from within or beyond Eastern Patagonia might be used to explore the validity of the results presented in this thesis. This is especially applicable to long-term meteorological measurements from Chile.

- Besides, the teleconnection mechanisms described in this study allow the comparison between various climate variables in remote places. This result offers potential for exploring climatic relationships within South America and also beyond that continent, in a spatial scale comprising other regions of the Southern Hemisphere (e.g. between precipitation in Oceania and SAT in SSA). This possibility is not only restricted to the instrumental period but may also hold for the climate of the past. However, caution should be taken due the possible non-stationary character of these associations.

- Because our results concerning the similarity between the mechanisms identified for the interannual and the intraseasonal timescales are not conclusive, further scientific questions arise around this subject: What builds up *warm summers*? Are they related to the frequency or rather to the intensity of intraseasonal heat waves or maybe rather to other parameters?

- In the intraseasonal timescale, the modulation of SAT in Patagonia by the MJO could serve as basis for an improved local SAT forecast, provided that forecasts of the MJO active phases are well achieved. In particular, the forecast skill of local heat waves could also be enhanced.

- The proposed tropical-extratropical interaction for the intraseasonal timescale, a mechanism leading to SAT modulation in Patagonia, should be analysed in a modelling framework. It provides a basis for a better understanding of climate dynamics in the South Pacific region and related climate phenomena occurring in South America.

Acknowledgments

Merci viumau…

This thesis is the result of the inspiration and work supported by many people.

I am a privileged person from a country with profound social inequalities, especially concerning the access to education of quality. In this sense, I am very grateful to the BecasChile scholarship programme that allowed me to pursue my PhD studies in Bern. My scholarship was financed by all the workers of Chile. Our goal for the modern Latin American society is that in the near future, all people with a thirst for knowledge will have the opportunity to develop their potential. Thanks also to the CLIMANDES project.

There are uncountable people living abroad while following an academic career. My admiration goes to all of them. For me, this way of life has been a winding but beautiful road to transit – an endless voyage of curiosity, doubts, and restlessness. Thanks for their support to my family and all my friends, from here and abroad, especially to those who were always with me in person or via a camera, a keyboard, a pen, or through sincere thoughts. Ustedes han sido mi red de contención.

My years in Switzerland have been embellished by diverse exciting activities and wonderful people. I am very glad to have played with Bernavernos and the Orchestra of the University of Bern. Life without music would be unimaginable to me. In this regard, thanks to my co-pilots who kept me up-to-date concerning melodies and news from the external world: Radio Universidad de Chile, Radio Uno, and Radio RaBe. Thanks to AxionChile and RadioActivos: there is an amazing revolutionary spirit in you. *Gracias* to my flatmates from Waldheim and Schänzlihalde: you were a family to me. *Un abrazo al mundo hispanoamericano, los representantes de la patria grande, que hacen de este lugar uno más amable y sensible*.

In Bern I have fallen in love and also confronted myself deeply. After all, short before turning 30, I am somehow content of facing more existential questions than answers.

E r k l ä r u n g

gemäss Art. 28 Abs. 2 RSL 05

Name/Vorname: Jacques Coper, Martín Sebastián

Matrikelnummer: 10-129-930

Studiengang: PhD in Climate Sciences

          Bachelor ☐   Master ☐   Dissertation ☑

Titel der Arbeit: A multiscale analysis of summer temperature variability

in Southern South America during the 20th century

LeiterIn der Arbeit: Prof. Dr. Stefan Brönnimann

Ich erkläre hiermit, dass ich diese Arbeit selbständig verfasst und keine anderen als die angegebenen Quellen benutzt habe. Alle Stellen, die wörtlich oder sinngemäss aus Quellen entnommen wurden, habe ich als solche gekennzeichnet. Mir ist bekannt, dass andernfalls der Senat gemäss Artikel 36 Absatz 1 Buchstabe o des Gesetztes vom 5. September 1996 über die Universität zum Entzug des auf Grund dieser Arbeit verliehenen Titels berechtigt ist.

....
Ort/Datum

                               ....
                                     Unterschrift

Curriculum Vitae

Personal		Martín Sebastián Jacques Coper
		Schänzlihalde 30, 3013 Bern, Switzerland
		Born September 8th, 1984, in Ciudad de México, Mexico

Personal	since end of 2010	PhD student in Climate Sciences,
		Oeschger Centre and Institute of Geography,
		University of Bern, Switzerland
	2007-2009	Master of Science in Geophysics
		(Meteorology and Climatology),
		Universidad de Chile, Chile
	2003-2007	Graduate Diploma (*Licenciatura en Ciencias)*
		in Geophysics,
		Universidad de Chile, Chile

Student Exchange	2006	Student of Geophysics and Meteorology,
		University of Vienna, Austria

Professional Experience	2010	Researcher at the Geophysics Department,
		Universidad de Chile, Chile
		Research internship at ForWind,
		University of Oldenburg, Germany
	2005-2010	Teaching assistant,
		Faculty of Physical and Mathematical Sciences,
		Universidad de Chile, Chile